ARTICLES
https://doi.org/10.1038/s41557-022-00899-z

nature chemistry

Insights from an information thermodynamics analysis of a synthetic molecular motor

Shuntaro Amano[1], Massimiliano Esposito[2], Elisabeth Kreidt[1], David A. Leigh[1]✉, Emanuele Penocchio[2]✉ and Benjamin M. W. Roberts[1]

Information is physical, a realization that has transformed the physics of measurement and communication. However, the flow between information, energy and mechanics in chemical systems remains largely unexplored. Here we analyse a minimalist autonomous chemically driven molecular motor in terms of information thermodynamics, a framework that quantitatively relates information to other thermodynamic parameters. The treatment reveals how directional motion is generated by free energy transfer from chemical to mechanical (conformational and/or co-conformational) processes by 'energy flow' and 'information flow'. It provides a thermodynamic level of understanding of molecular motors that is general, complements previous analyses based on kinetics and has practical implications for machine design. In line with kinetic analysis, we find that power strokes do not affect the directionality of chemically driven machines. However, we find that power strokes can modulate motor velocity, the efficiency of free energy transfer and the number of fuel molecules consumed per cycle. This may help explain the role of such (co-)conformational changes in biomachines and illustrates the interplay between energy and information in chemical systems.

Understanding how and why a machine works in the way it does is crucial for optimizing designs and inventing new ones. For macroscopic machines, such an understanding can be deduced from engineering principles and Newtonian physics. In contrast, at the molecular level there is no simple explanation for why individual components of biomachines move in a particular way. Is the movement of a specific amino acid in adenosine triphosphate synthase a key requisite for the mechanism, or does it occur incidentally as part of an evolutionary pathway that was overall successful? Biomolecular machines operate autonomously, apparently through Brownian ratchet mechanisms[1–5]. They use energy and information to rectify the directionality of random thermal movements of their components so that work can be performed. These types of machines include biological pumps and motors, in which the energy is generally provided in the form of a chemical potential gradient[6,7]. Chemists are learning how to design synthetic analogues of such machines[8–13], with examples including a minimalist autonomous chemically fuelled molecular rotary motor[14] (Fig. 1).

Kinetic models have proved useful[15–17] in describing the behaviour of molecular machines, but such analysis is inherently unable to give an account of free energy transfer from the fuel to the machine. The consideration of thermodynamics is essential to understand free energy transduction, how this drives directional motion and generates the capacity to perform work[18] and, hence, how to optimize the motor's design. Up to now, attempts[12,19–24] to design molecular motors have been led by chemical intuition, with little opportunity to reliably judge the effectiveness of a machine's design or performance unless and until it has been realized experimentally.

Recently, stochastic thermodynamics has emerged as a method for studying systems that operate at energies of the order of thermal fluctuations[25–28]. The theory is valid even when systems are driven far from equilibrium[25,29,30] and has been used to study nonequilibrium nanoscale systems[31–37]. A major achievement in this field was the connection made between stochastic thermodynamics and information theory[38], which gave birth to 'information thermodynamics'[39,40]. Information thermodynamics relates information to other thermodynamic quantities, such as free energy and entropy, and has proved particularly successful in resolving apparent thermodynamic paradoxes, such as Maxwell's demon[41].

In this Article we develop a quantitative understanding of the processes that drive an autonomous chemically fuelled molecular motor[14] (Fig. 1) using an analysis that incorporates concepts from information thermodynamics within the framework of nonequilibrium thermodynamics of open chemical reaction networks[42,43]. Contrary to common models in stochastic thermodynamics[25,30,37], our framework neglects fluctuations and describes macroscopic ensembles of chemical species characterized by experimentally measurable concentrations. The approach is consistent with kinetic models[16,17,44], but goes further by introducing a quantitative thermodynamic understanding of how autonomous molecular motors work. Two features—information flow and energy flow—contribute to the transfer of free energy from the fuel to the machine that is the origin of current (that is, the net rate of displacement of the macrocycle directionally along the track; Box 1) in the motor. The effect of changing chemical gating[15], power strokes[45–47] (a viscoelastic, free energy-releasing, large-amplitude conformational change[45,47]) and overall rates on current and efficiency (Box 1) are examined through simulations, revealing design principles for molecular motors. Particular insight is gained in terms of the role of power strokes in tuning a motor's performance while remaining consistent with core aspects of kinetic models[16,17,44–48], informing the current debate concerning the role of power strokes in biomolecular machines[44,46,47].

As a result, the mechanism of operation of the rotary motor can be understood in several different ways: through chemical design[14], reaction kinetics[15,49], molecular dynamics[50] and, now, nonequilibrium information thermodynamics. Accordingly, this minimalist molecular motor can act as a Rosetta Stone for relating these disparate frameworks[16,17,35,44,49–51], aiding the translation

[1]Department of Chemistry, University of Manchester, Manchester, UK. [2]Department of Physics and Materials Science, University of Luxembourg, Luxembourg City, Luxembourg. ✉e-mail: david.leigh@manchester.ac.uk; emanuele.penocchio@uni.lu

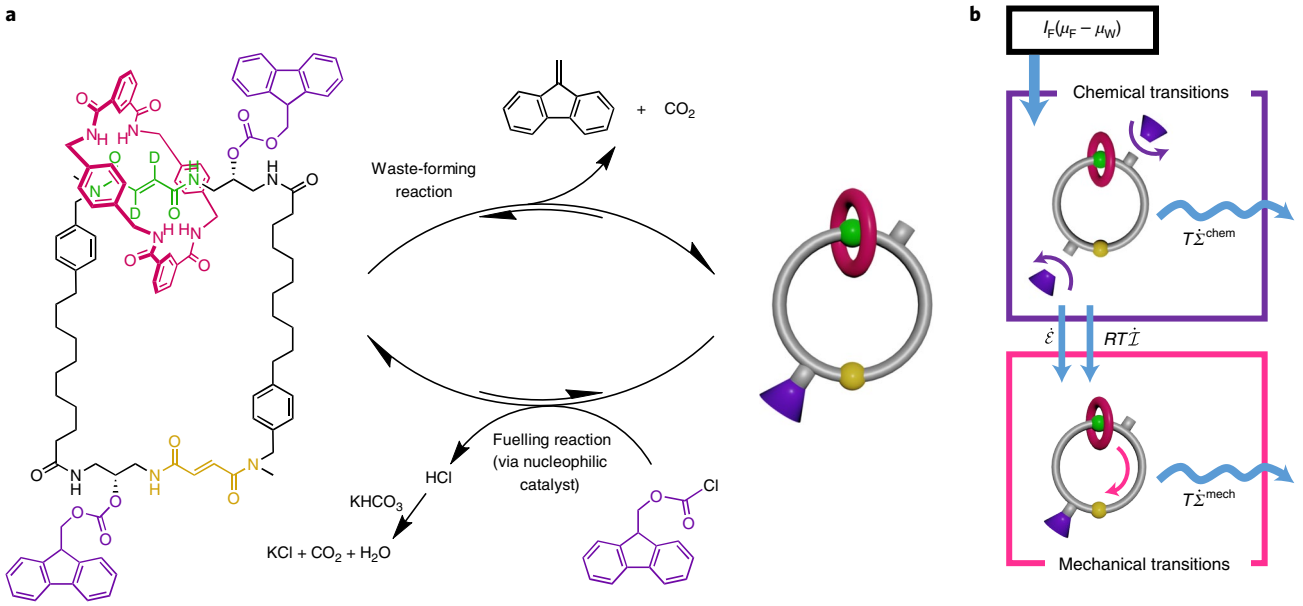

Fig. 1 | A Rosetta Stone for chemical (reactions and co-conformational dynamics) and information thermodynamics descriptions of a molecular motor: two distinct but complementary accounts of the processes involved in a minimalist, autonomous, chemically fuelled, molecular rotary motor. **a**, Chemical structure of the rotary motor and the chemical reactions involved in its operation. The motor comprises a benzylic amide macrocycle (magenta) and a track with two fumaramide binding sites (yellow, non-deuterated; green, deuterated for analytical purposes). The macrocycle randomly shuttles between the two fumaramide sites when its path is not blocked by Fmoc groups (purple). The fuelling reaction consumes the fuel (Fmoc-Cl) and attaches an Fmoc group to the track, and the waste-forming reaction removes the Fmoc group (allowing passage of the macrocycle) and generates waste species (dibenzofulvene and CO_2). The fuelling reaction is catalysed by a pyridine-based nucleophilic catalyst (for example, 4-dimethylaminopyridine or the bulky catalyst shown in Fig. 4a). Note that both reactions are considered reversible, even when the backward reactions (that is, regeneration of fuel via barrier removal and waste products reacting to give the barrier) are extremely rare events[66]. **b**, Information thermodynamics description of free energy transduction in the rotary motor. In the chemical transitions, free energy is supplied to the motor ($I_F(\mu_F-\mu_W)$), part of which is dissipated ($T\dot{\Sigma}^{chem}$). I_F is the rate at which the motor reacts with the fuel, $(\mu_F-\mu_W)$ is the chemical potential difference between the fuel and waste species, T is the temperature and $\dot{\Sigma}^{chem}$ is the entropy production rate of the chemical transitions. The rest of the free energy is supplied to the mechanical transitions either as energy ($\dot{\mathcal{E}}$) or information ($RT\dot{\mathcal{I}}$) flow, where R is the gas constant. Mechanical transitions dissipate this free energy ($T\dot{\Sigma}^{mech}$), generating directional motion of the macrocycle. When $\dot{\mathcal{E}}+RT\dot{\mathcal{I}}=0$, mechanical transitions are at equilibrium and no net mechanical displacement of the macrocycle can arise.

of concepts and relationships among energy, information, kinetics and molecular structure.

Results and discussion

A bipartite chemical reaction network for the minimalist rotary motor. The rotary motor in Fig. 1 comprises a cyclic track with two degenerate binding sites for a macrocycle[14]. One site is deuterium labelled to distinguish it from the other by ^{1}H NMR spectroscopy, although deuteration does not influence the chemical properties. Fluorenylmethoxycarbonyl (Fmoc) groups, which sterically prevent passage of the macrocycle, can be attached to hydroxy residues on the track (Fig. 2). When only one barrier is in place, macrocycle shuttling enables exchange between two co-conformers (co-conformers are structures that differ in the relative positions of the components[52]) that have the macrocycle either proximal (p) or distal (d) to the free hydroxy group. The fuelling reaction kinetically discriminates between the two co-conformers, favouring the reaction of the distal co-conformer over the proximal co-conformer. Under basic conditions, the waste-forming reaction removes barriers without any chemical gating. The chemical gating afforded by the biased fuelling reaction, and the free energy supplied by the fuel-to-waste conversion, result in directional movement of the macrocycle around the track. The rotary motor can be represented by a chemomechanical network of reactions (Fig. 2) in which mechanical and chemical transitions are coupled, as in common models for biological molecular motors[44] and minimal Brownian motors with external dichotomous noise[53]. Because no transitions enable simultaneous change in the mechanical and chemical states, this network is said to be bipartite[40,54].

Information thermodynamic analysis. As detailed in Supplementary Section I, the rotary motor is modelled as the isothermal open bipartite chemical reaction network[40,42,43] shown in Fig. 2. The concentrations of the six motor species, 2_H, 2_D, 1^H_D, 1^D_D, 1^H_H and 1^D_H (see Fig. 2 caption) evolve according to the rate constants of each reaction following mass-action kinetics. The system is open because the concentrations of fuel (Fmoc-Cl) and waste (HCl—liberated as part of the fuelling reaction and subsequently neutralized by $KHCO_3$, which is present to produce KCl, CO_2 and H_2O—and dibenzofulvene and CO_2 produced during the waste-forming reaction) species are kept constant through addition from, or removal to, an external source. An important quantity for our analysis is the chemical potential gradient between the fuel and waste species ($\mu_{Fmoc-Cl}-\mu_{HCl}-\mu_{dibenzofulvene}-\mu_{CO_2}$) which we denote $\mu_F-\mu_W$. For any thermodynamically consistent set of parameters (Methods), the system will evolve towards a stationary state in which the concentrations of all the motor species (that is, all co-conformations and chemical states of the motor) are constant in time, as are the thermodynamic properties of the system. The entropy production rate (the entropy changes in the system and in the reservoirs per unit time), denoted $\dot{\Sigma}$, measures how far from equilibrium the motor operates and has to be non-negative by virtue of the second law of thermodynamics[55]. When multiplied by temperature (T), this corresponds to the amount of free energy that is instantaneously

Box 1 | Definitions as applied to the minimalist rotary motor

Fuelling reaction	The reaction that consumes the fuel (Fmoc-Cl) and attaches an Fmoc group to the motor's track, generating HCl as waste product. Forward ($k^{p/d}_{+F}$) and backward ($k^{p/d}_{-F}$) rate constants may depend on the macrocycle being proximal (p) or distal (d) to the reaction site.
Waste-forming reaction	The reaction that removes the Fmoc group from the motor's track, generating dibenzofulvene and CO_2 as waste products. Forward ($k^{p/d}_{-W}$) and backward ($k^{p/d}_{+W}$) rate constants may depend on the macrocycle being proximal (p) or distal (d) to the reaction site.
Chemical gating	The bias of distal over proximal rate constants in fuelling and waste-forming reactions, quantified by k^{d}_{+F}/k^{p}_{+F} (fuelling gating) and k^{p}_{-W}/k^{d}_{-W} (waste-forming gating).
Overall reaction rate	The sum of the rate constants for a particular process: for example, Fmoc addition through fuelling reactions ($k^{d}_{+F} + k^{p}_{+F}$), Fmoc removal through waste-forming reactions ($k^{p}_{-W} + k^{d}_{-W}$), mechanical shuttling ($k_{+\Delta} + k_{-\Delta}$ or $k'_{+\Delta} + k'_{-\Delta}$, where the prime symbol indicates the case when the barrier close to the deuterated station is removed to allow for the shuttling).
Current	The net rate of directional displacement of the macrocycle along the track, quantified by equation (4).
Efficiency	The free energy available to the motor to dissipate as mechanical motion compared to the free energy available from the fuel-to-waste reaction, quantified by equation (5). This definition of efficiency does not take into account the background fuel decomposition.
Power stroke	The viscoelastic, free energy-releasing, mechanical shuttling of the macrocycle along the track. The free energy released is quantified by the change in standard chemical potential due to a net mechanical displacement of the macrocycle from the station proximal to the reacting hydroxy group (1^{D}_{H}, 1^{H}_{D}) to the one distal (1^{D}_{D}, 1^{H}_{H}): $\mu^{\circ}_{1^{D}_{H}} - \mu^{\circ}_{1^{D}_{D}}$ and $\mu^{\circ}_{1^{H}_{D}} - \mu^{\circ}_{1^{H}_{H}} \neq 0$.
Kinetic asymmetry	The kinetic preference for one direction over the other in a chemomechanical cycle, embodied by the ratcheting constant: $K_r = \frac{k_{+\Delta}k'_{+\Delta}(k^{p}_{-F}[HCl]+k^{p}_{-W})^2([Fmoc-Cl]k^{d}_{+F}+[CO_2][DBF]k^{d}_{+W})^2}{k_{-\Delta}k'_{-\Delta}([Fmoc-Cl]k^{p}_{+F}+[CO_2][DBF]k^{p}_{+W})^2(k^{d}_{-F}[HCl]+k^{d}_{-W})^2}$, where DBF stands for dibenzofulvene. When $K_r > 1$, the motor preferentially cycles in the forward direction, as is apparent from equation (4).

dissipated by the motor ($T\dot{\Sigma}$). In a stationary state (the only type of state considered in this Article), all the free energy from the conversion of the fuel to waste is dissipated by the motor: $T\dot{\Sigma} = I_F(\mu_F - \mu_W) \geq 0$, where I_F is the rate at which the fuel is consumed by the motor (we neglect the fuel-to-waste background reaction)[43]. This indicates that a non-null chemical potential gradient between fuel and waste species (we consider the case where $\mu_F > \mu_W$) is necessary to drive the system out of equilibrium and produce directed motion. However, this expression gives no information as to how free energy is consumed nor the amount of dissipation specifically devoted to sustain directional motion of the components.

To obtain a more in-depth understanding, we use information thermodynamics to split the free energy dissipation rate into two separately non-negative contributions (Fig. 1b), one due to the chemical transitions ($T\dot{\Sigma}^{chem}$) and the other due to the mechanical transitions ($T\dot{\Sigma}^{mech}$). This is possible because the Fmoc-motor chemical reaction network is bipartite[40]:

$$T\dot{\Sigma} = \overbrace{I_F(\mu_F - \mu_W) - \dot{\mathcal{E}} - RT\dot{\mathcal{I}}}^{T\dot{\Sigma}^{chem}\geq 0} + \overbrace{\dot{\mathcal{E}} + RT\dot{\mathcal{I}}}^{T\dot{\Sigma}^{mech}\geq 0} \geq 0. \quad (1)$$

This dissection of terms in equation (1) underlines that the free energy supplied by the fuel is only partially dissipated via the chemical processes as $T\dot{\Sigma}^{chem}$, while the remaining part is transferred to the mechanical processes and dissipated as $T\dot{\Sigma}^{mech}$. This transfer of free energy is composed of a standard free energy part, denoted 'energy flow':

$$\dot{\mathcal{E}} = J(\mu^{\circ}_{1^{D}_{H}} - \mu^{\circ}_{1^{D}_{D}} + \mu^{\circ}_{1^{H}_{D}} - \mu^{\circ}_{1^{H}_{H}}), \quad (2)$$

and a mutual information part[38], denoted 'information flow':

$$RT\dot{\mathcal{I}} = JRT\log\frac{[1^{D}_{H}][1^{H}_{D}]}{[1^{D}_{D}][1^{H}_{H}]}, \quad (3)$$

where R is the gas constant and J is the stationary clockwise (as viewed in Fig. 2) current at which the motor operates (Box 1). This current can be expressed as

$$J = k_{+\Delta}[1^{D}_{H}] - k_{-\Delta}[1^{D}_{D}] = k'_{+\Delta}[1^{H}_{D}] - k'_{-\Delta}[1^{H}_{H}] = \Gamma(K_r - 1) \quad (4)$$

where both Γ and K_r are positive quantities (for the derivation of equation (4) and the definition of Γ, see Supplementary Section V-B4 and Supplementary equation (69)), the latter denoting the ratcheting constant (recently applied in the context of dissipative self-assembly[17,49]), which quantifies the kinetic asymmetry of the motor[15,16,56] (Box 1).

Under the experimental conditions in which the motor was originally operated[14], the rotary motor is driven purely by information flow as the macrocycle binds with equal affinity to fumaramide stations adjacent to a hydroxy group and an Fmoc group (within the detection limits of ^{1}H NMR measurements), so there is no energy flow. However, when the standard chemical potentials of the distal and proximal co-conformers differ, energy flow arises according to equation (2). An example of this could arise if there was, say, a stabilizing interaction between the macrocycle and the Fmoc group, which would lead to an increase in energy of the macrocycle upon removal of the Fmoc-barrier close to it. As a consequence, the standard chemical potential would decrease, leading to the release of heat, each time net mechanical displacement occurs in the forward direction. This fits the definition of a 'power stroke'[45–47] (Box 1). Therefore, according to equation (2), the energy flow accounts for the part of the fuelling free energy that contributes to destabilizing the macrocycle during chemical transitions and which is subsequently dissipated in a power stroke.

Mutual information quantifies the correlation between the two parts of a bipartite system[40,54], here the chemical and mechanical states. For example, when $[1^{H}_{D}]$ (the concentration of species 1^{H}_{D}) and $[1^{H}_{H}]$ are larger than $[1^{H}_{H}]$ and $[1^{D}_{D}]$, respectively, a correlation is present between the mechanical and chemical states: when the motor's

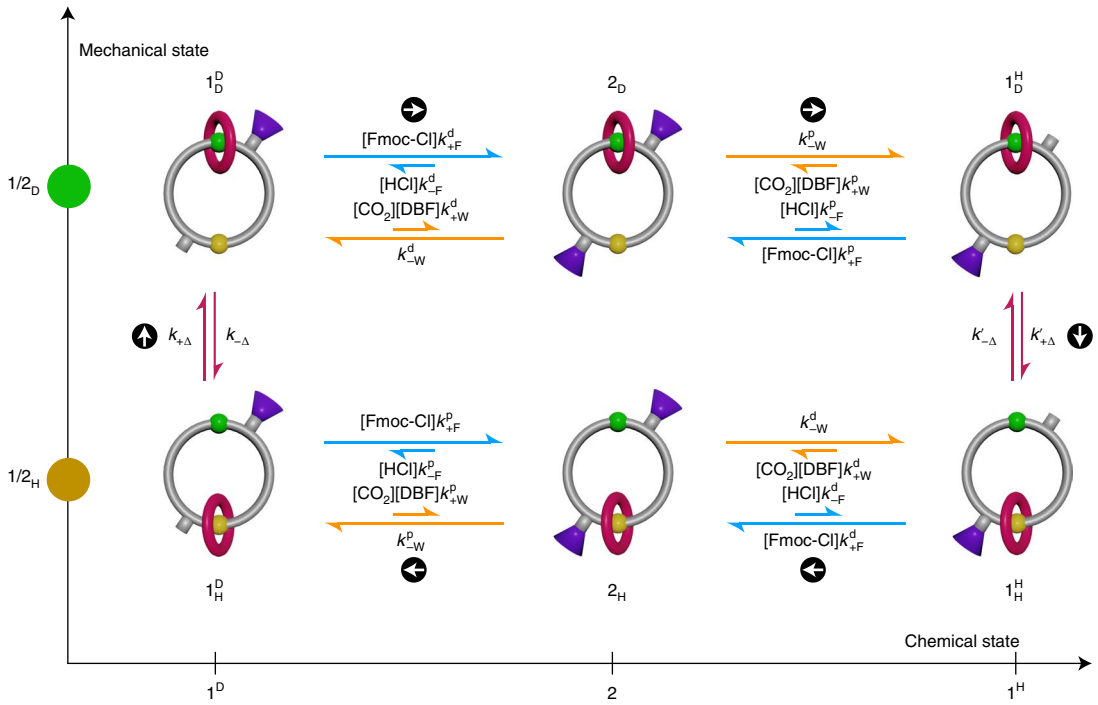

Fig. 2 | Rotary motor as an open and bipartite chemical reaction network. The state of the motor can be represented as a combination of two mechanical states (subscript D or H, expressing whether the macrocycle is binding to the deuterated or non-deuterated site on the track) and three chemical states (1^D, 2 or 1^H). The number in the chemical state shows the number of the Fmoc groups attached to the track, and the superscript H or D denotes the binding site close to the attached Fmoc group. Note that chemical states without any Fmoc group on the track are neglected as these are present in negligible concentration during machine operation due to the faster barrier formation than removal. The mechanical transitions involve displacement of the macrocycle, the rate constants for which are denoted $k_{+\Delta}$, $k_{-\Delta}$, $k'_{+\Delta}$ and $k'_{-\Delta}$. Subscript Δ indicates that they are the rate constants of mechanical transitions, which are only coupled to the thermal reservoir. Rate constants with and without the prime (′) are for the interconversion between 1^H_D and 1^H_H and the interconversion between 1^D_D and 1^D_H, respectively. The sign of the subscripts shows the direction of the transition (+ for the clockwise and − for the anticlockwise direction). The rate constants of the fuelling reaction and its reverse are denoted $k^{p/d}_{+F}$ and $k^{p/d}_{-F}$, respectively. The superscript shows whether the macrocycle is proximal (p) or distal (d) to the reacting hydroxy group. The rate constants of the waste-forming reaction and its reverse are denoted $k^{p/d}_{-W}$ and $k^{p/d}_{+W}$, respectively. In the experimental rotary motor, a clockwise current across the network is generated because $k^p_{+F} < k^d_{+F}$, $k^p_{-W} = k^d_{-W}$, and free energy is supplied to the motor by the fuel-to-waste conversion. The chemical gating in the fuelling reaction arises due to the steric crowding in the transition states of the proximal co-conformers (1^H_D and 1^D_H) compared to the distal co-conformers (1^D_D and 1^H_H). Arrows in circles represent the most probable (that is, most frequent) clockwise path. DBF, dibenzofulvene.

chemical state is 1^H, its mechanical state is more likely to be D than H. Similarly, when the motor's chemical state is 1^D, its mechanical state is more likely to be H than D. A concentration distribution with this kind of correlation has smaller (Shannon-like[38]) entropy than one without ($[1^H_D]$ and $[1^D_H]$ equal to $[1^H_H]$ and $[1^D_D]$, respectively). Therefore, correlation between the mechanical and chemical states (mutual information) generates an entropic driving force for a directional current (from $[1^H_D]$ to $[1^H_H]$ and from $[1^D_H]$ to $[1^D_D]$). From the thermodynamic viewpoint, mutual information constitutes the entropic contribution of the free energy that comes from the fuel. As mutual information is constant in the stationary state, changes in mutual information due to the chemical processes and mechanical processes are balanced[40]. If, as in the above situation, $\dot{\mathcal{I}} > 0$, the chemical transitions are producing mutual information that is consumed by the mechanical ones. Therefore, according to equation (3), the information flow accounts for the part of fuelling free energy that contributes to increasing the system's mutual information during chemical transitions and that is subsequently erased by mechanical shuttling.

Regimes where the free energy supplied by the chemical to the mechanical processes is exclusively due to the information flow ($RT\dot{\mathcal{I}}$), and thus lack any energy flow ($\dot{\mathcal{E}}$), are denoted as pure Maxwell demon regimes[40].

This analysis demonstrates that the free energy supplied to the mechanical processes by the energy and information flows, $RT\dot{\mathcal{I}} + \dot{\mathcal{E}}$, is the origin of net directional motion of the macrocycle around the track. Indeed, in the absence of such flow ($RT\dot{\mathcal{I}} + \dot{\mathcal{E}} = 0$), the mechanical transitions are at thermodynamic equilibrium ($\dot{\Sigma}^{\mathrm{mech}} = 0$), meaning a zero directional shuttling current ($J=0$; equation (4)). From an information thermodynamics perspective, the molecular motor operates by using chemical processes to transduce the free energy supplied by the fuel into the free energy supplied to the mechanical processes. The efficiency of this transduction is the ratio of the latter to the former and is bounded between zero and one due to the non-negativity of $\dot{\Sigma}^{\mathrm{chem}}$:

$$0 \leq \eta = \frac{RT\dot{\mathcal{I}} + \dot{\mathcal{E}}}{I_F(\mu_F - \mu_W)} = 1 - \frac{T\dot{\Sigma}^{\mathrm{chem}}}{I_F(\mu_F - \mu_W)} \leq 1. \qquad (5)$$

The efficiency of the transduction of the free energy of fuelling to the mechanical processes (η) is not directly comparable with the efficiencies usually reported for biological motors, which are often defined with respect to the work performed by the motor against an external force[35,47,57] or as the fraction of fuel molecules that are productively consumed, on average, over an operational cycle[50,58,59] (the latter measure of performance is computed in Supplementary Section VI for the rotary motor). In this set-up, the energy and information flows are entirely dissipated by the shuttling of the macrocycle as $T\dot{\Sigma}^{\mathrm{mech}}$. If the mechanical steps of the motor were

to work against a force (for example, if a load were attached to the macrocycle), $T\dot{\Sigma}^{\mathrm{mech}}$ would incorporate a negative work term in addition to $RT\dot{\mathcal{I}} + \dot{\mathcal{E}}$, which could serve to define the efficiency of the energy and information flows being converted into output work, instead of just being dissipated. The energy and information flows would thus constitute the maximum work output that can be delivered by the motor. A traditional thermodynamic analysis of such a motor[25,26,60] would exclusively focus on the efficiency with which the input free energy supplied by the fuel-to-waste chemical potential gradient is converted into output work, thus over-estimating the maximum work output as the overall free energy input $I_F(\mu_F - \mu_W)$. The present approach refines this analysis by showing how the input-to-output transduction is mediated by the free energy transfer within the motor, whose efficiency η (equation (5)) limits the maximum work output potentially deliverable by the motor. It also formally defines a thermodynamic efficiency that can be applied to motors while they perform no appreciable output work, as is the case for most of the synthetic molecular motors made so far, and can serve to compare the efficiencies of their operation.

The framework we have outlined can also be used to re-derive previous results obtained using kinetic arguments as a consequence of the second law of thermodynamics in bipartite systems. In Supplementary Section V-B, we show that the condition $T\dot{\Sigma}^{\mathrm{mech}} = 0$ implies $K_r = 1$, whereas the condition $T\dot{\Sigma}^{\mathrm{mech}} > 0$ implies $K_r \neq 1$, with forward movement when $K_r > 1$. This shows how the nonequilibrium thermodynamic framework, which focuses on energetic aspects quantified by the dissipation $T\dot{\Sigma}^{\mathrm{mech}}$, is consistent with previous analysis[15–17,49] focusing on kinetic aspects quantified by K_r, which determines the sign of the current J according to equation (4). This reiterates the effectiveness of this information thermodynamics-based approach and, again, demonstrates the usefulness of this minimalist molecular motor as a Rosetta Stone for the translation of meaning and understanding between different frameworks for describing phenomena.

Previously[17], the ratcheting constant has also been related to the ability of a dissipative self-assembly system to store free energy, but this connection is only valid in an operating regime where chemical transitions are substantially faster than mechanical ones. The information thermodynamics framework offers a general understanding of dissipative chemical systems and establishes limits to the maximum work deliverable by them that are valid in any operating regime, thanks to concepts such as the efficiency η introduced in equation (5).

Design principles for molecular motors. To demonstrate the use of our framework as a design tool, we explored the effects of altering the design features of the rotary motor on its current and efficiency (Supplementary Section VI). Basing the simulations on experimentally derived parameters[14] (Supplementary Section VI-A), we established that, under the experimental conditions employed, the rotary motor is driven purely by information flow as only the macrocycle distribution, rather than binding site affinity (within the detection limits of ^{1}H NMR measurements), is altered during operation. Under experimental conditions ([motor] = 10 mM, [Fmoc-Cl] = 30 mM, which is sustained by constant addition, [bulky catalyst] = 50 mM, [Et_3N] = 15 mM, [$KHCO_3$] = 200 mM, CH_2Cl_2, room temperature)[14], the current was estimated to be 2.1×10^{-8} mol dm^{-3} s^{-1}, requiring an average of seven fuel molecules per cycle per motor, although only 10^{-6}% of the free energy provided by the fuel is used to sustain the current (efficiency, $\eta = 10^{-8}$; equation (5)).

Varying the model parameters allows consideration of the effects of potential structural and chemical changes on the rotary motor (Supplementary Section VI-B1). Greater chemical gating for either the fuelling (Fig. 3a,b) or waste-forming reaction (Supplementary Section VI-B2) increases the current and efficiency by increasing information flow. The former has been achieved by increasing the steric bulk of the barrier-formation catalyst[14,61,62] (Fig. 4a) and the latter by catalysis of barrier removal by a proximal macrocycle (Fig. 4b)[24]. Gating of both fuelling and waste-forming reactions (Supplementary Section VI-B3) was recently demonstrated in a rotaxane information ratchet[24]. Inverting chemical gating is predicted to reverse the direction of the motor and could be achieved if the macrocycle activates, rather than hinders, proximal barrier formation (Fig. 4c). In the absence of a kinetic preference, or when gating from the fuelling and waste-forming reactions cancel out, the motor stops working, as this precludes information flow and hence mechanical dissipation ($\dot{\Sigma}^{\mathrm{mech}} = 0$). These results are consistent with kinetic models where kinetic asymmetry predicts the direction of the current[15–17].

The relevance of power strokes in molecular machinery is contentious, as power strokes are often observed experimentally in biological molecular motors[44–46], but, according to analysis based on kinetic asymmetry, the magnitude of the free energy released by such conformational changes does not affect the properties of chemically driven molecular machines, such as directionality and stopping force, and cannot improve the efficiency of a motor to work against an external force[47]. To reconcile differing viewpoints as to the importance of power strokes in molecular machines, we attempted to use our framework to understand the ways in which a power stroke can affect a molecular motor while staying kinetically and thermodynamically consistent. Power strokes can be used to induce energy flow (equation (2)) and, in principle, could be added to the rotary motor by introducing attractive interactions between the barrier and the macrocycle (Fig. 4d), stabilizing distal co-conformers $1^{\mathrm{D}}_{\mathrm{D}}$ and $1^{\mathrm{H}}_{\mathrm{H}}$ or, by adding repulsive interactions between the free barrier site and the macrocycle (Fig. 4e), destabilizing proximal co-conformers $1^{\mathrm{D}}_{\mathrm{H}}$ and $1^{\mathrm{H}}_{\mathrm{D}}$. Our simulations show that power strokes can change the magnitude of the current and efficiency of internal energy transduction (as defined in equations (4) and (5), respectively), despite kinetic asymmetry remaining unaltered (Methods and Supplementary Section VI-B4). This is because, while not altering K_r, power strokes can still increase the value of Γ in equation (4), reflecting their ability to favour forward cycles by inducing energy flow out of equilibrium (Fig. 3c,d). However, power strokes cannot drive directional motion in the absence of kinetic asymmetry ($RT\dot{\mathcal{I}} = -\dot{\mathcal{E}}$ when $K_r = 1$), nor can they invert directionality while the kinetic asymmetry remains constant. In these simulations, altering the power strokes and kinetic asymmetry together (Supplementary Section VI-B5) gave the greatest simulated efficiency (up to ~1%), suggesting that modifying both aspects may be important for optimizing the design of synthetic molecular motors. We note that improvements that occur through power strokes arise from the induced energy flow rather than from any special role for the energetically downhill nature of the power stroke in determining the motor's behaviour. As our analysis shows, a prerequisite for the motor's operation is the availability of free energy to dissipate through mechanical motion. Therefore, any design feature that enhances free energy transduction from the chemical to the mechanical transitions could equally well foster improvements in performance.

If power strokes cancel out over the motor cycle, then no net energy flow is introduced: free energy gained from one mechanical transition is lost in the other (Methods and Supplementary Section VI-B6). This could be realized in molecular form by using non-degenerate binding sites, for example, changing one fumaramide site to a more weakly binding succinamide unit (Figs. 3e,f and 4f), with a typical difference in binding energy of 23 kJ mol^{-1} (pink + symbol, Fig. 3e,f, equilibrium distribution > 99:1)[63] under experimental conditions similar to those used for rotary motor operation. Kinetic asymmetry remains unaltered in this scenario and, correspondingly, the direction of the motor could not be inverted in the simulation[15–17]. However, our analysis suggests that such a

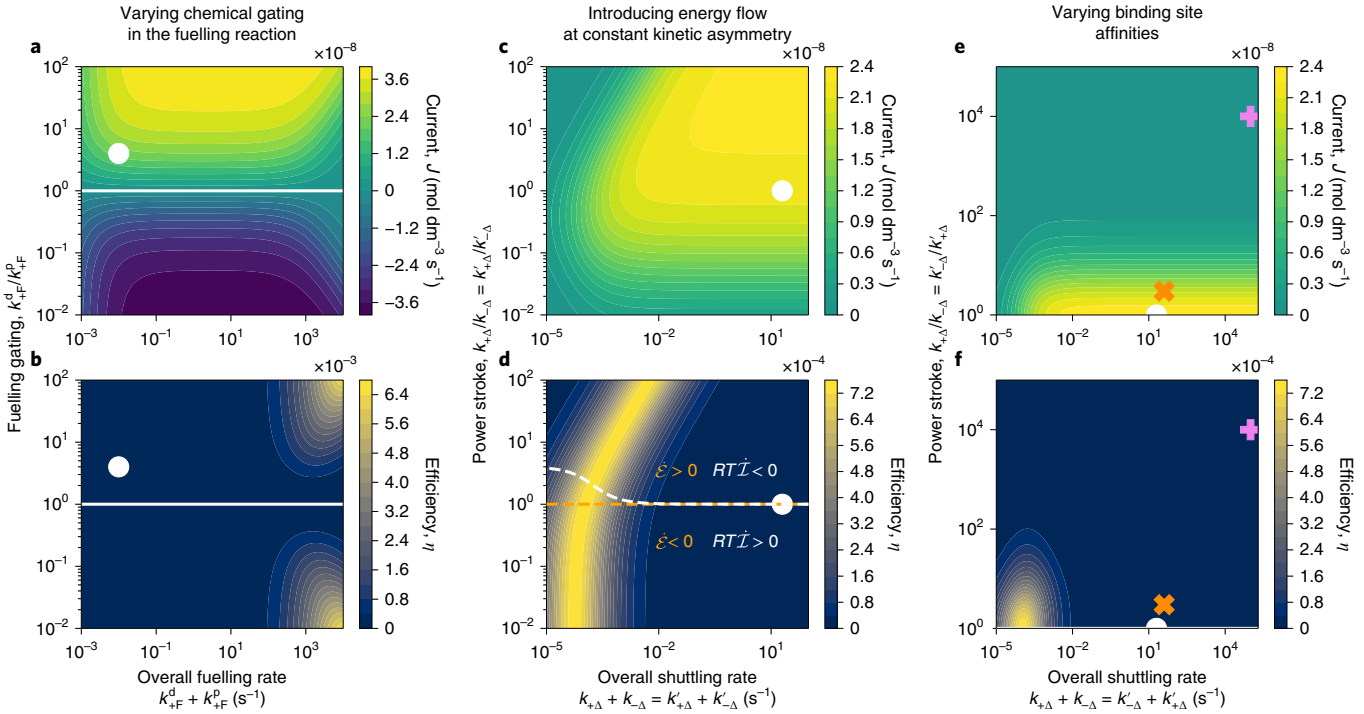

Fig. 3 | Numerical simulations of different molecular motor design modifications. a–f, Simulated current (J, top) and efficiency (η, bottom). Solid white lines indicate the regions of null current (and efficiency). White circles indicate the approximate parameters of the experimental rotary motor, giving a current of 2.1×10^{-8} mol dm^{-3} s^{-1} and efficiency of 10^{-6}%. Directional motion in the experimental rotary motor arises because distal fuelling reactions are approximately four times faster than proximal fuelling reactions (chemical gating, $k^{d}_{+F}/k^{p}_{+F} \approx 4$) due to the steric hindrance of the proximal transition state, whereas there was no chemical gating of waste-forming reactions ($k^{p}_{-W}/k^{d}_{-W} \approx 1$). In **a** and **b**, the overall rate of the fuelling reactions (x axis) and the fuelling gating (y axis) are varied. In **c** and **d**, the overall shuttling rate (x axis) and the ratio of forward and backward shuttling rates (indicative of power stroke magnitude; Methods) are varied. Power strokes are introduced in a way that induces energy flow ($\dot{\mathcal{E}}$) while keeping K_r constant. Below the dashed white lines, information flow ($RT\dot{\mathcal{I}}$) is positive and thus contributes to mechanical dissipation $\dot{\Sigma}^{mech}$. Above these lines, information flow is negative, requiring the motor to be driven by positive energy flow ($\dot{\mathcal{E}} > 0$). Negative energy flow is found below the orange dashed line. In **e** and **f**, the overall shuttling rate (x axis) and ratio of shuttling rate between stations (y axis) are varied. When this ratio diverges from one (indicating non-degenerate binding sites; Methods), both the current and efficiency drop. The pink + symbol indicates the position expected by changing one fumaramide group to a succinamide[63]. The orange × symbol indicates a position with a 3:1 difference in binding site affinity for the macrocycle.

change would be sufficient to effectively stall the motor, if operated under the original experimental conditions, despite the unchanged kinetic asymmetry. The simulations predict that, with power strokes cancelling out, any change from degenerate binding sites lowers the current and efficiency, although a smaller difference would leave the motor functional, albeit less effective. A 3:1 bias[61] (orange × symbol, Fig. 3e,f) is predicted to reduce the current by ~20%, rendering a design with non-degenerate binding sites plausible but less effective than a motor with binding sites of equal affinities.

In all of the cases considered, the highest efficiencies are predicted for when the rates of all the forward processes are approximately equal, leading to a cycle with no single rate-limiting step. Rate-limiting mechanical steps promote futile cycles, in which fuel is consumed without taking a forward step, as the unfavourable fuelling reaction is kinetically favoured over shuttling, decreasing both the current and efficiency. Rate-limiting chemical reactions result in lower thermodynamic efficiency but do not reduce the current or substantially change the fuel consumption per cycle. This is because relatively fast shuttling hinders the generation of a concentration bias (relative to mechanical equilibrium), which decreases the information flow in the steady state. The strong dependence of efficiency on shuttling rate indicates that, like macroscopic engines, the efficiency of a motor will be dependent on the load against which it is working[35]. As a consequence, instead of discussing a generic efficiency of a molecular motor, it is more proper to discuss the efficiency to work in a specific range of force/attached load. To use molecular machines most efficiently, they must either be tailored to the job they perform—such as using diesel engines for heavy loads—or they must use the equivalent of gears for macroscopic engines, to ensure they are working under optimal conditions.

Conclusions

Information thermodynamics-based analysis of a minimalist autonomous chemically driven molecular motor shows how information and energy flow, the two components of free energy transfer from chemical to mechanical transitions, enable the generation of directional motion from free energy supplied by a chemical fuel. The experimental rotary motor is a pure 'chemical Maxwell's demon', as information flow is the sole driving force. However, energy flow could potentially be introduced using power strokes, one of several design variations explored using our model. The predicted effect of energy flow is in line with observations made in biological motors[44] and contributes to the ongoing debate regarding the role of power strokes in molecular motors[46–48]. Information thermodynamics confirms that, in line with kinetic analysis, power strokes do not affect some key properties of chemically driven molecular machines, such as directionality. However, the magnitude of power strokes is able to affect the magnitude of the current (how fast the motor components rotate), the efficiency in terms of how free energy is dissipated, and the number of fuel molecules consumed per cycle. However,

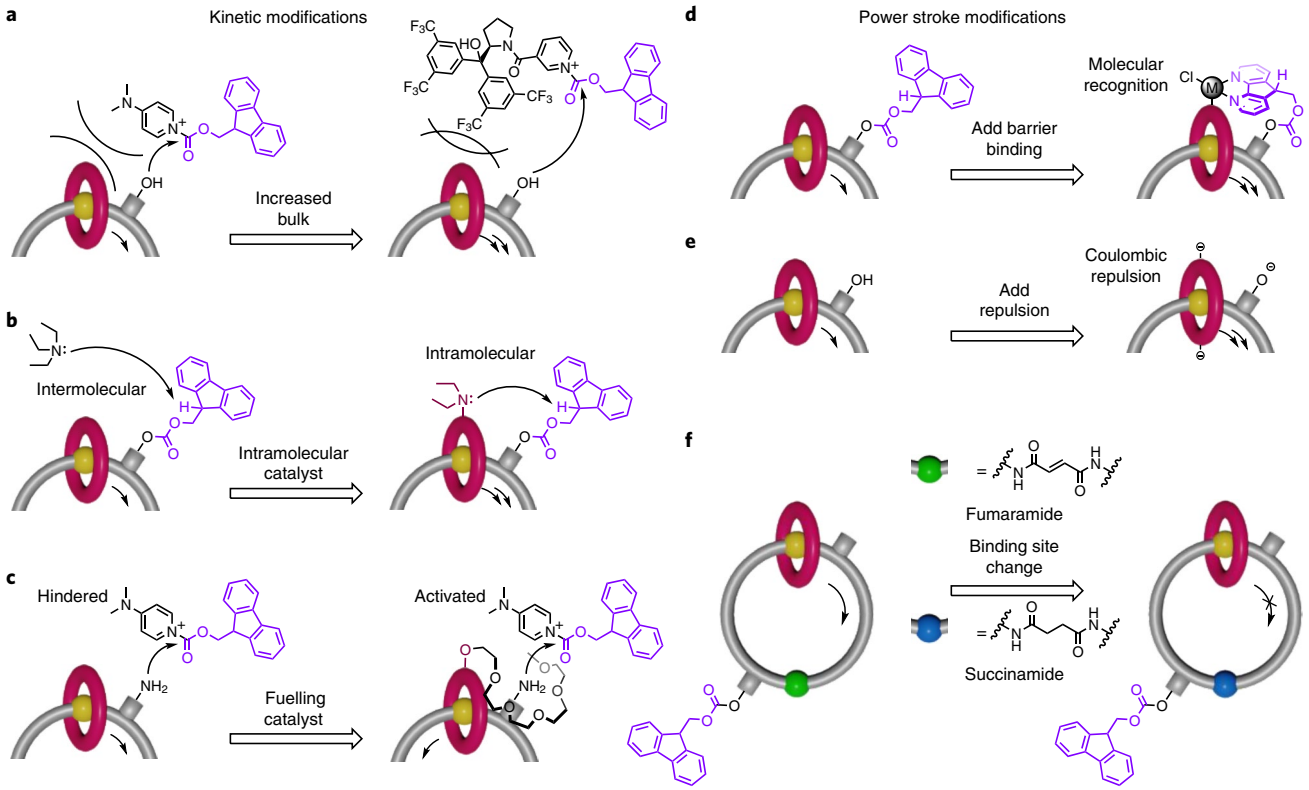

Fig. 4 | Potential ways of achieving different molecular motor design modifications. a, Increasing the steric bulk of the catalyst could be used to increase the fuelling chemical gating by slowing the undesired proximal reaction. **b**, Addition of a catalyst for the waste-forming reaction to the macrocycle could increase waste-formation chemical gating by increasing the rate of the proximal waste-forming reaction. **c**, Addition of a catalyst to the macrocycle that accelerates rather than hinders proximal barrier formation could negate chemical gating arising from steric hindrance, leading to an inversion of the directionality of the motor. **d**, Allowing the formation of a complex that binds the barrier and the macrocycle could allow the introduction of a power stroke by stabilizing the co-conformer in which the macrocycle is adjacent to the barrier. **e**, Conversely, a power stroke might be introduced by destabilizing the co-conformer with the macrocycle adjacent to the site with no barrier, for example, by the introduction of coulombic repulsion. **f**, Swapping one fumaramide binding site for a succinamide should, in principle, be sufficient to stall the rotary motor under the previous experimental operating conditions.

these results should not be misinterpreted as supporting a special importance of power strokes compared to other processes in the chemomechanical cycle. The information thermodynamics framework used in this Article should be generally applicable to other types of synthetic molecular machine, such as non-autonomous[10,12] and light-driven[8,9,11] motors, providing a quantitative basis through which to compare molecular machine designs. Additionally, it could, in principle, be extended to other types of (supra)molecular system (such as dissipative self-assembly[17]) powered by chemical engines[64]. We have uncovered substantial roles for 'energy flow' and 'information flow' in the mechanism of the transduction of free energy from chemical reactions by molecular machinery, although the exact nature of the connection of energy and information flow to energy and information ratcheting[1,65] remains to be clarified. The minimalist autonomous chemically driven molecular motor acts as a Rosetta Stone for relating energy, information, kinetics and molecular structure by aiding the translation of concepts and relationships between the 'languages' (that is, frameworks) of chemical kinetics, thermodynamics and chemical reactions.

Online content

Any methods, additional references, Nature Research reporting summaries, source data, extended data, supplementary information, acknowledgements, peer review information; details of author contributions and competing interests; and statements of data and code availability are available at https://doi.org/10.1038/s41557-022-00899-z.

Received: 4 July 2021; Accepted: 28 January 2022;
Published online: 17 March 2022

References

1. Chatterjee, M. N., Kay, E. R. & Leigh, D. A. Beyond switches: ratcheting a particle energetically uphill with a compartmentalized molecular machine. *J. Am. Chem. Soc.* **128**, 4058–4073 (2006).
2. Coskun, A., Banaszak, M., Astumian, R. D., Stoddart, J. F. & Grzybowski, B. A. Great expectations: can artificial molecular machines deliver on their promise? *Chem. Soc. Rev.* **41**, 19–30 (2012).
3. Erbas-Cakmak, S., Leigh, D. A., McTernan, C. T. & Nussbaumer, A. L. Artificial molecular machines. *Chem. Rev.* **115**, 10081–10206 (2015).
4. Qiu, Y., Feng, Y., Guo, Q.-H., Astumian, R. D. & Stoddart, J. F. Pumps through the ages. *Chem* **6**, 1952–1977 (2020).
5. Aprahamian, I. The future of molecular machines. *ACS Cent. Sci.* **6**, 347–358 (2020).
6. Howard, J. *Mechanics of Motor Proteins and the Cytoskeleton* (Oxford Univ. Press, 2001).
7. Astumian, R. D., Mukherjee, S. & Warshel, A. The physics and physical chemistry of molecular machines. *Chemphyschem* **17**, 1719–1741 (2016).
8. Koumura, N., Zijlstra, R. W. J., van Delden, R. A., Harada, N. & Feringa, B. L. Light-driven monodirectional molecular rotor. *Nature* **401**, 152–155 (1999).
9. Serreli, V., Lee, C.-F., Kay, E. R. & Leigh, D. A. A molecular information ratchet. *Nature* **445**, 523–527 (2007).
10. Cheng, C. et al. An artificial molecular pump. *Nat. Nanotechnol.* **10**, 547–553 (2015).
11. Ragazzon, G., Baroncini, M., Silvi, S., Venturi, M. & Credi, A. Light-powered autonomous and directional molecular motion of a dissipative self-assembling system. *Nat. Nanotechnol.* **10**, 70–75 (2015).
12. Erbas-Cakmak, S. et al. Rotary and linear molecular motors driven by pulses of a chemical fuel. *Science* **358**, 340–343 (2017).

13. Amano, S., Fielden, S. D. P. & Leigh, D. A. A catalysis-driven artificial molecular pump. *Nature* **594**, 529–534 (2021).
14. Wilson, M. R. et al. An autonomous chemically fuelled small-molecule motor. *Nature* **534**, 235–240 (2016).
15. Astumian, R. D. How molecular motors work—insights from the molecular machinist's toolbox: the Nobel Prize in Chemistry 2016. *Chem. Sci.* **8**, 840–845 (2017).
16. Astumian, R. D. Kinetic asymmetry allows macromolecular catalysts to drive an information ratchet. *Nat. Commun.* **10**, 3837 (2019).
17. Ragazzon, G. & Prins, L. J. Energy consumption in chemical fuel-driven self-assembly. *Nat. Nanotechnol.* **13**, 882–889 (2018).
18. Esposito, M. Open questions on nonequilibrium thermodynamics of chemical reaction networks. *Commun. Chem.* **3**, 107 (2020).
19. Kelly, T. R., De Silva, H. & Silva, R. A. Unidirectional rotary motion in a molecular system. *Nature* **401**, 150–152 (1999).
20. Mock, W. L. & Ochwat, K. J. Theory and example of a small-molecule motor. *J. Phys. Org. Chem.* **16**, 175–182 (2003).
21. Fletcher, S. P., Dumur, F., Pollard, M. M. & Feringa, B. L. A reversible, unidirectional molecular rotary motor driven by chemical energy. *Science* **310**, 80–82 (2005).
22. Collins, B. S. L., Kistemaker, J. C. M., Otten, E. & Feringa, B. L. A chemically powered unidirectional rotary molecular motor based on a palladium redox cycle. *Nat. Chem.* **8**, 860–866 (2016).
23. Zhang, Y. et al. A chemically driven rotary molecular motor based on reversible lactone formation with perfect unidirectionality. *Chem* **6**, 2420–2429 (2020).
24. Borsley, S., Leigh, D. A. & Roberts, B. M. W. A doubly kinetically-gated information ratchet autonomously driven by carbodiimide hydration. *J. Am. Chem. Soc.* **143**, 4414–4420 (2021).
25. Seifert, U. Stochastic thermodynamics, fluctuation theorems and molecular machines. *Rep. Prog. Phys.* **75**, 126001 (2012).
26. Parrondo, J. M. R. & de Cisneros, B. J. Energetics of Brownian motors: a review. *Appl. Phys. A* **75**, 179–191 (2002).
27. Esposito, M., Lindenberg, K. & Van den Broeck, C. Universality of efficiency at maximum power. *Phys. Rev. Lett.* **102**, 130602 (2009).
28. Benenti, G., Casati, G., Saito, K. & Whitney, R. S. Fundamental aspects of steady-state conversion of heat to work at the nanoscale. *Phys. Rep.* **694**, 1–124 (2017).
29. Jarzynski, C. Equalities and inequalities: irreversibility and the second law of thermodynamics at the nanoscale. *Annu. Rev. Condens. Matter Phys.* **2**, 329–351 (2011).
30. Peliti, L. & Pigolotti, S. *Stochastic Thermodynamics*: *An Introduction* (Princeton Univ. Press, 2021).
31. Andrieux, D. & Gaspard, P. Fluctuation theorems and the nonequilibrium thermodynamics of molecular motors. *Phys. Rev. E* **74**, 011906 (2006).
32. Lipowsky, R. & Liepelt, S. Chemomechanical coupling of molecular motors: thermodynamics, network representations, and balance conditions. *J. Stat. Phys.* **130**, 39–67 (2008).
33. Toyabe, S. et al. Nonequilibrium energetics of a single F_1-ATPase molecule. *Phys. Rev. Lett.* **104**, 198103 (2010).
34. Ariga, T., Tomishige, M. & Mizuno, D. Nonequilibrium energetics of molecular motor kinesin. *Phys. Rev. Lett.* **121**, 218101 (2018).
35. Brown, A. I. & Sivak, D. A. Theory of nonequilibrium free energy transduction by molecular machines. *Chem. Rev.* **120**, 434–459 (2020).
36. Ciliberto, S. Experiments in stochastic thermodynamics: short history and perspectives. *Phys. Rev. X* **7**, 021051 (2017).
37. McGrath, T., Jones, N. S., ten Wolde, P. R. & Ouldridge, T. E. Biochemical machines for the interconversion of mutual information and work. *Phys. Rev. Lett.* **118**, 028101 (2017).
38. Cover, T. M. & Thomas, J. A. *Elements of Information Theory* (Wiley, 2012).
39. Parrondo, J. M. R., Horowitz, J. M. & Sagawa, T. Thermodynamics of information. *Nat. Phys.* **11**, 131–139 (2015).
40. Horowitz, J. M. & Esposito, M. Thermodynamics with continuous information flow. *Phys. Rev. X* **4**, 031015 (2014).
41. Leff, H. S. & Rex, A. F. (eds) *Maxwell's Demon*: *Entropy*, *Information*, *Computing* (Princeton Univ. Press, 1990).
42. Rao, R. & Esposito, M. Nonequilibrium thermodynamics of chemical reaction networks: wisdom from stochastic thermodynamics. *Phys. Rev. X* **6**, 041064 (2016).
43. Penocchio, E., Rao, R. & Esposito, M. Thermodynamic efficiency in dissipative chemistry. *Nat. Commun.* **10**, 3865 (2019).
44. Wagoner, J. A. & Dill, K. A. Mechanisms for achieving high speed and efficiency in biomolecular machines. *Proc. Natl Acad. Sci. USA* **116**, 5902–5907 (2019).
45. Howard, J. Protein power strokes. *Curr. Biol.* **16**, R517–R519 (2006).
46. Hwang, W. & Karplus, M. Structural basis for power stroke vs. Brownian ratchet mechanisms of motor proteins. *Proc. Natl Acad. Sci. USA* **116**, 19777–19785 (2019).
47. Astumian, R. D. Irrelevance of the power stroke for the directionality, stopping force, and optimal efficiency of chemically driven molecular machines. *Biophys. J.* **108**, 291–303 (2015).
48. Pezzato, C., Cheng, C., Stoddart, J. F. & Astumian, R. D. Mastering the non-equilibrium assembly and operation of molecular machines. *Chem. Soc. Rev.* **46**, 5491–5507 (2017).
49. Das, K., Gabrielli, L. & Prins, L. J. Chemically-fueled self-assembly in biology and chemistry. *Angew. Chem. Int. Ed.* **60**, 20120–20143 (2021).
50. Albaugh, A. & Gingrich, T. R. Simulating a chemically-fueled molecular motor with nonequilibrium molecular dynamics. Preprint at https://doi.org/10.48550/arXiv.2102.06298 (2021).
51. Horowitz, J. M., Sagawa, T. & Parrondo, J. M. R. Imitating chemical motors with optimal information motors. *Phys. Rev. Lett.* **111**, 010602 (2013).
52. Fyfe, M. C. T. et al. Anion-assisted self-assembly. *Angew. Chem. Int. Ed.* **36**, 2068–2070 (1997).
53. Astumian, R. D. Design principles for Brownian molecular machines: how to swim in molasses and walk in a hurricane. *Phys. Chem. Chem. Phys.* **9**, 5067–5083 (2007).
54. Hartich, D., Barato, A. C. & Seifert, U. Stochastic thermodynamics of bipartite systems: transfer entropy inequalities and a Maxwell's demon interpretation. *J. Stat. Mech. Theory Exp.* **2014**, P02016 (2014).
55. Kondepudi, D. K. & Prigogine, I. *Modern Thermodynamics*: *From Heat Engines to Dissipative Structures* (Wiley, 2015).
56. Astumian, R. & Bier, M. Mechanochemical coupling of the motion of molecular motors to ATP hydrolysis. *Biophys. J.* **70**, 637–653 (1996).
57. Kinosita, K. Jr., Yasuda, R., Noji, H. & Adachi, K. A rotary molecular motor that can work at near 100% efficiency. *Philos. Trans. R. Soc. Lond. B* **355**, 473–489 (2000).
58. Watt, I. N., Montgomery, M. G., Runswick, M. J., Leslie, A. G. W. & Walker, J. E. Bioenergetic cost of making an adenosine triphosphate molecule in animal mitochondria. *Proc. Natl Acad. Sci. USA* **107**, 16823–16827 (2010).
59. Petersen, J., Förster, K., Turina, P. & Gräber, P. Comparison of the H^+/ATP ratios of the H^+-ATP synthases from yeast and from chloroplast. *Proc. Natl Acad. Sci. USA* **109**, 11150–11155 (2012).
60. Hill, T. L. *Free Energy Transduction in Biology* (Academic Press, 1977).
61. Alvarez-Pérez, M., Goldup, S. M., Leigh, D. A. & Slawin, A. M. Z. A chemically-driven molecular information ratchet. *J. Am. Chem. Soc.* **130**, 1836–1838 (2008).
62. Carlone, A., Goldup, S. M., Lebrasseur, N., Leigh, D. A. & Wilson, A. A three-compartment chemically-driven molecular information ratchet. *J. Am. Chem. Soc.* **134**, 8321–8323 (2012).
63. Lussis, P. et al. A single synthetic small molecule that generates force against a load. *Nat. Nanotechnol.* **6**, 553–557 (2011).
64. Amano, S., Borsley, S., Leigh, D. A. & Sun, Z. Chemical engines: driving systems away from equilibrium through catalyst reaction cycles. *Nat. Nanotechnol.* **16**, 1057–1067 (2021).
65. Kay, E. R., Leigh, D. A. & Zerbetto, F. Synthetic molecular motors and mechanical machines. *Angew. Chem. Int. Ed.* **46**, 72–191 (2007).
66. Blackmond, D. G. 'If pigs could fly' chemistry: a tutorial on the principle of microscopic reversibility. *Angew. Chem. Int. Ed.* **48**, 2648–2654 (2009).

Methods

Wegscheider's conditions. To ensure that the system reaches thermodynamic equilibrium (detailed balance), when there is no chemical potential gradient between fuel and waste species ($\mu_F - \mu_W = 0$), the rate constants must satisfy Wegscheider's conditions[42]. These are equivalent to the constraints on the rate constants imposed in previous kinetic analyses[4,16,48] and dictate that the product of the forward rate constants along each independent cyclic pathway of reactions in the network, with neither net consumption nor net production of fuel or waste species, must equal the product of the corresponding backward rate constants:

$$k^{\mathrm{p}}_{-\mathrm{F}}k_{+\Delta}k^{\mathrm{d}}_{+\mathrm{F}}k^{\mathrm{p}}_{-\mathrm{F}}k'_{+\Delta}k^{\mathrm{d}}_{+\mathrm{F}} = k^{\mathrm{p}}_{+\mathrm{F}}k_{-\Delta}k^{\mathrm{d}}_{-\mathrm{F}}k^{\mathrm{p}}_{+\mathrm{F}}k'_{-\Delta}k^{\mathrm{d}}_{-\mathrm{F}} \quad (6)$$

$$k^{\mathrm{p}}_{-\mathrm{W}}k_{+\Delta}k^{\mathrm{d}}_{+\mathrm{W}}k^{\mathrm{p}}_{-\mathrm{W}}k'_{+\Delta}k^{\mathrm{d}}_{+\mathrm{W}} = k^{\mathrm{p}}_{+\mathrm{W}}k_{-\Delta}k^{\mathrm{d}}_{-\mathrm{W}}k^{\mathrm{p}}_{+\mathrm{W}}k'_{-\Delta}k^{\mathrm{d}}_{-\mathrm{W}}. \quad (7)$$

See Supplementary Section III for the derivation. These conditions were always imposed in numerical simulations to guarantee thermodynamic consistency[66].

Local detailed balance. In Fig. 3, variations in the power stroke magnitude have been related to changes in the ratio of shutting rate constants by virtue of the so-called 'principle of local detailed balance' (see below), which relates the log-ratio of forward and backward rate constants of a single chemical reaction to the difference in standard chemical potentials between its reagents and products[42] (Supplementary equation (33)). For example, it implies the relation

$$RT\log\left(\frac{k_{+\Delta}k'_{+\Delta}}{k_{-\Delta}k'_{-\Delta}}\right) = \mu^{\circ}_{1_{\mathrm{H}}^{\mathrm{D}}} - \mu^{\circ}_{1_{\mathrm{D}}^{\mathrm{D}}} + \mu^{\circ}_{1_{\mathrm{D}}^{\mathrm{H}}} - \mu^{\circ}_{1_{\mathrm{H}}^{\mathrm{H}}}, \quad (8)$$

which was employed in the numerical simulations.

In addition, Wegscheider's conditions (equations (6) and (7)) imply that a variation in the power stroke magnitude must always be compensated by a variation in the fuelling and waste-forming rate constants, because the following constraint (equation (9)) must always hold for thermodynamic consistency:

$$\frac{k_{+\Delta}}{k_{-\Delta}} \times \frac{k'_{+\Delta}}{k'_{-\Delta}} = \frac{k^{\mathrm{p}}_{+\mathrm{F}}k^{\mathrm{d}}_{-\mathrm{F}}}{k^{\mathrm{p}}_{-\mathrm{F}}k^{\mathrm{d}}_{+\mathrm{F}}} \times \frac{k^{\mathrm{p}}_{+\mathrm{W}}k^{\mathrm{d}}_{-\mathrm{W}}}{k^{\mathrm{p}}_{-\mathrm{W}}k^{\mathrm{d}}_{+\mathrm{W}}}. \quad (9)$$

When energy flow-inducing power strokes were introduced in Fig. 3c,d, the constraint in equation (9) was imposed by changing rate constants $k^{\mathrm{p}}_{+\mathrm{W}}$ and $k^{\mathrm{p}}_{+\mathrm{F}}$ according to variations in the shuttling rate constants. By doing so, kinetic asymmetry (K_{r}) is not altered during the simulation, but the magnitude of the current in equation (4) can still change by virtue of alterations in the value of the positive factor Γ (for its mathematical expression, see Supplementary equation (69)). Instead, in Supplementary Fig. 5, rate constants $k^{\mathrm{p}}_{+\mathrm{W}}$ and $k^{\mathrm{p}}_{-\mathrm{F}}$ were changed to vary the energy flow and K_{r} together. Experimentally, this could correspond to introducing an interaction between the macrocycle and the Fmoc group that affects (Supplementary Fig. 5) or not (Fig. 3c,d) the transition state of the proximal fuelling reaction, without affecting the transition state of the proximal waste-forming reaction. Note that, when binding affinities are modified as in Fig. 3e,f, the left-hand side of equation (9) stays constant and the constraint is automatically satisfied.

We end by noting that the terminology 'local detailed balance' comes from statistical physics[67], where it has become the central concept to formulate thermodynamically consistent dynamics[68,69]. Its chemical counterpart[42] (Supplementary equation (33)) is fully equivalent to the usual conditions imposed on the rate constants to ensure that microscopic reversibility holds[47] (see, for example, equation (5) in ref. [16]). We note that use of the term 'local detailed balance' in this context is considered contentious by some[16]. For a more detailed discussion see Supplementary Section III.

Data availability

All data needed to reproduce the numerical results are reported in the Supplementary Information.

Code availability

The code that generated the plots is available at the following link: gitlab.com/emanuele.penocchio/infothermorotmot

References

67. Katz, S., Lebowitz, J. L. & Spohn, H. Phase transitions in stationary nonequilibrium states of model lattice systems. *Phys. Rev. B* **28**, 1655–1658 (1983).
68. Esposito, M. Stochastic thermodynamics under coarse graining. *Phys. Rev. E* **85**, 041125 (2012).
69. Maes, C. Local detailed balance. *SciPost Phys. Lect. Notes* **32**, https://doi.org/10.48550/arXiv.2102.06298 (2021).

Acknowledgements

We acknowledge support from the European Research Council (ERC Consolidator grant no. 681456 to M.E. and funding to E.P.; ERC Advanced grant no. 786630 to D.A.L.), the FQXi Foundation, project 'Information as a fuel in colloids and superconducting quantum circuits' (grant no. FQXi-IAF19-05 to M.E.), the Engineering and Physical Sciences Research Council (EPSRC; grant no. EP/P027067/1 to D.A.L.), the Deutsche Forschungsgemeinschaft (a postdoctoral fellowship to E.K.) and the University of Manchester and EPSRC for PhD studentships to S.A. and B.M.W.R. D.A.L. is a Royal Society Research Professor. We thank R. D. Astumian for valuable discussions regarding the science in this study as well as robust debate regarding the use of the term 'local detailed balance' within the stochastic thermodynamics community.

Author contributions

S.A., B.M.W.R. and E.K. proposed the collaboration. E.P. developed the theoretical model. S.A., B.M.W.R., E.P. and E.K. carried out the theoretical analysis and simulations. D.A.L. and M.E. directed the research. All authors contributed to the analysis of the results and the writing of the manuscript.

Competing interests

The authors declare no competing interests.

Additional information

Supplementary information The online version contains supplementary material available at https://doi.org/10.1038/s41557-022-00899-z.

Correspondence and requests for materials should be addressed to David A. Leigh or Emanuele Penocchio.

Peer review information *Nature Chemistry* thanks the anonymous reviewers for their contribution to the peer review of this work.

Reprints and permissions information is available at www.nature.com/reprints.

nature portfolio

https://doi.org/10.1038/s41557-022-00899-z

Supplementary information

Insights from an information thermodynamics analysis of a synthetic molecular motor

In the format provided by the authors and unedited

Supplementary information for *Insights from an information thermodynamics analysis of a synthetic molecular motor*

Shuntaro Amano,[1] Massimiliano Esposito,[2] Elisabeth Kreidt,[1] David A. Leigh*,[1] Emanuele Penocchio*,[2] and Benjamin M. W. Roberts[1]

[1] *Department of Chemistry, University of Manchester, Oxford Road, Manchester M13 9PL, United Kingdom*
[2] *Complex Systems and Statistical Mechanics, Department of Physics and Materials Science, University of Luxembourg, L-1511 Luxembourg City, G.D. Luxembourg*

*email: david.leigh@manchester.ac.uk, emanuele.penocchio@uni.lu

CONTENTS

I. The model 2
A. Coarse-graining 2

II. Dynamics 4
A. Topological properties 5
B. Stationary state 6

III. Thermodynamics 7
A. Steady state entropy production and J^{ss}/I_F^{ss} 9

IV. Information Thermodynamics Perspective 9

V. Thermodynamic constraints on the stationary state dynamics and connection with kinetic asymmetry: the rotary motor as a Rosetta Stone for kinetic and thermodynamic analysis 12
A. Condition for directional J^{ss} 12
B. Connection to kinetic asymmetry and K_r 12
1. Equilibrium condition 13
2. Proof of the implication $\dot{\Sigma}^{mech} > 0 \rightarrow K_r \neq 1$ 13
3. Special proof for the experimental case 14
4. On the magnitude of the stationary state current J^{ss} 14

VI. Numerical Simulations 15
A. Parameters 15
B. Supplementary analysis of the numerical simulations 15
1. Chemical gating of the fueling reaction 15
2. Chemical gating of the waste-forming reaction 17
3. Further exploration of chemical gating 17
4. Introducing energy flow with power strokes without varying kinetic asymmetry 18
5. Introducing energy flow with a power stroke together with varying kinetic asymmetry 19
6. Causing power strokes to cancel out 20
7. Conclusion 21

References 21

I. THE MODEL

As stated in the main text, we treat the autonomous chemically-fueled molecular motor[1] as an open bipartite chemical reaction network. We consider an isothermal, isobaric, and well-stirred ideal dilute solution containing species undergoing the 10 reactions represented in Fig. 2 of the main text, which we collect in the vector $\boldsymbol{\rho} = \{1\mathrm{F}^{(\mathrm{p})}, 1\mathrm{W}^{(\mathrm{p})}, 2\Delta, 3\mathrm{F}^{(\mathrm{d})}, 3\mathrm{W}^{(\mathrm{d})}, 4\mathrm{F}^{(\mathrm{p})}, 4\mathrm{W}^{(\mathrm{p})}, 5\Delta', 6\mathrm{F}^{(\mathrm{d})}, 6\mathrm{W}^{(\mathrm{d})}\}$:

$$
\begin{aligned}
1\mathrm{F}^{(\mathrm{p})}: &\quad 2_{\mathrm{H}} + \mathrm{HCl} \underset{k^{\mathrm{p}}_{+\mathrm{F}}}{\overset{k^{\mathrm{p}}_{-\mathrm{F}}}{\rightleftharpoons}} 1^{\mathrm{D}}_{\mathrm{H}} + \mathrm{Fmoc{-}Cl} \qquad
4\mathrm{F}^{(\mathrm{p})}: &\quad 2_{\mathrm{D}} + \mathrm{HCl} \underset{k^{\mathrm{p}}_{+\mathrm{F}}}{\overset{k^{\mathrm{p}}_{-\mathrm{F}}}{\rightleftharpoons}} 1^{\mathrm{H}}_{\mathrm{D}} + \mathrm{Fmoc{-}Cl} \\
1\mathrm{W}^{(\mathrm{p})}: &\quad 2_{\mathrm{H}} \underset{k^{\mathrm{p}}_{+\mathrm{W}}}{\overset{k^{\mathrm{p}}_{-\mathrm{W}}}{\rightleftharpoons}} 1^{\mathrm{D}}_{\mathrm{H}} + \mathrm{DBF} + \mathrm{CO_2} \qquad
4\mathrm{W}^{(\mathrm{p})}: &\quad 2_{\mathrm{D}} \underset{k^{\mathrm{p}}_{+\mathrm{W}}}{\overset{k^{\mathrm{p}}_{-\mathrm{W}}}{\rightleftharpoons}} 1^{\mathrm{H}}_{\mathrm{D}} + \mathrm{DBF} + \mathrm{CO_2} \\
2\Delta: &\quad 1^{\mathrm{D}}_{\mathrm{H}} \underset{k_{-\Delta}}{\overset{k_{+\Delta}}{\rightleftharpoons}} 1^{\mathrm{D}}_{\mathrm{D}} \qquad
5\Delta': &\quad 1^{\mathrm{H}}_{\mathrm{D}} \underset{k'_{-\Delta}}{\overset{k'_{+\Delta}}{\rightleftharpoons}} 1^{\mathrm{H}}_{\mathrm{H}} \\
3\mathrm{F}^{(\mathrm{d})}: &\quad 1^{\mathrm{D}}_{\mathrm{D}} + \mathrm{Fmoc{-}Cl} \underset{k^{\mathrm{d}}_{-\mathrm{F}}}{\overset{k^{\mathrm{d}}_{+\mathrm{F}}}{\rightleftharpoons}} 2_{\mathrm{D}} + \mathrm{HCl} \qquad
6\mathrm{F}^{(\mathrm{d})}: &\quad 1^{\mathrm{H}}_{\mathrm{H}} + \mathrm{Fmoc{-}Cl} \underset{k^{\mathrm{d}}_{-\mathrm{F}}}{\overset{k^{\mathrm{d}}_{+\mathrm{F}}}{\rightleftharpoons}} 2_{\mathrm{H}} + \mathrm{HCl} \\
3\mathrm{W}^{(\mathrm{d})}: &\quad 1^{\mathrm{D}}_{\mathrm{D}} + \mathrm{DBF} + \mathrm{CO_2} \underset{k^{\mathrm{d}}_{-\mathrm{W}}}{\overset{k^{\mathrm{d}}_{+\mathrm{W}}}{\rightleftharpoons}} 2_{\mathrm{D}} \qquad
6\mathrm{W}^{(\mathrm{d})}: &\quad 1^{\mathrm{H}}_{\mathrm{H}} + \mathrm{DBF} + \mathrm{CO_2} \underset{k^{\mathrm{d}}_{-\mathrm{W}}}{\overset{k^{\mathrm{d}}_{+\mathrm{W}}}{\rightleftharpoons}} 2_{\mathrm{H}}
\end{aligned}
$$

Here and in the rest of the SI, the abbreviation DBF stands for dibenzofulvene. The symbols Δ and Δ' label thermal shuttlings (*i.e.*, mechanical processes) which change the mechanical state of the system, while all the other reactions constitute the chemical processes changing the chemical state of the system. Note that the latter are not elementary reactions, as detailed in the next section. The system is said to be open because during the experiment fuel (F = {Fmoc−Cl}) and waste (W = {HCl, DBF, CO_2}) species undergo other (not included in $\boldsymbol{\rho}$) processes: Fmoc−Cl is constantly added to the solution to compensate for its depletion, CO_2 exits the system as a gas, and HCl is readily buffered by the presence of $KHCO_3$ in the solution. With the exception of DBF, whose accumulation does not affect the rest of the system as it is unreactive under the experimental conditions, the concentrations of fuel and waste species are kept approximately constant by external processes. This is modeled with the concept of *chemostats*: large chemical reservoirs in contact with the system which fix the chemical potentials (and thus the concentrations in the ideal dilute solution setting) of F and W species in the system. These species are therefore said to be chemostatted.

In the experimental case, the following symmetries between rate constants hold:

$$k_{+\Delta} = k_{-\Delta} = k'_{+\Delta} = k'_{-\Delta} \coloneqq k_{\Delta}\,, \tag{1a}$$

$$k^{\mathrm{p}}_{+\mathrm{W}} = k^{\mathrm{d}}_{+\mathrm{W}} \coloneqq k_{+\mathrm{W}} \quad \text{and} \quad k^{\mathrm{p}}_{-\mathrm{W}} = k^{\mathrm{d}}_{-\mathrm{W}} \coloneqq k_{-\mathrm{W}}\,. \tag{1b}$$

A. Coarse-graining

Consider the fueling reaction pathway, catalyzed by a pyridine-based nucleophilic catalyst (denoted Cat):

$$\mathrm{Fmoc{-}Cl} + \mathrm{Cat} \underset{k_{-1\mathrm{F}}}{\overset{k_{+1\mathrm{F}}}{\rightleftharpoons}} \mathrm{Fmoc{-}Cat \cdot Cl} \tag{2a}$$

$$\mathrm{Fmoc{-}Cat \cdot Cl} + \underbrace{\mathrm{HO{-}R}}_{e.g.:\, 1^{\mathrm{D}}_{\mathrm{D}}} \underset{k_{-2\mathrm{F}}}{\overset{k_{+2\mathrm{F}}}{\rightleftharpoons}} \mathrm{Fmoc{-}Cat{-}O{-}R} + \mathrm{HCl} \tag{2b}$$

$$\mathrm{Fmoc{-}Cat{-}O{-}R} \underset{k_{-3\mathrm{F}}}{\overset{k_{+3\mathrm{F}}}{\rightleftharpoons}} \underbrace{\mathrm{Fmoc{-}O{-}R}}_{e.g.:\, 2_{\mathrm{D}}} + \mathrm{Cat} \tag{2c}$$

which has the net effect of adding one Fmoc group to the motor. In principle, we could explicitly include the above steps in our analysis and this wouldn't change the main outcomes of the work, thus uselessly complicating the mathematical treatment. For the sake of simplifying our model without losing its relevant thermodynamic features, we then consider a coarse-grained version of the fueling process based on the assumption that $k_{+2\mathrm{F}}$ and $k_{+3\mathrm{F}}$ are much larger than $k_{-2\mathrm{F}}$ and $k_{-3\mathrm{F}}$. In addition, given that in the original experiment Fmoc−Cl is continuously added to the system, the catalyst Cat, whose total amount is denoted by L_{Cat} can be assumed to be saturated by the Fmoc−Cl ($[\mathrm{Fmoc{-}Cat \cdot Cl}] \approx L_{\mathrm{Cat}}$). This is an additional level of control on the fueling process, since the availability of Fmoc−Cl to react with the motor

species is regulated by the amount of catalyst in the system. As a consequence of these assumptions, scheme (2) can be coarse-grained via a standard steady-state approximation of the intermediates to get[2]:

$$\mathrm{HO{-}R + Fmoc{-}Cl} \underset{k_{-\mathrm{F}}}{\overset{k_{+\mathrm{F}}}{\rightleftharpoons}} \mathrm{Fmoc{-}O{-}R + HCl} \tag{3}$$

where we defined the rate constants

$$k_{+\mathrm{F}} = \Omega \cdot k_{+1\mathrm{F}} k_{+2\mathrm{F}} k_{+3\mathrm{F}} \quad , \qquad k_{-\mathrm{F}} = \Omega \cdot k_{-1\mathrm{F}} k_{-2\mathrm{F}} k_{-3\mathrm{F}} \, , \tag{4}$$

with the kinetic factor

$$\Omega = \frac{L_{\mathrm{Cat}}}{[\mathrm{Fmoc{-}Cl}] k_{+1\mathrm{F}} k_{+3\mathrm{F}} + [\mathrm{HCl}][\mathrm{Fmoc{-}Cl}] k_{+1\mathrm{F}} k_{-2\mathrm{F}} + [\mathrm{HCl}][\mathrm{Fmoc{-}O{-}R}] k_{-2\mathrm{F}} k_{-3\mathrm{F}}} \approx \frac{L_{\mathrm{Cat}}}{[\mathrm{Fmoc{-}Cl}] k_{+1\mathrm{F}} k_{+3\mathrm{F}}} \, . \tag{5}$$

The final approximation highlights that, in the experimental conditions, the fueling rate is strongly determined by $[\mathrm{Fmoc{-}Cat \cdot Cl}] \approx L_{\mathrm{Cat}}$, regardless the actual value of [Fmoc−Cl]. Indeed, we could also have considered the species Fmoc−Cat · Cl as the actual chemostatted fuel without altering the results of our analysis. However, the way we proceeded here is more general and equation (3) holds also for situations where the catalysts is not saturated[3].

Similar considerations apply to the waste-forming reaction pathway catalyzed by triethylamine ($\mathrm{NEt_3}$), which has the net effect of removing one Fmoc group from the track. Let us consider the following reaction pathway:

$$\underbrace{\mathrm{Fmoc{-}O{-}R}}_{e.g.:\, 2_{\mathrm{D}}} + \mathrm{NEt_3} \underset{k_{-1\mathrm{W}}}{\overset{k_{+1\mathrm{W}}}{\rightleftharpoons}} \mathrm{HNEt_3^+ \cdot Fmoc{-}O{-}R^-} \tag{6a}$$

$$\mathrm{HNEt_3^+ \cdot Fmoc{-}O{-}R^-} \underset{k_{-2\mathrm{W}}}{\overset{k_{+2\mathrm{W}}}{\rightleftharpoons}} \mathrm{HNEt_3^+ \cdot R{-}OCOO^-} + \mathrm{DBF} \tag{6b}$$

$$\mathrm{HNEt_3^+ \cdot R{-}OCOO^-} \underset{k_{-3\mathrm{W}}}{\overset{k_{+3\mathrm{W}}}{\rightleftharpoons}} \mathrm{HNEt_3^+ \cdot R{-}O^-} + \mathrm{CO_2} \tag{6c}$$

$$\mathrm{HNEt_3^+ \cdot R{-}O^-} \underset{k_{-4\mathrm{W}}}{\overset{k_{+4\mathrm{W}}}{\rightleftharpoons}} \underbrace{\mathrm{R{-}OH}}_{e.g.:\, 1_{\mathrm{D}}^{\mathrm{D}}} + \mathrm{NEt_3} \tag{6d}$$

By considering the forward processes to be faster than the backward ones, here the coarse-graining of the intermediates through a stationary state approximation leads to

$$\mathrm{Fmoc{-}O{-}R} \underset{k_{+\mathrm{W}}}{\overset{k_{-\mathrm{W}}}{\rightleftharpoons}} \mathrm{R{-}OH + DBF + CO_2} \tag{7}$$

where

$$k_{-\mathrm{W}} = \Psi \cdot k_{+1\mathrm{W}} k_{+2\mathrm{W}} k_{+3\mathrm{W}} k_{+4\mathrm{W}} \quad , \qquad k_{+\mathrm{W}} = \Psi \cdot k_{-1\mathrm{W}} k_{-2\mathrm{W}} k_{-3\mathrm{W}} k_{-4\mathrm{W}} \, , \tag{8}$$

with kinetic factor

$$\Psi = \frac{L_{\mathrm{NEt_3}}}{k_{+2\mathrm{W}} k_{+3\mathrm{W}} k_{+4\mathrm{W}} + k_{-1\mathrm{W}}(k_{+3\mathrm{W}} k_{+4\mathrm{W}} + [\mathrm{DBF}] k_{-2\mathrm{W}}([\mathrm{CO_2}] k_{-3\mathrm{W}} + k_{+4\mathrm{W}}))} \approx \frac{L_{\mathrm{NEt_3}}}{k_{+3\mathrm{W}} k_{+4\mathrm{W}}(k_{-1\mathrm{W}} + k_{+2\mathrm{W}})} \, . \tag{9}$$

The symbol $L_{\mathrm{NEt_3}}$ denotes the total amount of $\mathrm{NEt_3}$ added to the system to catalyze the waste-forming process. The final approximation is based on the assumption that $k_{-2\mathrm{W}}$ and $k_{-3\mathrm{W}}$ are small compared to the other rate constants.

Expressions (3) and (7) are commonly adopted in the literature to model this kind of fueling and waste-forming processes[4–6]. Here, we have shown under which (reasonable) assumptions they can be considered as the coarse-grained versions of elementary reaction pathways, whose fast dynamics can be safely neglected. We stress that the results in the following do not rely on the chosen elementary model and can be extended also to more complicated schemes. Crucially, it has been shown that the coarse-graining procedure described above is thermodynamically consistent, namely it exactly retains the stationary state entropy production of the system, which is the key observable in our analysis[3,7].

II. DYNAMICS

The evolution in time of the concentrations of the motor species $\boldsymbol{X} = \{2_H, 2_D, 1^H_H, 1^H_D, 1^D_H, 1^D_D\}$ is ruled by the following rate equations. Note that, from now on, we will abbreviate Fmoc−Cl as F, as it is the only fuel species.

$$\mathrm{d}_t \underbrace{\begin{pmatrix}[2_H]\\ [2_D]\\ [1^D_H]\\ [1^D_D]\\ [1^H_H]\\ [1^H_D]\end{pmatrix}}_{[\boldsymbol{X}]} = \underbrace{\begin{array}{c}\begin{matrix}1\mathrm{F}^{(\mathrm{p})} & 1\mathrm{W}^{(\mathrm{p})} & 2\Delta & 3\mathrm{F}^{(\mathrm{d})} & 3\mathrm{W}^{(\mathrm{d})} & 4\mathrm{F}^{(\mathrm{p})} & 4\mathrm{W}^{(\mathrm{p})} & 5\Delta' & 6\mathrm{F}^{(\mathrm{d})} & 6\mathrm{W}^{(\mathrm{d})}\end{matrix}\\ \begin{pmatrix}-1 & -1 & 0 & 0 & 0 & 0 & 0 & 0 & 1 & 1\\ 0 & 0 & 0 & 1 & 1 & -1 & -1 & 0 & 0 & 0\\ 1 & 1 & -1 & 0 & 0 & 0 & 0 & 0 & 0 & 0\\ 0 & 0 & 1 & -1 & -1 & 0 & 0 & 0 & 0 & 0\\ 0 & 0 & 0 & 0 & 0 & 0 & 0 & 1 & -1 & -1\\ 0 & 0 & 0 & 0 & 0 & 1 & 1 & -1 & 0 & 0\end{pmatrix}\end{array}}_{\mathbb{S}^{\mathrm{X}}} \cdot \underbrace{\begin{pmatrix}k^{\mathrm{p}}_{-\mathrm{F}}[2_H][\mathrm{HCl}] - k^{\mathrm{p}}_{+\mathrm{F}}[\mathrm{F}][1^D_H]\\ k^{\mathrm{p}}_{-\mathrm{W}}[2_H] - k^{\mathrm{p}}_{+\mathrm{W}}[\mathrm{CO_2}][\mathrm{DBF}][1^D_H]\\ k_{+\Delta}[1^D_H] - k_{-\Delta}[1^D_D]\\ k^{\mathrm{d}}_{+\mathrm{F}}[\mathrm{F}][1^D_D] - k^{\mathrm{d}}_{-\mathrm{F}}[\mathrm{HCl}][2_D]\\ k^{\mathrm{d}}_{+\mathrm{W}}[\mathrm{CO_2}][\mathrm{DBF}][1^D_D] - k^{\mathrm{d}}_{-\mathrm{W}}[2_D]\\ k^{\mathrm{p}}_{-\mathrm{F}}[\mathrm{HCl}][2_D] - k^{\mathrm{p}}_{+\mathrm{F}}[\mathrm{F}][1^H_D]\\ k^{\mathrm{p}}_{-\mathrm{W}}[2_D] - k^{\mathrm{p}}_{+\mathrm{W}}[\mathrm{CO_2}][\mathrm{DBF}][1^H_D]\\ k'_{+\Delta}[1^H_D] - k'_{-\Delta}[1^H_H]\\ k^{\mathrm{d}}_{+\mathrm{F}}[\mathrm{F}][1^H_H] - k^{\mathrm{d}}_{-\mathrm{F}}[\mathrm{HCl}][2_H]\\ k^{\mathrm{d}}_{+\mathrm{W}}[\mathrm{CO_2}][\mathrm{DBF}][1^H_H] - k^{\mathrm{d}}_{-\mathrm{W}}[2_H]\end{pmatrix}}_{\boldsymbol{J} = \boldsymbol{J}_+ - \boldsymbol{J}_-} . \tag{10}$$

The balance equations for concentrations of chemostatted species $\boldsymbol{Y} = \{\mathrm{F}, \mathrm{HCl}, \mathrm{DBF}, \mathrm{CO_2}\}$ read

$$\mathbf{0} = \mathrm{d}_t \underbrace{\begin{pmatrix}[\mathrm{F}]\\ [\mathrm{HCl}]\\ [\mathrm{DBF}]\\ [\mathrm{CO_2}]\end{pmatrix}}_{[\boldsymbol{Y}]} = \underbrace{\begin{array}{c}\begin{matrix}1\mathrm{F}^{(\mathrm{p})} & 1\mathrm{W}^{(\mathrm{p})} & 2\Delta & 3\mathrm{F}^{(\mathrm{d})} & 3\mathrm{W}^{(\mathrm{d})} & 4\mathrm{F}^{(\mathrm{p})} & 4\mathrm{W}^{(\mathrm{p})} & 5\Delta' & 6\mathrm{F}^{(\mathrm{d})} & 6\mathrm{W}^{(\mathrm{d})}\end{matrix}\\ \begin{pmatrix}1 & 0 & 0 & -1 & 0 & 1 & 0 & 0 & -1 & 0\\ -1 & 0 & 0 & 1 & 0 & -1 & 0 & 0 & 1 & 0\\ 0 & 1 & 0 & 0 & -1 & 0 & 1 & 0 & 0 & -1\\ 0 & 1 & 0 & 0 & -1 & 0 & 1 & 0 & 0 & -1\end{pmatrix}\end{array}}_{\mathbb{S}^{\mathrm{Y}}} \cdot \underbrace{\begin{pmatrix}k^{\mathrm{p}}_{-\mathrm{F}}[\mathrm{HCl}][2_H] - k^{\mathrm{p}}_{+\mathrm{F}}[\mathrm{F}][1^D_H]\\ k^{\mathrm{p}}_{-\mathrm{W}}[2_H] - k^{\mathrm{p}}_{+\mathrm{W}}[\mathrm{CO_2}][\mathrm{DBF}][1^D_H]\\ k_{+\Delta}[1^D_H] - k_{-\Delta}[1^D_D]\\ k^{\mathrm{d}}_{+\mathrm{F}}[\mathrm{F}][1^D_D] - k^{\mathrm{d}}_{-\mathrm{F}}[\mathrm{HCl}][2_D]\\ k^{\mathrm{d}}_{+\mathrm{W}}[\mathrm{CO_2}][\mathrm{DBF}][1^D_D] - k^{\mathrm{d}}_{-\mathrm{W}}[2_D]\\ k^{\mathrm{p}}_{-\mathrm{F}}[\mathrm{HCl}][2_D] - k^{\mathrm{p}}_{+\mathrm{F}}[\mathrm{F}][1^H_D]\\ k^{\mathrm{p}}_{-\mathrm{W}}[2_D] - k^{\mathrm{p}}_{+\mathrm{W}}[\mathrm{CO_2}][\mathrm{DBF}][1^H_D]\\ k'_{+\Delta}[1^H_D] - k'_{-\Delta}[1^H_H]\\ k^{\mathrm{d}}_{+\mathrm{F}}[\mathrm{F}][1^H_H] - k^{\mathrm{d}}_{-\mathrm{F}}[\mathrm{HCl}][2_H]\\ k^{\mathrm{d}}_{+\mathrm{W}}[\mathrm{CO_2}][\mathrm{DBF}][1^H_H] - k^{\mathrm{d}}_{-\mathrm{W}}[2_H]\end{pmatrix}}_{\boldsymbol{J} = \boldsymbol{J}_+ - \boldsymbol{J}_-} + \underbrace{\begin{pmatrix}I_{\mathrm{F}}\\ I_{\mathrm{HCl}}\\ I_{\mathrm{DBF}}\\ I_{\mathrm{CO_2}}\end{pmatrix}}_{\boldsymbol{I}}, \tag{11}$$

with $\boldsymbol{I}$ collecting currents of the chemostatting processes which keep the corresponding concentrations constant. For instance, from equation (11) we obtain the following expression for the fuelling current:

$$I_{\mathrm{F}} = J_{3\mathrm{F}^{(\mathrm{d})}} + J_{6\mathrm{F}^{(\mathrm{d})}} - J_{1\mathrm{F}^{(\mathrm{p})}} - J_{4\mathrm{F}^{(\mathrm{p})}} . \tag{12}$$

To conclude this part, we introduce an alternative representation of the dynamics which will prove useful in some of the following derivations. The reader who is not interested in detailed derivations may safely skip the following formula (as well as all the equations marked with an asterisk).

$$\mathrm{d}_t \underbrace{\begin{pmatrix}[2_H]\\ [2_D]\\ [1^D_H]\\ [1^D_D]\\ [1^H_H]\\ [1^H_D]\end{pmatrix}}_{[\boldsymbol{X}]} = \underbrace{\begin{array}{c}\begin{matrix}2_H & 2_D & 1^D_H & 1^D_D & 1^H_H & 1^H_D\end{matrix}\\ \begin{pmatrix}-(\tilde{k}^{\mathrm{p}}_{-} + \tilde{k}^{\mathrm{d}}_{-}) & 0 & \tilde{k}^{\mathrm{p}}_{+} & 0 & \tilde{k}^{\mathrm{d}}_{+} & 0\\ 0 & -(\tilde{k}^{\mathrm{d}}_{-} + \tilde{k}^{\mathrm{p}}_{-}) & 0 & \tilde{k}^{\mathrm{d}}_{+} & 0 & \tilde{k}^{\mathrm{p}}_{+}\\ \tilde{k}^{\mathrm{p}}_{-} & 0 & -(\tilde{k}^{\mathrm{p}}_{+} + \tilde{k}_{+\Delta}) & \tilde{k}_{-\Delta} & 0 & 0\\ 0 & \tilde{k}^{\mathrm{d}}_{-} & \tilde{k}_{+\Delta} & -(\tilde{k}^{\mathrm{d}}_{+} + \tilde{k}_{-\Delta}) & 0 & 0\\ \tilde{k}^{\mathrm{d}}_{-} & 0 & 0 & 0 & -(\tilde{k}^{\mathrm{d}}_{+} + \tilde{k}'_{-\Delta}) & \tilde{k}'_{+\Delta}\\ 0 & \tilde{k}^{\mathrm{p}}_{-} & 0 & 0 & \tilde{k}'_{-\Delta} & -(\tilde{k}^{\mathrm{p}}_{+} + \tilde{k}'_{+\Delta})\end{pmatrix}\end{array}}_{\mathbb{W}} \cdot \underbrace{\begin{pmatrix}[2_H]\\ [2_D]\\ [1^D_H]\\ [1^D_D]\\ [1^H_H]\\ [1^H_D]\end{pmatrix}}_{[\boldsymbol{X}]} . \tag{13*}$$

The above equations are equivalent to equations (10), and we will make use of the $\mathbb{W}$ matrix in the following. Note that we defined new pseudo first-order rate constants marked with a tilde: the ones referring to mechanical transitions are identical to the ones introduced before (*e.g.*, $\tilde{k}_{+\Delta} = k_{+\Delta}$), while for chemical transitions fuelling and waste-forming rate constants are lumped together (*e.g.*, $\tilde{k}^{\mathrm{d}}_{+} = k^{\mathrm{d}}_{+\mathrm{F}}[\mathrm{F}] + k^{\mathrm{d}}_{+\mathrm{W}}[\mathrm{DBF}][\mathrm{CO_2}]$ and $\tilde{k}^{\mathrm{p}}_{-} = k^{\mathrm{p}}_{-\mathrm{F}}[\mathrm{HCl}] + k^{\mathrm{p}}_{-\mathrm{W}}$). Despite symbols redundancy, the use of the latter rate constants will be convenient in § V B 2.

A. Topological properties

The stoichiometric matrix $\mathbb{S} \equiv (\mathbb{S}^{\mathrm{X}}, \mathbb{S}^{\mathrm{Y}})^{\mathsf{T}}$ in Equations (10) and (11) encodes the topological properties of the chemical reaction network (CRN). The first class of them can be accessed by determining the cokernel of $\mathbb{S}$, which is spanned by the following vectors

$$\boldsymbol{\ell}_{\mathrm{M}} = \begin{array}{c} \begin{matrix} {}^{2_{\mathrm{H}}} & {}^{2_{\mathrm{D}}} & {}^{1^{\mathrm{D}}_{\mathrm{H}}} & {}^{1^{\mathrm{D}}_{\mathrm{D}}} & {}^{1^{\mathrm{H}}_{\mathrm{H}}} & {}^{1^{\mathrm{H}}_{\mathrm{D}}} & \mathrm{F} & \mathrm{HCl} & \mathrm{DBF} & \mathrm{CO_2} \end{matrix} \\ \begin{pmatrix} 1 & 1 & 1 & 1 & 1 & 1 & 0 & 0 & 0 & 0 \end{pmatrix} \end{array}, \tag{14}$$

$$\boldsymbol{\ell}_{\mathrm{CO_2}} = \begin{array}{c} \begin{matrix} {}^{2_{\mathrm{H}}} & {}^{2_{\mathrm{D}}} & {}^{1^{\mathrm{D}}_{\mathrm{H}}} & {}^{1^{\mathrm{D}}_{\mathrm{D}}} & {}^{1^{\mathrm{H}}_{\mathrm{H}}} & {}^{1^{\mathrm{H}}_{\mathrm{D}}} & \mathrm{F} & \mathrm{HCl} & \mathrm{DBF} & \mathrm{CO_2} \end{matrix} \\ \begin{pmatrix} 1 & 1 & 0 & 0 & 0 & 0 & 1 & 0 & 0 & 1 \end{pmatrix} \end{array}, \tag{15}$$

$$\boldsymbol{\ell}_{\mathrm{DBF}} = \begin{array}{c} \begin{matrix} {}^{2_{\mathrm{H}}} & {}^{2_{\mathrm{D}}} & {}^{1^{\mathrm{D}}_{\mathrm{H}}} & {}^{1^{\mathrm{D}}_{\mathrm{D}}} & {}^{1^{\mathrm{H}}_{\mathrm{H}}} & {}^{1^{\mathrm{H}}_{\mathrm{D}}} & \mathrm{F} & \mathrm{HCl} & \mathrm{DBF} & \mathrm{CO_2} \end{matrix} \\ \begin{pmatrix} 1 & 1 & 0 & 0 & 0 & 0 & 1 & 0 & 1 & 0 \end{pmatrix} \end{array}, \tag{16}$$

$$\boldsymbol{\ell}_{\mathrm{Cl}} = \begin{array}{c} \begin{matrix} {}^{2_{\mathrm{H}}} & {}^{2_{\mathrm{D}}} & {}^{1^{\mathrm{D}}_{\mathrm{H}}} & {}^{1^{\mathrm{D}}_{\mathrm{D}}} & {}^{1^{\mathrm{H}}_{\mathrm{H}}} & {}^{1^{\mathrm{H}}_{\mathrm{D}}} & \mathrm{F} & \mathrm{HCl} & \mathrm{DBF} & \mathrm{CO_2} \end{matrix} \\ \begin{pmatrix} 0 & 0 & 0 & 0 & 0 & 0 & 1 & 1 & 0 & 0 \end{pmatrix} \end{array}. \tag{17}$$

The first of these vectors identifies a conserved quantity

$$\begin{aligned} L_{\mathrm{M}} &= \boldsymbol{\ell}_{\mathrm{M}} \cdot \begin{pmatrix} [\boldsymbol{X}] \\ [\boldsymbol{Y}] \end{pmatrix} = [2_{\mathrm{H}}] + [2_{\mathrm{D}}] + [1^{\mathrm{D}}_{\mathrm{H}}] + [1^{\mathrm{D}}_{\mathrm{D}}] + [1^{\mathrm{H}}_{\mathrm{H}}] + [1^{\mathrm{H}}_{\mathrm{D}}] \\ \mathrm{d}_t L_{\mathrm{M}} &= 0\,, \end{aligned} \tag{18}$$

which is proved through the rate equations (10) and (11). It expresses the fact that the total concentration of the motor species is determined by the initial conditions and cannot be altered by the dynamics. The other three vectors identify what we call *broken* conserved quantities

$$L_{\mathrm{CO_2}} = \boldsymbol{\ell}_{\mathrm{CO_2}} \cdot \begin{pmatrix} [\boldsymbol{X}] \\ [\boldsymbol{Y}] \end{pmatrix} = [2_{\mathrm{H}}] + [2_{\mathrm{D}}] + [\mathrm{F}] + [\mathrm{CO_2}]\,, \tag{19}$$

$$L_{\mathrm{DBF}} = \boldsymbol{\ell}_{\mathrm{DBF}} \cdot \begin{pmatrix} [\boldsymbol{X}] \\ [\boldsymbol{Y}] \end{pmatrix} = [2_{\mathrm{H}}] + [2_{\mathrm{D}}] + [\mathrm{F}] + [\mathrm{DBF}]\,, \tag{20}$$

$$L_{\mathrm{Cl}} = \boldsymbol{\ell}_{\mathrm{Cl}} \cdot \begin{pmatrix} [\boldsymbol{X}] \\ [\boldsymbol{Y}] \end{pmatrix} = [\mathrm{F}] + [\mathrm{HCl}]\,. \tag{21}$$

They express the total concentrations of moieties (specific groups of atoms) whose number in the system is not determined by the initial conditions, as they are exchanged with the exterior through the chemostatting. Indeed, by using again the rate equations, it can be shown that

$$\mathrm{d}_t L_{\mathrm{CO_2}} = I_{\mathrm{F}} + I_{\mathrm{CO_2}}\,, \tag{22}$$

$$\mathrm{d}_t L_{\mathrm{DBF}} = I_{\mathrm{F}} + I_{\mathrm{DBF}}\,, \tag{23}$$

$$\mathrm{d}_t L_{\mathrm{Cl}} = I_{\mathrm{F}} + I_{\mathrm{HCl}}\,. \tag{24}$$

Namely, quantities $L_{\mathrm{CO_2}}$, L_{DBF} and L_{Cl} change only due to the exchange of fuel and waste species with the chemostats. If the CRN was closed, they would be conserved by the dynamics like L_{M}.

The other useful piece of information contained in the stoichiometric matrix $\mathbb{S}$ is given by cycles. A cycle is a vector in the kernel of $\mathbb{S}^{\mathrm{X}}$, which corresponds to a series of reactions which upon completion leaves the concentrations of each motor species unchanged. They play an important role at the steady state, where reaction currents can only flow across

cycles.

$$\boldsymbol{c}_{\mathrm{F}}^{\mathrm{T}} = \begin{pmatrix} {\scriptstyle 1\mathrm{F}^{(\mathrm{p})}} & {\scriptstyle 1\mathrm{W}^{(\mathrm{p})}} & {\scriptstyle 2\Delta} & {\scriptstyle 3\mathrm{F}^{(\mathrm{d})}} & {\scriptstyle 3\mathrm{W}^{(\mathrm{d})}} & {\scriptstyle 4\mathrm{F}^{(\mathrm{p})}} & {\scriptstyle 4\mathrm{W}^{(\mathrm{p})}} & {\scriptstyle 5\Delta'} & {\scriptstyle 6\mathrm{F}^{(\mathrm{d})}} & {\scriptstyle 6\mathrm{W}^{(\mathrm{d})}} \\ 1 & 0 & 1 & 1 & 0 & 1 & 0 & 1 & 1 & 0 \end{pmatrix}, \tag{25a}$$

$$\boldsymbol{c}_{\mathrm{W}}^{\mathrm{T}} = \begin{pmatrix} {\scriptstyle 1\mathrm{F}^{(\mathrm{p})}} & {\scriptstyle 1\mathrm{W}^{(\mathrm{p})}} & {\scriptstyle 2\Delta} & {\scriptstyle 3\mathrm{F}^{(\mathrm{d})}} & {\scriptstyle 3\mathrm{W}^{(\mathrm{d})}} & {\scriptstyle 4\mathrm{F}^{(\mathrm{p})}} & {\scriptstyle 4\mathrm{W}^{(\mathrm{p})}} & {\scriptstyle 5\Delta'} & {\scriptstyle 6\mathrm{F}^{(\mathrm{d})}} & {\scriptstyle 6\mathrm{W}^{(\mathrm{d})}} \\ 0 & 1 & 1 & 0 & 1 & 0 & 1 & 1 & 0 & 1 \end{pmatrix}, \tag{25b}$$

$$\boldsymbol{c}_{\mathrm{a}}^{\mathrm{T}} = \begin{pmatrix} {\scriptstyle 1\mathrm{F}^{(\mathrm{p})}} & {\scriptstyle 1\mathrm{W}^{(\mathrm{p})}} & {\scriptstyle 2\Delta} & {\scriptstyle 3\mathrm{F}^{(\mathrm{d})}} & {\scriptstyle 3\mathrm{W}^{(\mathrm{d})}} & {\scriptstyle 4\mathrm{F}^{(\mathrm{p})}} & {\scriptstyle 4\mathrm{W}^{(\mathrm{p})}} & {\scriptstyle 5\Delta'} & {\scriptstyle 6\mathrm{F}^{(\mathrm{d})}} & {\scriptstyle 6\mathrm{W}^{(\mathrm{d})}} \\ 1 & -1 & 0 & 0 & 0 & -1 & 1 & 0 & 0 & 0 \end{pmatrix}, \tag{25c}$$

$$\boldsymbol{c}_{\mathrm{b}}^{\mathrm{T}} = \begin{pmatrix} {\scriptstyle 1\mathrm{F}^{(\mathrm{p})}} & {\scriptstyle 1\mathrm{W}^{(\mathrm{p})}} & {\scriptstyle 2\Delta} & {\scriptstyle 3\mathrm{F}^{(\mathrm{d})}} & {\scriptstyle 3\mathrm{W}^{(\mathrm{d})}} & {\scriptstyle 4\mathrm{F}^{(\mathrm{p})}} & {\scriptstyle 4\mathrm{W}^{(\mathrm{p})}} & {\scriptstyle 5\Delta'} & {\scriptstyle 6\mathrm{F}^{(\mathrm{d})}} & {\scriptstyle 6\mathrm{W}^{(\mathrm{d})}} \\ -1 & 1 & 0 & -1 & 1 & 0 & 0 & 0 & 0 & 0 \end{pmatrix}, \tag{25d}$$

$$\boldsymbol{c}_{\epsilon}^{\mathrm{T}} = \begin{pmatrix} {\scriptstyle 1\mathrm{F}^{(\mathrm{p})}} & {\scriptstyle 1\mathrm{W}^{(\mathrm{p})}} & {\scriptstyle 2\Delta} & {\scriptstyle 3\mathrm{F}^{(\mathrm{d})}} & {\scriptstyle 3\mathrm{W}^{(\mathrm{d})}} & {\scriptstyle 4\mathrm{F}^{(\mathrm{p})}} & {\scriptstyle 4\mathrm{W}^{(\mathrm{p})}} & {\scriptstyle 5\Delta'} & {\scriptstyle 6\mathrm{F}^{(\mathrm{d})}} & {\scriptstyle 6\mathrm{W}^{(\mathrm{d})}} \\ 0 & 1 & 1 & 1 & 0 & 0 & 1 & 1 & 1 & 0 \end{pmatrix}. \tag{25e}$$

In the above vectors, each entry represents the number of times the corresponding reaction has to be performed in order to complete the corresponding cycle. Minus signs indicate that the corresponding reaction is performed backwards in the cycle, considering the clockwise cycling in Figure 2 of the main text as the forward direction (the same convention is adopted for the reactions at the beginning of Sec. I, where left-to-right is considered as forward direction). Cycles $\boldsymbol{c}_{\mathrm{F}}$, $\boldsymbol{c}_{\mathrm{W}}$, $\boldsymbol{c}_{\mathrm{a}}$ and $\boldsymbol{c}_{\mathrm{b}}$ would be present also if the system was closed (fuel and waste species not chemostatted and free to vary) and we call them *internal* cycles (mathematically, they are also right-null vectors of the whole $\mathbb{S}$ matrix[8]). They set thermodynamic constraints on the rate constants that will be introduced later (Wegscheider's conditions, equations (36)). The cycle $\boldsymbol{c}_{\epsilon}$ involves a net exchange of chemicals with chemostats, and we call it *emergent* cycle because it arises only when the system is open. Note that the set of vectors (25) is a complete basis for the cycles in the system, but it is not unique. Another useful basis that we will exploit in § III A is the following, obtained from linear combinations of vectors (25):

$$\boldsymbol{c}_{\epsilon}^{\mathrm{T}} = \begin{pmatrix} {\scriptstyle 1\mathrm{F}^{(\mathrm{p})}} & {\scriptstyle 1\mathrm{W}^{(\mathrm{p})}} & {\scriptstyle 2\Delta} & {\scriptstyle 3\mathrm{F}^{(\mathrm{d})}} & {\scriptstyle 3\mathrm{W}^{(\mathrm{d})}} & {\scriptstyle 4\mathrm{F}^{(\mathrm{p})}} & {\scriptstyle 4\mathrm{W}^{(\mathrm{p})}} & {\scriptstyle 5\Delta'} & {\scriptstyle 6\mathrm{F}^{(\mathrm{d})}} & {\scriptstyle 6\mathrm{W}^{(\mathrm{d})}} \\ 0 & 1 & 1 & 1 & 0 & 0 & 1 & 1 & 1 & 0 \end{pmatrix}, \tag{26a}$$

$$\boldsymbol{c}_{1\mathrm{p}}^{\mathrm{T}} = \frac{1}{2}(\boldsymbol{c}_{\epsilon}^{\mathrm{T}} - \boldsymbol{c}_{\mathrm{F}}^{\mathrm{T}} - \boldsymbol{c}_{\mathrm{a}}^{\mathrm{T}}) = \begin{pmatrix} {\scriptstyle 1\mathrm{F}^{(\mathrm{p})}} & {\scriptstyle 1\mathrm{W}^{(\mathrm{p})}} & {\scriptstyle 2\Delta} & {\scriptstyle 3\mathrm{F}^{(\mathrm{d})}} & {\scriptstyle 3\mathrm{W}^{(\mathrm{d})}} & {\scriptstyle 4\mathrm{F}^{(\mathrm{p})}} & {\scriptstyle 4\mathrm{W}^{(\mathrm{p})}} & {\scriptstyle 5\Delta'} & {\scriptstyle 6\mathrm{F}^{(\mathrm{d})}} & {\scriptstyle 6\mathrm{W}^{(\mathrm{d})}} \\ -1 & 1 & 0 & 0 & 0 & 0 & 0 & 0 & 0 & 0 \end{pmatrix}, \tag{26b}$$

$$\boldsymbol{c}_{3\mathrm{d}}^{\mathrm{T}} = \boldsymbol{c}_{1\mathrm{p}}^{\mathrm{T}} - \boldsymbol{c}_{\mathrm{b}}^{\mathrm{T}} = \begin{pmatrix} {\scriptstyle 1\mathrm{F}^{(\mathrm{p})}} & {\scriptstyle 1\mathrm{W}^{(\mathrm{p})}} & {\scriptstyle 2\Delta} & {\scriptstyle 3\mathrm{F}^{(\mathrm{d})}} & {\scriptstyle 3\mathrm{W}^{(\mathrm{d})}} & {\scriptstyle 4\mathrm{F}^{(\mathrm{p})}} & {\scriptstyle 4\mathrm{W}^{(\mathrm{p})}} & {\scriptstyle 5\Delta'} & {\scriptstyle 6\mathrm{F}^{(\mathrm{d})}} & {\scriptstyle 6\mathrm{W}^{(\mathrm{d})}} \\ 0 & 0 & 0 & 1 & -1 & 0 & 0 & 0 & 0 & 0 \end{pmatrix}, \tag{26c}$$

$$\boldsymbol{c}_{4\mathrm{p}}^{\mathrm{T}} = \boldsymbol{c}_{\mathrm{a}}^{\mathrm{T}} + \boldsymbol{c}_{1\mathrm{p}}^{\mathrm{T}} = \begin{pmatrix} {\scriptstyle 1\mathrm{F}^{(\mathrm{p})}} & {\scriptstyle 1\mathrm{W}^{(\mathrm{p})}} & {\scriptstyle 2\Delta} & {\scriptstyle 3\mathrm{F}^{(\mathrm{d})}} & {\scriptstyle 3\mathrm{W}^{(\mathrm{d})}} & {\scriptstyle 4\mathrm{F}^{(\mathrm{p})}} & {\scriptstyle 4\mathrm{W}^{(\mathrm{p})}} & {\scriptstyle 5\Delta'} & {\scriptstyle 6\mathrm{F}^{(\mathrm{d})}} & {\scriptstyle 6\mathrm{W}^{(\mathrm{d})}} \\ 0 & 0 & 0 & 0 & 0 & -1 & 1 & 0 & 0 & 0 \end{pmatrix}, \tag{26d}$$

$$\boldsymbol{c}_{6\mathrm{d}}^{\mathrm{T}} = \boldsymbol{c}_{\epsilon}^{\mathrm{T}} - \boldsymbol{c}_{\mathrm{W}}^{\mathrm{T}} - \boldsymbol{c}_{3\mathrm{d}}^{\mathrm{T}} = \begin{pmatrix} {\scriptstyle 1\mathrm{F}^{(\mathrm{p})}} & {\scriptstyle 1\mathrm{W}^{(\mathrm{p})}} & {\scriptstyle 2\Delta} & {\scriptstyle 3\mathrm{F}^{(\mathrm{d})}} & {\scriptstyle 3\mathrm{W}^{(\mathrm{d})}} & {\scriptstyle 4\mathrm{F}^{(\mathrm{p})}} & {\scriptstyle 4\mathrm{W}^{(\mathrm{p})}} & {\scriptstyle 5\Delta'} & {\scriptstyle 6\mathrm{F}^{(\mathrm{d})}} & {\scriptstyle 6\mathrm{W}^{(\mathrm{d})}} \\ 0 & 0 & 0 & 0 & 0 & 0 & 0 & 0 & 1 & -1 \end{pmatrix}. \tag{26e}$$

For instance, the vector $\boldsymbol{c}_{1\mathrm{p}}$ describes the sequence of reactions $2_{\mathrm{H}} \xrightarrow{1\mathrm{W}^{(\mathrm{p})}} 1_{\mathrm{H}}^{\mathrm{D}} \xrightarrow{1\mathrm{F}^{(\mathrm{p})}} 2_{\mathrm{H}}$. Cycles $\boldsymbol{c}_{1\mathrm{p}}$, $\boldsymbol{c}_{3\mathrm{d}}$, $\boldsymbol{c}_{4\mathrm{p}}$, and $\boldsymbol{c}_{6\mathrm{d}}$ are called *futile* cycles, since they consume fuel molecules without contributing to a forward step of the motor.

B. Stationary state

Given a set of values for the kinetic parameters and the total concentration of motor species L_{M} (defined in equation (18)), for any choice of the chemostatted concentrations in $\boldsymbol{Y}$ the system will reach a stationary state distribution (mathematically, this is because the network is complex balanced and confined[9]) such that $\mathrm{d}_t[\boldsymbol{X}]_{\mathrm{ss}} = 0$ in equation (10). It can be analytically computed using graph-theoretical techniques[10–12] (see also Appendix A of reference 3 for a short introduction):

$$[X_\alpha]_{\mathrm{ss}} = \frac{L_{\mathrm{M}}}{\mathcal{N}} \sum_{t \in \mathcal{T}_\alpha} \prod_{\lambda \in t} \tilde{k}_\lambda \,. \tag{27*}$$

In the above expression, $\mathcal{N} = \sum_\alpha \sum_{t \in \mathcal{T}_\alpha} \prod_{\lambda \in t} \tilde{k}_\lambda$ is a normalizing denominator and $\mathcal{T}_\alpha$ is the set of spanning trees rooted in vertex α of the chemical reaction network representing the motor. The index λ runs over all forward and backward reactions such that $\tilde{k}_\lambda$ are the pseudo-first-order rate constants as defined in equation (13*). A rooted spanning tree is a spanning tree with its edges oriented such that all edges point towards the root.

For the experimental case where equations (1) hold, the above equations boil down to:

$$\begin{pmatrix}[2_{\mathrm{H}}]_{\mathrm{ss}}\\ [2_{\mathrm{D}}]_{\mathrm{ss}}\\ [1^{\mathrm{D}}_{\mathrm{H}}]_{\mathrm{ss}}\\ [1^{\mathrm{D}}_{\mathrm{D}}]_{\mathrm{ss}}\\ [1^{\mathrm{H}}_{\mathrm{H}}]_{\mathrm{ss}}\\ [1^{\mathrm{H}}_{\mathrm{D}}]_{\mathrm{ss}}\end{pmatrix} = \frac{L_{\mathrm{M}}}{\mathcal{N}}\begin{pmatrix}(k^{\mathrm{p}}_{+\mathrm{F}}[\mathrm{F}]+k_{+\mathrm{W}}[\mathrm{CO_2}][\mathrm{DBF}])(k^{\mathrm{d}}_{+\mathrm{F}}[\mathrm{F}]+k_{+\mathrm{W}}[\mathrm{CO_2}][\mathrm{DBF}])+(k^{\mathrm{p}}_{+\mathrm{F}}[\mathrm{F}]+k^{\mathrm{d}}_{+\mathrm{F}}[\mathrm{F}]+2k_{+\mathrm{W}}[\mathrm{CO_2}][\mathrm{DBF}])k_{\Delta}\\ (k^{\mathrm{p}}_{+\mathrm{F}}[\mathrm{F}]+k_{+\mathrm{W}}[\mathrm{CO_2}][\mathrm{DBF}])(k^{\mathrm{d}}_{+\mathrm{F}}[\mathrm{F}]+k_{+\mathrm{W}}[\mathrm{CO_2}][\mathrm{DBF}])+(k^{\mathrm{p}}_{+\mathrm{F}}[\mathrm{F}]+k^{\mathrm{d}}_{+\mathrm{F}}[\mathrm{F}]+2k_{+\mathrm{W}}[\mathrm{CO_2}][\mathrm{DBF}])k_{\Delta}\\ (k^{\mathrm{p}}_{-\mathrm{F}}[\mathrm{HCl}]+k_{-\mathrm{W}})(k^{\mathrm{d}}_{+\mathrm{F}}[\mathrm{F}]+k_{+\mathrm{W}}[\mathrm{CO_2}][\mathrm{DBF}])+(k^{\mathrm{p}}_{-\mathrm{F}}[\mathrm{HCl}]+k^{\mathrm{d}}_{-\mathrm{F}}[\mathrm{HCl}]+2k_{-\mathrm{W}})k_{\Delta}\\ (k^{\mathrm{d}}_{-\mathrm{F}}[\mathrm{HCl}]+k_{-\mathrm{W}})(k^{\mathrm{p}}_{+\mathrm{F}}[\mathrm{F}]+k_{+\mathrm{W}}[\mathrm{CO_2}][\mathrm{DBF}])+(k^{\mathrm{p}}_{-\mathrm{F}}[\mathrm{HCl}]+k^{\mathrm{d}}_{-\mathrm{F}}[\mathrm{HCl}]+2k_{-\mathrm{W}})k_{\Delta}\\ (k^{\mathrm{d}}_{-\mathrm{F}}[\mathrm{HCl}]+k_{-\mathrm{W}})(k^{\mathrm{p}}_{+\mathrm{F}}[\mathrm{F}]+k_{+\mathrm{W}}[\mathrm{CO_2}][\mathrm{DBF}])+(k^{\mathrm{p}}_{-\mathrm{F}}[\mathrm{HCl}]+k^{\mathrm{d}}_{-\mathrm{F}}[\mathrm{HCl}]+2k_{-\mathrm{W}})k_{\Delta}\\ (k^{\mathrm{p}}_{-\mathrm{F}}[\mathrm{HCl}]+k_{-\mathrm{W}})(k^{\mathrm{d}}_{+\mathrm{F}}[\mathrm{F}]+k_{+\mathrm{W}}[\mathrm{CO_2}][\mathrm{DBF}])+(k^{\mathrm{p}}_{-\mathrm{F}}[\mathrm{HCl}]+k^{\mathrm{d}}_{-\mathrm{F}}[\mathrm{HCl}]+2k_{-\mathrm{W}})k_{\Delta}\end{pmatrix}. \tag{28}$$

It is easy to see that if the steric hindrance caused by the macrocycle did not affect the rates of the fueling reaction (*i.e.*, $k^{\mathrm{p}}_{+\mathrm{F}} = k^{\mathrm{d}}_{+\mathrm{F}}$ and $k^{\mathrm{p}}_{-\mathrm{F}} = k^{\mathrm{d}}_{-\mathrm{F}}$), the stationary state would be symmetric ($[1^{\mathrm{H}}_{\mathrm{H}}]_{\mathrm{ss}} = [1^{\mathrm{H}}_{\mathrm{D}}]_{\mathrm{ss}} = [1^{\mathrm{D}}_{\mathrm{H}}]_{\mathrm{ss}} = [1^{\mathrm{D}}_{\mathrm{D}}]_{\mathrm{ss}}$).

From equation (10), it follows that the stationary state current vector $\boldsymbol{J}_{\mathrm{ss}}$ must be a right null vector of the matrix $\mathbb{S}^{\mathrm{X}}$. As anticipated in the previous section (§ II A), this implies that the stationary state currents can be decomposed on a basis of cycles:

$$\boldsymbol{J}_{\mathrm{ss}} = \sum_i \psi_i \boldsymbol{c}_i\,, \tag{29}$$

where the index i runs over the elements of a complete basis of cycles and terms ψ_i are the currents flowing across each cycle. Considering vectors (25) and (26) as basis sets:

$$\begin{pmatrix}J^{\mathrm{ss}}_{1\mathrm{F}^{(\mathrm{p})}}\\ J^{\mathrm{ss}}_{1\mathrm{W}^{(\mathrm{p})}}\\ J^{\mathrm{ss}}_{2\Delta}\\ J^{\mathrm{ss}}_{3\mathrm{F}^{(\mathrm{d})}}\\ J^{\mathrm{ss}}_{3\mathrm{W}^{(\mathrm{d})}}\\ J^{\mathrm{ss}}_{4\mathrm{F}^{(\mathrm{p})}}\\ J^{\mathrm{ss}}_{4\mathrm{W}^{(\mathrm{p})}}\\ J^{\mathrm{ss}}_{5\Delta'}\\ J^{\mathrm{ss}}_{6\mathrm{F}^{(\mathrm{d})}}\\ J^{\mathrm{ss}}_{6\mathrm{W}^{(\mathrm{d})}}\end{pmatrix} = \begin{pmatrix}\psi_{\boldsymbol{c}_{\mathrm{F}}}+\psi_{\boldsymbol{c}_{\mathrm{a}}}-\psi_{\boldsymbol{c}_{\mathrm{b}}}\\ \psi_{\boldsymbol{c}_{\mathrm{W}}}-\psi_{\boldsymbol{c}_{\mathrm{a}}}+\psi_{\boldsymbol{c}_{\mathrm{b}}}+\psi_{\boldsymbol{c}_{\epsilon}}\\ \psi_{\boldsymbol{c}_{\mathrm{F}}}+\psi_{\boldsymbol{c}_{\mathrm{W}}}+\psi_{\boldsymbol{c}_{\epsilon}}\\ \psi_{\boldsymbol{c}_{\mathrm{F}}}-\psi_{\boldsymbol{c}_{\mathrm{b}}}+\psi_{\boldsymbol{c}_{\epsilon}}\\ \psi_{\boldsymbol{c}_{\mathrm{W}}}+\psi_{\boldsymbol{c}_{\mathrm{b}}}\\ \psi_{\boldsymbol{c}_{\mathrm{F}}}-\psi_{\boldsymbol{c}_{\mathrm{a}}}\\ \psi_{\boldsymbol{c}_{\mathrm{W}}}+\psi_{\boldsymbol{c}_{\mathrm{a}}}+\psi_{\boldsymbol{c}_{\epsilon}}\\ \psi_{\boldsymbol{c}_{\mathrm{F}}}+\psi_{\boldsymbol{c}_{\mathrm{W}}}+\psi_{\boldsymbol{c}_{\epsilon}}\\ \psi_{\boldsymbol{c}_{\mathrm{F}}}+\psi_{\boldsymbol{c}_{\epsilon}}\\ \psi_{\boldsymbol{c}_{\mathrm{W}}}\end{pmatrix} = \begin{pmatrix}-\psi_{\boldsymbol{c}_{1\mathrm{p}}}\\ \psi_{\boldsymbol{c}_{1\mathrm{p}}}+\psi'_{\boldsymbol{c}_{\epsilon}}\\ \psi'_{\boldsymbol{c}_{\epsilon}}\\ \psi_{\boldsymbol{c}_{3\mathrm{d}}}+\psi'_{\boldsymbol{c}_{\epsilon}}\\ -\psi_{\boldsymbol{c}_{3\mathrm{d}}}\\ -\psi_{\boldsymbol{c}_{4\mathrm{p}}}\\ \psi_{\boldsymbol{c}_{4\mathrm{p}}}+\psi'_{\boldsymbol{c}_{\epsilon}}\\ \psi'_{\boldsymbol{c}_{\epsilon}}\\ \psi_{\boldsymbol{c}_{6\mathrm{d}}}+\psi'_{\boldsymbol{c}_{\epsilon}}\\ -\psi_{\boldsymbol{c}_{6\mathrm{d}}}\end{pmatrix}. \tag{30}$$

Note that, depending on the chosen basis set, the same cycle may be associated with a different cycle current (*i.e.*, $\psi_{\boldsymbol{c}_\epsilon} \neq \psi'_{\boldsymbol{c}_\epsilon}$) in equation (30). We will come back to this point at the end of the next section (§ III A), when the set of fundamental cycles and corresponding currents will be identified. Here, we conclude by noticing that equation (30) implies the following relations between steady state currents:

$$J^{\mathrm{ss}} := J^{\mathrm{ss}}_{1\mathrm{F}^{(\mathrm{p})}} + J^{\mathrm{ss}}_{1\mathrm{W}^{(\mathrm{p})}} = J^{\mathrm{ss}}_{2\Delta} = J^{\mathrm{ss}}_{3\mathrm{F}^{(\mathrm{d})}} + J^{\mathrm{ss}}_{3\mathrm{W}^{(\mathrm{d})}} = J^{\mathrm{ss}}_{4\mathrm{F}^{(\mathrm{p})}} + J^{\mathrm{ss}}_{4\mathrm{W}^{(\mathrm{p})}} = J^{\mathrm{ss}}_{5\Delta'} = J^{\mathrm{ss}}_{6\mathrm{F}^{(\mathrm{d})}} + J^{\mathrm{ss}}_{6\mathrm{W}^{(\mathrm{d})}} = \psi_{\boldsymbol{c}_\epsilon} + \psi_{\boldsymbol{c}_{\mathrm{W}}} + \psi_{\boldsymbol{c}_{\mathrm{F}}} = \psi'_{\boldsymbol{c}_\epsilon}\,, \tag{31a}$$

$$I^{\mathrm{ss}}_{\mathrm{F}} = J^{\mathrm{ss}}_{3\mathrm{F}^{(\mathrm{d})}} + J^{\mathrm{ss}}_{6\mathrm{F}^{(\mathrm{d})}} - J^{\mathrm{ss}}_{1\mathrm{F}^{(\mathrm{p})}} - J^{\mathrm{ss}}_{4\mathrm{F}^{(\mathrm{p})}} = 2\psi_{\boldsymbol{c}_\epsilon} = 2\psi'_{\boldsymbol{c}_\epsilon} + \psi_{\boldsymbol{c}_{1\mathrm{p}}} + \psi_{\boldsymbol{c}_{3\mathrm{d}}} + \psi_{\boldsymbol{c}_{4\mathrm{p}}} + \psi_{\boldsymbol{c}_{6\mathrm{d}}}\,, \tag{31b}$$

where J^{ss} corresponds to the rate of net displacement of the macrocycle along the track in the stationary state. Note that J^{ss} and $I^{\mathrm{ss}}_{\mathrm{F}}$ are respectively expressed as J and I_{F} in the main text, where we unambiguously refer to the stationary state.

III. THERMODYNAMICS

Each species is thermodynamically characterized by chemical potentials of the form

$$\mu_X = \mu^{\circ}_X + RT\ln[X]\,, \quad \mu_Y = \mu^{\circ}_Y + RT\ln[Y]\,, \tag{32}$$

where μ°_X and μ°_Y are standard-state chemical potentials. As in the main text, we will denote the sum of the chemical potentials of waste species as $\mu_{\mathrm{W}} = \mu_{\mathrm{HCl}}+\mu_{\mathrm{DBF}}+\mu_{\mathrm{CO_2}}$. Note that in the experimental Fmoc rotary motor (see equations (1))

we have $\mu^\circ_{1^{\rm D}_{\rm H}} = \mu^\circ_{1^{\rm D}_{\rm D}} = \mu^\circ_{1^{\rm H}_{\rm D}} = \mu^\circ_{1^{\rm H}_{\rm H}} := \mu^\circ_1$, since the benzylic amide macrocycle only interacts with the two identical fumaramide sites. The equality $\mu^\circ_{2_{\rm H}} = \mu^\circ_{2_{\rm D}} = \mu^\circ_2$ also holds in the experimental case.

Dynamics and thermodynamics can be connected via the so-called "principle of local detailed balance"[8] which relates the ratio of forward and backward rate constants of a single elementary reaction to the difference of standard-state chemical potentials between its reagents and products, and thus to the free-energy exchanged with the reservoirs (thermal bath and chemostats) each time the reaction happens:

$$RT \ln \frac{k_{+\rho}}{k_{-\rho}} = -\sum_X \mu^\circ_X \mathbb{S}^X_\rho - \sum_Y \mu^\circ_Y \mathbb{S}^Y_\rho \,, \tag{33}$$

where indexes X and Y run over motor's and chemostatted species, respectively, while index ρ runs over all the 10 reactions introduced in Section I. For closed systems, this relation is essentially the law of mass action which has been known since the nineteen's century in chemistry. Its open systems formulation was later extensively used and was derived to ensure that microreversibility holds at equilibrium[11,13,14]. In the broader context of statistical mechanics, similar relations were explicitly formulated in reference 15 and to the best of our knowledge the terminology "local detailed balance" first appeared in reference 16 to denote a constructive principle for formulating physically sound models describing nonequilibrium phenomena. It is nowadays the central concept underlying stochastic thermodynamics, the theory that formulates the general principles for building nonequilibrium thermodynamics for a variety of dynamics,[17,18] not always related to chemical processes. Under certain conditions, local detailed balance also holds for nonelementary reactions as shown in references 3 and 7. This is indeed the case for the coarse-grained rate constants of the fueling and waste-forming reaction (see § I A), as commonly assumed[4,5].

We note that the local detailed balance as stated in (33), is different from how local detailed balance is discussed in references 5 and 19. Indeed, only in contexts where there is only one possible transition (e.g. one chemical reaction reaction) connecting a pair of states (e.g. two motor species), local detailed balance reduces to a constraint on the forward and backward transition rates connecting the two. But in the cases where there are multiple transitions between a couple of states (e.g. two reactions involving the same motor species but different chemostats), local detailed balance only holds at the level of each single transition[16,17,20], as done in equation (33), and not at the level of the net (i.e. summed) transition rates. This important point is also discussed in comment 21.

At equilibrium, the thermodynamic forces driving each reaction (also called *affinities* in the literature, a term not adopted here to avoid confusion with binding affinities) vanish

$$A^{\rm eq}_\rho = -\textstyle\sum_X \mu^{\rm eq}_X \mathbb{S}^X_\rho - \sum_Y \mu^{\rm eq}_Y \mathbb{S}^Y_\rho = 0 \,, \tag{34}$$

as well as all reaction currents

$$J^{\rm eq}_\rho = J^{\rm eq}_{+\rho} - J^{\rm eq}_{-\rho} = 0 \,. \tag{35}$$

Equations (33) imply the Wegscheider's conditions for the internal cycles: the product of the forward rate constants along each internal cycle must be equal to that of the backward rate constants

$$\text{from } \boldsymbol{c}_{\rm F}: \qquad k^{\rm p}_{-{\rm F}} k_{+\Delta} k^{\rm d}_{+{\rm F}} k^{\rm p}_{-{\rm F}} k'_{+\Delta} k^{\rm d}_{+{\rm F}} = k^{\rm p}_{+{\rm F}} k_{-\Delta} k^{\rm d}_{-{\rm F}} k^{\rm p}_{+{\rm F}} k'_{-\Delta} k^{\rm d}_{-{\rm F}} \,, \tag{36a}$$

$$\text{from } \boldsymbol{c}_{\rm W}: \qquad k^{\rm p}_{-{\rm W}} k_{+\Delta} k^{\rm d}_{+{\rm W}} k^{\rm p}_{-{\rm W}} k'_{+\Delta} k^{\rm d}_{+{\rm W}} = k^{\rm p}_{+{\rm W}} k_{-\Delta} k^{\rm d}_{-{\rm W}} k^{\rm p}_{+{\rm W}} k'_{-\Delta} k^{\rm d}_{-{\rm W}} \,, \tag{36b}$$

$$\text{from } \boldsymbol{c}_{\rm a}: \qquad k^{\rm p}_{-{\rm F}} k^{\rm p}_{+{\rm W}} k^{\rm p}_{+{\rm F}} k^{\rm p}_{-{\rm W}} = k^{\rm p}_{+{\rm F}} k^{\rm p}_{-{\rm W}} k^{\rm p}_{-{\rm F}} k^{\rm p}_{+{\rm W}} \,, \tag{36c}$$

$$\text{from } \boldsymbol{c}_{\rm b}: \qquad k^{\rm p}_{+{\rm F}} k^{\rm p}_{-{\rm W}} k^{\rm d}_{-{\rm F}} k^{\rm d}_{+{\rm W}} = k^{\rm p}_{-{\rm F}} k^{\rm p}_{+{\rm W}} k^{\rm d}_{+{\rm F}} k^{\rm d}_{-{\rm W}} \,. \tag{36d}$$

They set thermodynamic constraints that the kinetic parameters must satisfy, thus reducing freedom in their choice. Note that, due to symmetries in the system (*i.e.*, rate constants of reactions $1{\rm F}^{(\rm p)}$ and $4{\rm F}^{(\rm p)}$ are considered identical), condition (36c) is trivially satisfied and condition (36d) is implied by (36a) and (36b), which are therefore the only ones reported in the main text.

The dissipation of the process is captured by the entropy production rate times the temperature T:

$$T\dot\Sigma = RT \sum_\rho J_\rho \ln \frac{J_{+\rho}}{J_{-\rho}} \geq 0 \,, \tag{37}$$

which also vanishes at equilibrium. Equation (37) shows that each of the 10 reactions in the vector $\boldsymbol{\rho}$ (see Section I) brings a positive contribution to the total dissipation. We will use this property in Section IV to identify the specific contributions of chemical and mechanical processes.

By using the rate equations and the local detailed balance (33), the dissipation in equation (37) can be rewritten as

$$T\dot\Sigma = -{\rm d}_t \mathcal{G} + \dot{\mathcal{W}}_{\rm fuel} \,, \tag{38}$$

where

$$\begin{aligned}\mathcal{G} =&[1_{\mathrm{H}}^{\mathrm{D}}]\mu_{1_{\mathrm{H}}^{\mathrm{D}}} + [1_{\mathrm{D}}^{\mathrm{D}}]\mu_{1_{\mathrm{D}}^{\mathrm{D}}} + [1_{\mathrm{H}}^{\mathrm{H}}]\mu_{1_{\mathrm{H}}^{\mathrm{H}}} + [1_{\mathrm{D}}^{\mathrm{H}}]\mu_{1_{\mathrm{D}}^{\mathrm{H}}} + [2_{\mathrm{H}}]\left(\mu_{2_{\mathrm{H}}} - \mu_{\mathrm{DBF}} - \mu_{\mathrm{CO}_2}\right) + [2_{\mathrm{D}}]\left(\mu_{2_{\mathrm{D}}} - \mu_{\mathrm{DBF}} - \mu_{\mathrm{CO}_2}\right) + \\ &+ [\mathrm{F}]\,(\mu_{\mathrm{F}} - \mu_{\mathrm{W}}) - RT\left(L_{\mathrm{M}} + [\mathrm{F}] + [\mathrm{HCl}] + [\mathrm{DBF}] + [\mathrm{CO}_2]\right)\end{aligned} \tag{39}$$

is the *semigrand* Gibbs potential of the system[8], and

$$\dot{\mathcal{W}}_{\mathrm{fuel}} = I_{\mathrm{F}}(\mu_{\mathrm{F}} - \mu_{\mathrm{W}}) \tag{40}$$

is the fueling chemical work per unit of time (*i.e.*, the fueling power). If $\mu_{\mathrm{F}} = \mu_{\mathrm{W}}$, equation (38) shows that $\mathcal{G}$ is a monotonically decreasing function in time, given that $T\dot{\Sigma} \geq 0$.

A. Steady state entropy production and $J^{\mathrm{ss}}/I_{\mathrm{F}}^{\mathrm{ss}}$

As pointed out in the main text, at stationary state (see § II B) the dissipation in equation (38) boils down to:

$$T\dot{\Sigma}^{\mathrm{ss}} = \dot{\mathcal{W}}_{\mathrm{fuel}}^{\mathrm{ss}} = I_{\mathrm{F}}^{\mathrm{ss}}(\mu_{\mathrm{F}} - \mu_{\mathrm{W}})\,. \tag{41}$$

It is instructive to look at the equivalent expressions of equation (41) which are obtained by decomposing the stationary I_F^{ss} current on both cycles basis (25) and (26):

$$T\dot{\Sigma}^{\mathrm{ss}} = 2\psi_{\boldsymbol{c}_\epsilon}(\mu_{\mathrm{F}} - \mu_{\mathrm{W}}) = (\psi_{\boldsymbol{c}_{1\mathrm{p}}} + \psi_{\boldsymbol{c}_{3\mathrm{d}}} + \psi_{\boldsymbol{c}_{4\mathrm{p}}} + \psi_{\boldsymbol{c}_{6\mathrm{d}}} + 2\psi'_{\boldsymbol{c}_\epsilon})(\mu_{\mathrm{F}} - \mu_{\mathrm{W}})\,. \tag{42}$$

The first equality (decomposition according to the basis of vectors (25)) identifies the cycle current $\psi_{\boldsymbol{c}_\epsilon}$ as the fundamental current in the stationary regime: it accounts for total dissipation once multiplied by its conjugated fundamental force $2(\mu_{\mathrm{F}} - \mu_{\mathrm{W}})$, also denoted *cycle's affinity*; this is a consequence of the presence of a unique emergent cycle. The second one (decomposition according to the basis of vectors (26)) highlights how the consumption of fuel can be thought of as happening due to 5 different processes: the directional cycling of the macrocycle ($\psi'_{\boldsymbol{c}_\epsilon}$, which one would like to enhance), and four futile cycles consuming fuel without inducing directional movement of the macrocycle ($\psi_{\boldsymbol{c}_{1\mathrm{p}}}$, $\psi_{\boldsymbol{c}_{3\mathrm{d}}}$, $\psi_{\boldsymbol{c}_{4\mathrm{p}}}$, and $\psi_{\boldsymbol{c}_{6\mathrm{d}}}$ which one would like to suppress). From the latter perspective, we use relations (31) to introduce the following *coefficient of performance* ($J^{\mathrm{ss}}/I_{\mathrm{F}}^{\mathrm{ss}}$) quantifying how many fuel molecules are needed on average to complete a directional cycle:

$$\frac{J^{\mathrm{ss}}}{I_{\mathrm{F}}^{\mathrm{ss}}} = \frac{\psi'_{\boldsymbol{c}_\epsilon}}{\psi_{\boldsymbol{c}_{1\mathrm{p}}} + \psi_{\boldsymbol{c}_{3\mathrm{d}}} + \psi_{\boldsymbol{c}_{4\mathrm{p}}} + \psi_{\boldsymbol{c}_{6\mathrm{d}}} + 2\psi'_{\boldsymbol{c}_\epsilon}}\,. \tag{43}$$

In the best possible scenario, namely when futile currents vanish and the fuel consumption is tightly coupled with macrocycle directional movement, we have an average of 2 fuel molecules consumed per cycle, leading to an optimal $J^{\mathrm{ss}}/I_{\mathrm{F}}^{\mathrm{ss}}$ of 0.5. Equation (43) allows to quantify how much the motor deviates from the optimal condition and will be employed in the supplementary simulations of § VI B to further compare different designs. In particular, the values of $J^{\mathrm{ss}}/I_{\mathrm{F}}^{\mathrm{ss}}$ for the rotary motor can be directly compared with similar data measured for biological molecular motors. For instance, in reference 22 ATP-synthase in yeast mitochondria was found to use on average about 3.9 H^+ ions to synthetize one ATP molecule, when the expected theoretical value predicted by models was 3.3 (85% of the theoretical limit). As anticipated in the main text, our minimalist rotary motor consumes on average seven fuel molecules per cycle, corresponding to a $J^{\mathrm{ss}}/I_{\mathrm{F}}^{\mathrm{ss}}$ of 0.15 (30% of the theoretical limit) in the experimental condition.

IV. INFORMATION THERMODYNAMICS PERSPECTIVE

If we stick to the description above, the motor appears as an autonomous system exploiting the chemical gradient $\mu_{\mathrm{F}} - \mu_{\mathrm{W}}$ to sustain currents. We can evaluate its performance through equation (43), but questions such as how effectively the free energy harvested from the fuel is transduced by the motor to produce directional motion remain open. The detailed mechanism is better understood when the motor is thought of as a bipartite system, where we distinguish between "mechanical" states **mech** = {H, D} referring to the position of the macrocycle, and "chemical" ones **chem** = $\{2, 1^{\mathrm{H}}, 1^{\mathrm{D}}\}$ indicating the state of the track (how many stoppers attached, if one, where). With this structure in mind, the entropy production in equation (37) can be split as:

$$
\begin{aligned}
T\dot{\Sigma} = RT\sum_{\rho} J_\rho \ln\frac{J_{+\rho}}{J_{-\rho}} &= \underbrace{T\,R\sum_{\rho} J_\rho \ln\left(\frac{k_{+\rho}}{k_{-\rho}} Y_\sigma^{-\mathbb{S}^{Y}{}_{\rho}^{\sigma}}\right)}_{\dot{S}_{\mathrm{r}}} + \underbrace{T\,R\sum_{\rho} J_\rho \ln X_\sigma^{-\mathbb{S}^{X}{}_{\rho}^{\sigma}}}_{\mathrm{d}_t S} = \\
&= \underbrace{RTJ_{2\Delta}\ln\frac{k_{+\Delta}}{k_{-\Delta}} + RTJ_{5\Delta'}\ln\frac{k'_{+\Delta}}{k'_{-\Delta}}}_{T\dot{S}_{\mathrm{r}}^{\mathrm{mech}}} + \underbrace{RTJ_{2\Delta}\ln\frac{[1^{\mathrm{D}}_{\mathrm{H}}]}{[1^{\mathrm{D}}_{\mathrm{D}}]} + RTJ_{5\Delta'}\ln\frac{[1^{\mathrm{H}}_{\mathrm{D}}]}{[1^{\mathrm{H}}_{\mathrm{H}}]}}_{T\text{đ}_t S^{\mathrm{mech}}} + \\
&+ \underbrace{RT(J_{1\mathrm{F}^{(\mathrm{p})}} + J_{4\mathrm{F}^{(\mathrm{p})}})\ln\frac{k^{\mathrm{p}}_{-\mathrm{F}}[\mathrm{HCl}]}{k^{\mathrm{p}}_{+\mathrm{F}}[\mathrm{F}]} + RT(J_{3\mathrm{F}^{(\mathrm{d})}} + J_{6\mathrm{F}^{(\mathrm{d})}})\ln\frac{k^{\mathrm{d}}_{+\mathrm{F}}[\mathrm{F}]}{k^{\mathrm{d}}_{-\mathrm{F}}[\mathrm{HCl}]}}_{T\dot{S}_{\mathrm{r}}^{\mathrm{chem,F}}} + \\
&+ \underbrace{RT(J_{1\mathrm{W}^{(\mathrm{p})}} + J_{4\mathrm{W}^{(\mathrm{p})}})\ln\frac{k^{\mathrm{p}}_{-\mathrm{W}}}{k^{\mathrm{p}}_{+\mathrm{W}}[\mathrm{DBF}][\mathrm{CO_2}]} + RT(J_{3\mathrm{W}^{(\mathrm{d})}} + J_{6\mathrm{W}^{(\mathrm{d})}})\ln\frac{k^{\mathrm{d}}_{+\mathrm{W}}[\mathrm{DBF}][\mathrm{CO_2}]}{k^{\mathrm{d}}_{-\mathrm{W}}}}_{T\dot{S}_{\mathrm{r}}^{\mathrm{chem,W}}} + \\
&+ \underbrace{RT(J_{1\mathrm{F}^{(\mathrm{p})}} + J_{1\mathrm{W}^{(\mathrm{p})}})\ln\frac{[2_{\mathrm{H}}]}{[1^{\mathrm{D}}_{\mathrm{H}}]} + RT(J_{3\mathrm{F}^{(\mathrm{d})}} + J_{3\mathrm{W}^{(\mathrm{d})}})\ln\frac{[1^{\mathrm{D}}_{\mathrm{D}}]}{[2_{\mathrm{D}}]} + RT(J_{4\mathrm{F}^{(\mathrm{p})}} + J_{4\mathrm{W}^{(\mathrm{p})}})\ln\frac{[2_{\mathrm{D}}]}{[1^{\mathrm{H}}_{\mathrm{D}}]} + RT(J_{6\mathrm{F}^{(\mathrm{d})}} + J_{6\mathrm{W}^{(\mathrm{d})}})\ln\frac{[1^{\mathrm{H}}_{\mathrm{H}}]}{[2_{\mathrm{H}}]}}_{T\text{đ}_t S^{\mathrm{chem}}} \geq 0\,,
\end{aligned}
\tag{44}
$$

where terms

$$
T\dot{S}_{\mathrm{r}}^{\mathrm{mech}} = J_{2\Delta}(\mu^{\circ}_{1^{\mathrm{D}}_{\mathrm{H}}} - \mu^{\circ}_{1^{\mathrm{D}}_{\mathrm{D}}}) + J_{5\Delta'}(\mu^{\circ}_{1^{\mathrm{H}}_{\mathrm{D}}} - \mu^{\circ}_{1^{\mathrm{H}}_{\mathrm{H}}}) \tag{45a}
$$

$$
\begin{aligned}
T\dot{S}_{\mathrm{r}}^{\mathrm{chem,F}} + T\dot{S}_{\mathrm{r}}^{\mathrm{chem,W}} = \overbrace{I_{\mathrm{F}}(\mu_{\mathrm{F}} - \mu_{\mathrm{W}})}^{\dot{w}_{\mathrm{fuel}}} &+ (J_{1\mathrm{F}^{(\mathrm{p})}} + J_{1\mathrm{W}^{(\mathrm{p})}})(\mu^{\circ}_{2_{\mathrm{H}}} - \mu^{\circ}_{1^{\mathrm{D}}_{\mathrm{H}}} - \mu_{\mathrm{DBF}} - \mu_{\mathrm{CO_2}}) + \\
&+ (J_{4\mathrm{F}^{(\mathrm{p})}} + J_{4\mathrm{W}^{(\mathrm{p})}})(\mu^{\circ}_{2_{\mathrm{D}}} - \mu^{\circ}_{1^{\mathrm{H}}_{\mathrm{D}}} - \mu_{\mathrm{DBF}} - \mu_{\mathrm{CO_2}}) + (J_{3\mathrm{F}^{(\mathrm{d})}} + J_{3\mathrm{W}^{(\mathrm{d})}})(\mu^{\circ}_{1^{\mathrm{D}}_{\mathrm{D}}} - \mu^{\circ}_{2_{\mathrm{D}}} + \mu_{\mathrm{DBF}} + \mu_{\mathrm{CO_2}}) + \\
&+ (J_{6\mathrm{F}^{(\mathrm{d})}} + J_{6\mathrm{W}^{(\mathrm{d})}})(\mu^{\circ}_{1^{\mathrm{H}}_{\mathrm{H}}} - \mu^{\circ}_{2_{\mathrm{H}}} + \mu_{\mathrm{DBF}} + \mu_{\mathrm{CO_2}})
\end{aligned}
\tag{45b}
$$

keep track of the free energy exchanged with the reservoirs by each of the two sets of degrees of freedom. Note that fueling work by the chemostats is done on chemical degrees of freedom only. Terms $\text{đ}_t S^{\mathrm{mech}}$ and $\text{đ}_t S^{\mathrm{chem}}$ can be rewritten by introducing cumulative concentrations for the chemical subsystem: $[2] = [2_{\mathrm{H}}] + [2_{\mathrm{D}}]$, $[1^{\mathrm{H}}] = [1^{\mathrm{H}}_{\mathrm{D}}] + [1^{\mathrm{H}}_{\mathrm{H}}]$, $[1^{\mathrm{D}}] = [1^{\mathrm{D}}_{\mathrm{D}}] + [1^{\mathrm{D}}_{\mathrm{H}}]$; and for the mechanical one: $[\mathrm{H}^{\mathrm{mech}}] = [2_{\mathrm{H}}] + [1^{\mathrm{H}}_{\mathrm{H}}] + [1^{\mathrm{D}}_{\mathrm{H}}]$, $[\mathrm{D}^{\mathrm{mech}}] = [2_{\mathrm{D}}] + [1^{\mathrm{H}}_{\mathrm{D}}] + [1^{\mathrm{D}}_{\mathrm{D}}]$. We thus have:

$$
\text{đ}_t S^{\mathrm{mech}}/R = \underbrace{(J_{2\Delta} - J_{5\Delta'})\ln\frac{[\mathrm{H}^{\mathrm{mech}}]}{[\mathrm{D}^{\mathrm{mech}}]}}_{\mathrm{d}_t S^{\mathrm{mech}}/R} \underbrace{- J_{2\Delta}\ln\frac{[\mathrm{H}^{\mathrm{mech}}][1^{\mathrm{D}}_{\mathrm{D}}]}{[\mathrm{D}^{\mathrm{mech}}][1^{\mathrm{D}}_{\mathrm{H}}]} - J_{5\Delta'}\ln\frac{[\mathrm{D}^{\mathrm{mech}}][1^{\mathrm{H}}_{\mathrm{H}}]}{[\mathrm{H}^{\mathrm{mech}}][1^{\mathrm{H}}_{\mathrm{D}}]}}_{-\dot{I}^{\mathrm{mech}}}
$$

$$
\begin{aligned}
\text{đ}_t S^{\mathrm{chem}}/R = &\underbrace{(J_{1\mathrm{F}^{(\mathrm{p})}} + J_{1\mathrm{W}^{(\mathrm{p})}} - J_{3\mathrm{F}^{(\mathrm{d})}} - J_{3\mathrm{W}^{(\mathrm{d})}})\ln\frac{[2]}{[1^{\mathrm{D}}]} + (J_{4\mathrm{F}^{(\mathrm{p})}} + J_{4\mathrm{W}^{(\mathrm{p})}} - J_{6\mathrm{F}^{(\mathrm{d})}} - J_{6\mathrm{W}^{(\mathrm{d})}})\ln\frac{[2]}{[1^{\mathrm{H}}]}}_{\mathrm{d}_t S^{\mathrm{chem}}/R} + \\
&\underbrace{-(J_{1\mathrm{F}^{(\mathrm{p})}} + J_{1\mathrm{W}^{(\mathrm{p})}})\ln\frac{[2][1^{\mathrm{D}}_{\mathrm{H}}]}{[1^{\mathrm{D}}][2_{\mathrm{H}}]} - (J_{3\mathrm{F}^{(\mathrm{d})}} + J_{3\mathrm{W}^{(\mathrm{d})}})\ln\frac{[1^{\mathrm{D}}][2_{\mathrm{D}}]}{[2][1^{\mathrm{D}}_{\mathrm{D}}]} - (J_{4\mathrm{F}^{(\mathrm{p})}} + J_{4\mathrm{W}^{(\mathrm{p})}})\ln\frac{[2][1^{\mathrm{H}}_{\mathrm{D}}]}{[1^{\mathrm{H}}][2_{\mathrm{D}}]} - (J_{6\mathrm{F}^{(\mathrm{d})}} + J_{6\mathrm{W}^{(\mathrm{d})}})\ln\frac{[1^{\mathrm{H}}][2_{\mathrm{H}}]}{[2][1^{\mathrm{H}}_{\mathrm{H}}]}}_{-\dot{I}^{\mathrm{chem}}}\,.
\end{aligned}
\tag{46}
$$

Now the interpretation of $\mathrm{d}_t S^{\mathrm{mech}}$ and $\mathrm{d}_t S^{\mathrm{chem}}$ is clear: they are the time derivatives of the subsystem's Shannon-like entropies[8,23]. If we could measure the two subsystems separately, the entropy production rates we would assign to them

would be:

$$\sigma^{\text{mech}} := \dot{S}_{\text{r}}^{\text{mech}} + \mathrm{d}_t S^{\text{mech}} \tag{47}$$

$$\sigma^{\text{chem}} := \dot{S}_{\text{r}}^{\text{chem,F}} + \dot{S}_{\text{r}}^{\text{chem,W}} + \mathrm{d}_t S^{\text{chem}} \,. \tag{48}$$

Concerning the other terms, we now justify the names $\dot{\mathcal{I}}^{\text{mech}}$ and $\dot{\mathcal{I}}^{\text{chem}}$ by showing that their sum gives the time variation of the mutual information between the two subsystems. The reader who is not interested in technical details can directly go to equation (51).

If we focus on the stochastic behavior of a single motor unit, the joint probability to find it in a certain mechanical and chemical state evolves according to the following master equation:

$$\mathrm{d}_t \boldsymbol{p}(\text{chem}, \text{mech}) = \sum_{\text{mech}',\text{chem}'} \left[\mathbb{W}_{(\text{chem},\text{mech}),(\text{chem}',\text{mech}')} p(\text{chem}', \text{mech}') \right] \,. \tag{49*}$$

For instance, it is analogous to the one employed in reference 24 to study another example of a molecular motor. Note how the structure of equation (49*) is analogous to the equation (13*) evolving the concentrations of the various motor species. Indeed, when the number N of single motor units in the system is large, the probabilities $\boldsymbol{p}(\text{mech}, \text{chem})$ for each chemical species become sharply peaked on their average values. Thus, we can perform the substitution $\boldsymbol{p}(\text{mech}, \text{chem}) = \frac{\boldsymbol{N}(\text{mech},\text{chem})}{N} = \frac{[X]}{L_{\text{M}}}$, which shows that equation (13*) is the macroscopic limit of equation (49*). This is crucial, because it implies that for such a case taking the macroscopic limit of stochastic quantities just means to switch from the probability of a certain state to its concentrations. In this case, the stochastic mutual information between mechanical and chemical subsystems reads:

$$\mathcal{I}_{\text{M}} = \sum_{\text{mech,chem}} p(\text{mech}, \text{chem}) \ln \frac{p(\text{mech}, \text{chem})}{p(\text{mech}) p(\text{chem})} \geq 0 \,, \tag{50*}$$

which is a measure of the correlation between the two sets of degrees of freedom. In the above equation, $p(\text{mech}) = \sum_{\text{chem}} p(\text{mech}, \text{chem})$ and $p(\text{chem}) = \sum_{\text{mech}} p(\text{mech}, \text{chem})$. Thus, the mutual information in terms of macroscopic concentrations can be defined as:

$$\begin{aligned} \mathcal{I} := L_{\text{M}} \mathcal{I}_{\text{M}} = \Bigg(& [2_{\text{H}}] \ln \frac{[2_{\text{H}}]}{[\text{H}^{\text{mech}}][2]} + [2_{\text{D}}] \ln \frac{[2_{\text{D}}]}{[\text{D}^{\text{mech}}][2]} + [1^{\text{D}}_{\text{H}}] \ln \frac{[1^{\text{D}}_{\text{H}}]}{[\text{H}^{\text{mech}}][1^{\text{D}}]} + \\ & + [1^{\text{D}}_{\text{D}}] \ln \frac{[1^{\text{D}}_{\text{D}}]}{[\text{D}^{\text{mech}}][1^{\text{D}}]} + [1^{\text{H}}_{\text{D}}] \ln \frac{[1^{\text{H}}_{\text{D}}]}{[\text{D}^{\text{mech}}][1^{\text{H}}]} + [1^{\text{H}}_{\text{H}}] \ln \frac{[1^{\text{H}}_{\text{H}}]}{[\text{H}^{\text{mech}}][1^{\text{H}}]} \Bigg) + L_{\text{M}} \ln(L_{\text{M}}) \,, \end{aligned} \tag{51}$$

and by straightforward computation and equation (18) we get

$$\mathrm{d}_t \mathcal{I} = \dot{\mathcal{I}}^{\text{mech}} + \dot{\mathcal{I}}^{\text{chem}} \,. \tag{52}$$

To summarize, we showed that the entropy production of the full system can be written as a sum of two individually positive terms:

$$T\dot{\Sigma} = T\dot{\Sigma}^{\text{mech}} + T\dot{\Sigma}^{\text{chem}} = \underbrace{T\sigma^{\text{mech}} - RT\dot{\mathcal{I}}^{\text{mech}}}_{\geq 0} + \underbrace{T\sigma^{\text{chem}} - RT\dot{\mathcal{I}}^{\text{chem}}}_{\geq 0} \,. \tag{53}$$

Indeed, by substituting into equation (53) expressions (48), (46) and (45), we find

$$\begin{aligned} T\dot{\Sigma}^{\text{mech}} &= T\dot{S}_{\text{r}}^{\text{mech}} + T\mathrm{đ}_t S^{\text{mech}} = RT \sum_{\rho^{\text{mech}}} J_{\rho^{\text{mech}}} \ln \frac{J_{+\rho^{\text{mech}}}}{J_{-\rho^{\text{mech}}}} \geq 0 \\ T\dot{\Sigma}^{\text{chem}} &= T\dot{S}_{\text{r}}^{\text{chem}} + T\mathrm{đ}_t S^{\text{chem}} = RT \sum_{\rho^{\text{chem}}} J_{\rho^{\text{chem}}} \ln \frac{J_{+\rho^{\text{chem}}}}{J_{-\rho^{\text{chem}}}} \geq 0 \end{aligned} \tag{54}$$

where $\rho^{\text{mech}} = \{2\Delta, 5\Delta'\}$ and $\rho^{\text{chem}} = \{1\text{F}^{(\text{p})}, 1\text{W}^{(\text{p})}, 3\text{F}^{(\text{d})}, 3\text{W}^{(\text{d})}, 4\text{F}^{(\text{p})}, 4\text{W}^{(\text{p})}, 6\text{F}^{(\text{d})}, 6\text{W}^{(\text{d})}\}$ denote the reactions changing the mechanical and the chemical state of the motor, respectively.

At stationary state, we have that $\mathrm{d}_t \mathcal{I} = 0 = \dot{\mathcal{I}}^{\text{mech}}_{\text{ss}} + \dot{\mathcal{I}}^{\text{chem}}_{\text{ss}}$ (equation (51)), and also $\mathrm{d}_t S^{\text{mech}}$ and $\mathrm{d}_t S^{\text{chem}}$ vanish, as they are state functions. By specializing equation (53) to the stationary state (where relations (31) are employed to simplify the final expression) and defining $\dot{\mathcal{I}}^{\text{mech}}_{\text{ss}} = -\dot{\mathcal{I}}^{\text{chem}}_{\text{ss}} = -\dot{\mathcal{I}}$ and $T\dot{S}^{\text{mech}}_{\text{r,ss}} = \dot{\mathcal{E}}$, we finally get the equation reported in the main text (where the ss symbol has been dropped since there we unambiguously refer to the stationary state):

$$T\dot{\Sigma}^{\text{ss}} = T\dot{\Sigma}^{\text{chem}}_{\text{ss}} + T\dot{\Sigma}^{\text{mech}}_{\text{ss}} = \underbrace{I^{\text{ss}}_{\text{F}}(\mu_{\text{F}} - \mu_{\text{W}}) - \dot{\mathcal{E}} - RT\dot{\mathcal{I}}}_{\geq 0} + \underbrace{\dot{\mathcal{E}} + RT\dot{\mathcal{I}}}_{\geq 0} \geq 0 \,. \tag{55}$$

V. THERMODYNAMIC CONSTRAINTS ON THE STATIONARY STATE DYNAMICS AND CONNECTION WITH KINETIC ASYMMETRY: THE ROTARY MOTOR AS A ROSETTA STONE FOR KINETIC AND THERMODYNAMIC ANALYSIS

In this section, we examine in detail how equation (55) implies previous results obtained in the literature, namely the kinetic asymmetry rule[4,5]. In general, we can distinguish three possible stationary states for this system. The equilibrium (i) is always reached when the chemical potential gradient acting on the system is null ($\mu_F = \mu_W$), no matter the values of the rate constants (provided they fulfill Wegscheider's conditions in equations (36)). At equilibrium each reaction current vanishes ($J_\rho^{eq} = J_{+\rho}^{eq} - J_{-\rho}^{eq} = 0$) and no average net displacement of the macrocycle with respect to the track can be observed. Whenever the chemical potentials of fuel and waste species are kept different (*e.g.*, $\mu_F > \mu_W$), a nonequilibrium stationary state with net currents is reached in the long time limit (see § II B). This situation can be "symmetric" (ii) – always when the position of the macrocycle does not affect the rates of the fueling and waste-forming reactions – or "asymmetric" (iii) – the general case for the experiment we are considering. The latter is the interesting one from the point of view of directionality, because it corresponds to an average directional motion of the macrocycle along the track characterized by a non-null stationary state current J^{ss} (equation (31)).

A. Condition for directional J^{ss}

By considering the decomposition of the dissipation in equation (55):

$$T\dot{\Sigma}^{ss} = \overbrace{I_F^{ss}(\mu_F - \mu_W) - \dot{\mathcal{E}} - RT\dot{\mathcal{I}}}^{T\dot{\Sigma}_{ss}^{chem}} + \overbrace{\underbrace{J^{ss}RT\ln\frac{k_{+\Delta}k'_{+\Delta}}{k_{-\Delta}k'_{-\Delta}}}_{\dot{\mathcal{E}}} + \underbrace{J^{ss}RT\ln\frac{[1_H^D]_{ss}[1_D^H]_{ss}}{[1_D^D]_{ss}[1_H^H]_{ss}}}_{RT\dot{\mathcal{I}}}}^{T\dot{\Sigma}_{ss}^{mech}}, \tag{56}$$

the following inequalities hold by virtue of the second law of thermodynamics for bipartite systems:

$$T\dot{\Sigma}_{ss}^{chem} = {I_F}^{ss}(\mu_F - \mu_W) - T\dot{\Sigma}_{ss}^{mech} \geq 0 \tag{57a}$$

$$T\dot{\Sigma}_{ss}^{mech} = \dot{\mathcal{E}} + RT\dot{\mathcal{I}} = J^{ss}RT\left(\ln\frac{k_{+\Delta}k'_{+\Delta}}{k_{-\Delta}k'_{-\Delta}} + \ln\frac{[1_H^D]_{ss}[1_D^H]_{ss}}{[1_D^D]_{ss}[1_H^H]_{ss}}\right) \geq 0\,. \tag{57b}$$

As highlighted in the main text, net directional displacement of the macrocycle in the stationary state can be observed only in the presence of mechanical dissipation ($T\dot{\Sigma}_{ss}^{mech} > 0$), as directed motion is a nonequilibrium behaviour. This implies that in order to have a non null J^{ss}, a positive fueling work is required (${I_F}^{ss}(\mu_F - \mu_W) > 0$ in equation (57a), otherwise the stationary state would be an equilibrium one). This is not sufficient, since the sum of energy and information flow in equation (57b) must be positive too, namely a net free energy transfer from chemical to mechanical processes must be present.

The condition for a net directional displacement of the macrocycle in the stationary state can then be written as:

$$\ln\frac{k_{+\Delta}k'_{+\Delta}}{k_{-\Delta}k'_{-\Delta}} + \ln\frac{[1_H^D]_{ss}[1_D^H]_{ss}}{[1_D^D]_{ss}[1_H^H]_{ss}} = \ln\frac{J_{+2\Delta}^{ss}J_{+5\Delta'}^{ss}}{J_{-2\Delta}^{ss}J_{-5\Delta'}^{ss}} \neq 0\,. \tag{58}$$

Thanks to equation (31), it's easy to realize that whenever the quantity in equation (58) is positive, J^{ss} is positive too, and vice-versa, thus guaranteeing equation (57b) to always hold. We will now show how the condition (58) (obtained with nonequilibrium thermodynamic arguments) is equivalent to previous results obtained in the literature (based on kinetic arguments).

B. Connection to kinetic asymmetry and K_r

According to references 25 and 6, the condition for having directional currents in nonequilibrium chemical systems ($J^{ss} \neq 0$) can be expressed in terms of the ratcheting constant, which for the motor under study reads

$$K_r = \frac{k_{+\Delta}k'_{+\Delta}(k_{-F}^p[HCl] + k_{-W}^p)^2([F]k_{+F}^d + [CO_2][DBF]k_{+W}^d)^2}{k_{-\Delta}k'_{-\Delta}([F]k_{+F}^p + [CO_2][DBF]k_{+W}^p)^2(k_{-F}^d[HCl] + k_{-W}^d)^2} \neq 1\,, \tag{59}$$

with $K_r > 1$ implying a positive forward current, and vice-versa. By using Wegscheider's conditions (36), K_r can be rewritten as[4,5,25,26]:

$$K_r = \underbrace{\frac{k_{+\Delta}k'_{+\Delta}(k^p_{-F}[HCl])^2([F]k^d_{+F})^2}{k_{-\Delta}k'_{-\Delta}([F]k^p_{+F})^2(k^d_{-F}[HCl])^2}}_{=1,\text{ see equation (36a)}} \frac{(1+\frac{k^p_{-W}}{k^p_{-F}[HCl]})^2(1+\frac{[CO_2][DBF]k^d_{+W}}{[F]k^d_{+F}})^2}{(1+\frac{[CO_2][DBF]k^p_{+W}}{[F]k^p_{+F}})^2(1+\frac{k^d_{-W}}{k^d_{-F}[HCl]})^2} = \frac{(1+\frac{k^p_{-W}}{k^p_{-F}[HCl]})^2(1+\frac{[CO_2][DBF]k^d_{+W}}{[F]k^d_{+F}})^2}{(1+\frac{[CO_2][DBF]k^p_{+W}}{[F]k^p_{+F}})^2(1+\frac{k^d_{-W}}{k^d_{-F}[HCl]})^2}\,. \tag{60}$$

In the following, we show how the condition $K_r \neq 1$ for a directional current $J^{ss} \neq 0$ is implied by equations (58).

1. *Equilibrium condition*

The expression of the ratcheting constant in equation (60) can be further rearranged thanks to equations (32) and (33) to get (see also Eq. (5) in 4):

$$K_r = \frac{(1+\frac{k^p_{-W}}{k^p_{-F}[HCl]})^2(1+\frac{k^d_{-W}}{k^d_{-F}[HCl]}e^{-\frac{\mu_F-\mu_W}{RT}})^2}{(1+\frac{k^p_{-W}}{k^p_{-F}[HCl]}e^{-\frac{\mu_F-\mu_W}{RT}})^2(1+\frac{k^d_{-W}}{k^d_{-F}[HCl]})^2}\,, \tag{61}$$

which nicely shows that $K_r = 1$ (and then $J^{ss} = 0$) whenever $\mu_F = \mu_W$, in analogy with equation (57a). Regardless of the values of the rate constants, if there is no thermodynamic force ($\mu_F - \mu_W = 0$), the motor will relax to an equilibrium stationary state with no directional currents, and the quantity in equation (58) will be zero.

2. *Proof of the implication* $\dot{\Sigma}^{mech} > 0 \rightarrow K_r \neq 1$

We now prove that the condition on K_r in equation (59) directly follows from equation (58). We do so by relying on some results and techniques from graph theory (see appendixes of reference 3 for an introduction). The reader who is not familiar with this kind of techniques can directly go to the next paragraph, where a simpler proof valid for the experimental case (where equations 1 hold) is presented.

First of all, we define K_r in terms of the pseudo rate constants introduced in equation (13*):

$$K_r = \frac{\tilde{k}_{+\Delta}\tilde{k}'_{+\Delta}(\tilde{k}^p_-\tilde{k}^d_+)^2}{\tilde{k}_{-\Delta}\tilde{k}'_{-\Delta}(\tilde{k}^p_+\tilde{k}^d_-)^2} = \frac{\mathcal{P}_{cw}}{\mathcal{P}_{ccw}}\,, \tag{62}$$

where $\mathcal{P}_{cw}$ and $\mathcal{P}_{ccw}$ are the product of all forward clockwise and counterclockwise pseudo reaction constants, respectively. By plugging the analytical expression (27*) for the steady state concentrations into the condition (58), the latter can be rewritten as

$$\left(\tilde{k}_{+\Delta}\sum_{t\in\mathcal{T}^D_{1_H}}\prod_{\rho\in t}\tilde{k}_\rho\right)\cdot\left(\tilde{k}'_{+\Delta}\sum_{t\in\mathcal{T}^H_{1_D}}\prod_{\rho\in t}\tilde{k}_\rho\right)-\left(\tilde{k}_{-\Delta}\sum_{t\in\mathcal{T}^D_{1_D}}\prod_{\rho\in t}\tilde{k}_\rho\right)\cdot\left(\tilde{k}'_{-\Delta}\sum_{t\in\mathcal{T}^H_{1_H}}\prod_{\rho\in t}\tilde{k}_\rho\right)\neq 0\,. \tag{63*}$$

We recall that, for instance, the symbol $\mathcal{T}^D_{1_H}$ denotes the set of spanning trees rooted in vertex 1^D_H of the chemical reaction network representing the motor. Therefore, each parenthesis in the above expression contains a sum of 6 terms that are

each the product of 6 pseudo reaction constants. We can manipulate expression (63*) to get

$$\begin{aligned}
&\left(\tilde{k}_{+\Delta}\sum_{t\in\mathcal{T}_{\mathrm{i}_\mathrm{H}^\mathrm{D}}\wedge\tilde{k}_{-\Delta}\in t}\prod_{\rho\in t}\tilde{k}_\rho+\mathcal{P}_{\mathrm{cw}}\right)\cdot\left(\tilde{k}'_{+\Delta}\sum_{t\in\mathcal{T}_{\mathrm{i}_\mathrm{D}^\mathrm{H}}\wedge\tilde{k}'_{-\Delta}\in t}\prod_{\rho\in t}\tilde{k}_\rho+\mathcal{P}_{\mathrm{cw}}\right)\\
&-\left(\tilde{k}_{-\Delta}\sum_{t\in\mathcal{T}_{\mathrm{i}_\mathrm{D}^\mathrm{D}}\wedge\tilde{k}_{+\Delta}\in t}\prod_{\rho\in t}\tilde{k}_\rho+\mathcal{P}_{\mathrm{ccw}}\right)\cdot\left(\tilde{k}'_{-\Delta}\sum_{t\in\mathcal{T}_{\mathrm{i}_\mathrm{H}^\mathrm{H}}\wedge\tilde{k}'_{+\Delta}\in t}\prod_{\rho\in t}\tilde{k}_\rho+\mathcal{P}_{\mathrm{ccw}}\right)=\\
&0+(\mathcal{P}_{\mathrm{cw}}^2-\mathcal{P}_{\mathrm{ccw}}^2)+\mathcal{P}_{\mathrm{cw}}\underbrace{\left[\tilde{k}_{+\Delta}\sum_{t\in\mathcal{T}_{\mathrm{i}_\mathrm{H}^\mathrm{D}}\wedge\tilde{k}_{-\Delta}\in t}\prod_{\rho\in t}\tilde{k}_\rho+\tilde{k}'_{+\Delta}\sum_{t\in\mathcal{T}_{\mathrm{i}_\mathrm{D}^\mathrm{H}}\wedge\tilde{k}'_{-\Delta}\in t}\prod_{\rho\in t}\tilde{k}_\rho\right]}_{\Phi}\\
&-\mathcal{P}_{\mathrm{ccw}}\underbrace{\left[\tilde{k}_{-\Delta}\sum_{t\in\mathcal{T}_{\mathrm{i}_\mathrm{D}^\mathrm{D}}\wedge\tilde{k}_{+\Delta}\in t}\prod_{\rho\in t}\tilde{k}_\rho+\tilde{k}'_{-\Delta}\sum_{t\in\mathcal{T}_{\mathrm{i}_\mathrm{H}^\mathrm{H}}\wedge\tilde{k}'_{+\Delta}\in t}\prod_{\rho\in t}\tilde{k}_\rho\right]}_{\Phi}=(\mathcal{P}_{\mathrm{cw}}-\mathcal{P}_{\mathrm{ccw}})\cdot(\mathcal{P}_{\mathrm{cw}}+\mathcal{P}_{\mathrm{ccw}}+\Phi)\neq 0\,.
\end{aligned}\tag{64*}$$

Since $\mathcal{P}_{\mathrm{cw}}$, $\mathcal{P}_{\mathrm{ccw}}$, and Φ are positive quantities, the above condition is satisfied if and only if $\mathcal{P}_{\mathrm{cw}}-\mathcal{P}_{\mathrm{ccw}}\neq 0$ or, alternatively, $\mathcal{P}_{\mathrm{cw}}/\mathcal{P}_{\mathrm{ccw}}\neq 1$, thus fully proving the equivalence between condition (59) from references 4, 25, 5, and 6 and condition (58) derived from the second law (57) for bipartite systems[23].

3. *Special proof for the experimental case*

Here, we repeat the above proof for the special case of the experimental rotary motor, where the symmetries in equations (1) hold and the expressions for stationary state concentrations is given by equations (28). By plugging the latter in equation (58), the condition for directional current boils down to:

$$\frac{(k^{\mathrm{p}}_{-\mathrm{F}}[\mathrm{HCl}]+k_{-\mathrm{W}})(k^{\mathrm{d}}_{+\mathrm{F}}[\mathrm{F}]+k_{+\mathrm{W}}[\mathrm{CO_2}][\mathrm{DBF}])+(k^{\mathrm{p}}_{-\mathrm{F}}[\mathrm{HCl}]+k^{\mathrm{d}}_{-\mathrm{F}}[\mathrm{HCl}]+2k_{-\mathrm{W}})k_{\Delta}}{(k^{\mathrm{d}}_{-\mathrm{F}}[\mathrm{HCl}]+k_{-\mathrm{W}})(k^{\mathrm{p}}_{+\mathrm{F}}[\mathrm{F}]+k_{+\mathrm{W}}[\mathrm{CO_2}][\mathrm{DBF}])+(k^{\mathrm{p}}_{-\mathrm{F}}[\mathrm{HCl}]+k^{\mathrm{d}}_{-\mathrm{F}}[\mathrm{HCl}]+2k_{-\mathrm{W}})k_{\Delta}}\neq 1\,,\tag{65}$$

which is equivalent to

$$(k^{\mathrm{p}}_{-\mathrm{F}}[\mathrm{HCl}]+k_{-\mathrm{W}})(k^{\mathrm{d}}_{+\mathrm{F}}[\mathrm{F}]+k_{+\mathrm{W}}[\mathrm{CO_2}][\mathrm{DBF}])\neq(k^{\mathrm{d}}_{-\mathrm{F}}[\mathrm{HCl}]+k_{-\mathrm{W}})(k^{\mathrm{p}}_{+\mathrm{F}}[\mathrm{F}]+k_{+\mathrm{W}}[\mathrm{CO_2}][\mathrm{DBF}])\,,\tag{66}$$

and so

$$\frac{(k^{\mathrm{p}}_{-\mathrm{F}}[\mathrm{HCl}]+k_{-\mathrm{W}})(k^{\mathrm{d}}_{+\mathrm{F}}[\mathrm{F}]+k_{+\mathrm{W}}[\mathrm{CO_2}][\mathrm{DBF}])}{(k^{\mathrm{d}}_{-\mathrm{F}}[\mathrm{HCl}]+k_{-\mathrm{W}})(k^{\mathrm{p}}_{+\mathrm{F}}[\mathrm{F}]+k_{+\mathrm{W}}[\mathrm{CO_2}][\mathrm{DBF}])}\neq 1\,,\tag{67}$$

which is exactly the square root of K_{r} in equation (59) specialized for the experimental case.

4. *On the magnitude of the stationary state current J^{ss}*

We conclude this section by deriving the expression of the stationary state current displayed in equation (4) of the main text, which proves particularly useful to rationalize and discuss numerical simulations in the main text and in § VI B.

First of all, we rewrite the stationary state current defined in equation (31a) and equation (4) of the main text in terms of the pseudo rate constants introduced in equation (13*):

$$J^{\mathrm{ss}}=\tilde{k}_{+\Delta}[1^{\mathrm{D}}_{\mathrm{H}}]_{\mathrm{ss}}-\tilde{k}_{-\Delta}[1^{\mathrm{D}}_{\mathrm{D}}]_{\mathrm{ss}}=\tilde{k}'_{+\Delta}[1^{\mathrm{H}}_{\mathrm{D}}]_{\mathrm{ss}}-\tilde{k}'_{-\Delta}[1^{\mathrm{H}}_{\mathrm{H}}]_{\mathrm{ss}}\,.\tag{68}$$

This rewriting is trivial, since $\tilde{k}_{+\Delta} = k_{+\Delta}$, $\tilde{k}_{-\Delta} = k_{-\Delta}$, $\tilde{k}'_{+\Delta} = k'_{+\Delta}$, and $\tilde{k}'_{-\Delta} = k'_{-\Delta}$ (see equation (13*)), but by plugging the analytical expression (27*) for stationary state concentrations into equation (68) we get

$$
\begin{aligned}
J^{\mathrm{ss}} =& \frac{L_{\mathrm{M}}}{\mathcal{N}} \left(\tilde{k}_{+\Delta} \sum_{t \in \mathcal{T}_{\substack{\mathrm{1D} \\ \mathrm{H}}}} \prod_{\lambda \in t} \tilde{k}_{\lambda} - \tilde{k}_{-\Delta} \sum_{t \in \mathcal{T}_{\substack{\mathrm{1D} \\ \mathrm{D}}}} \prod_{\lambda \in t} \tilde{k}_{\lambda} \right) = \\
=& \frac{L_{\mathrm{M}}}{\mathcal{N}} \left(\tilde{k}_{+\Delta} \sum_{t \in \mathcal{T}_{\substack{\mathrm{1D} \\ \mathrm{H}}} \wedge \tilde{k}_{-\Delta} \in t} \prod_{\rho \in t} \tilde{k}_{\rho} + \mathcal{P}_{\mathrm{cw}} - \tilde{k}_{-\Delta} \sum_{t \in \mathcal{T}_{\substack{\mathrm{1D} \\ \mathrm{D}}} \wedge \tilde{k}_{+\Delta} \in t} \prod_{\rho \in t} \tilde{k}_{\rho} - \mathcal{P}_{\mathrm{ccw}} \right) = \frac{L_{\mathrm{M}}}{\mathcal{N}} \left(\mathcal{P}_{\mathrm{cw}} - \mathcal{P}_{\mathrm{ccw}} \right) = \\
=& \frac{L_{\mathrm{M}} \mathcal{P}_{\mathrm{ccw}}}{\mathcal{N}} (K_{\mathrm{r}} - 1) = \Gamma (K_{\mathrm{r}} - 1) \,, \qquad (69^*)
\end{aligned}
$$

where we introduced the positive quantity Γ appearing in equation (4) of the main text. All the other symbols appearing in the above equation have been defined in equations (27*) and (62). Equation (69) shows that the sign of the current J^{ss} is determined by K_{r} being smaller or greater than 1, with no current for $K_{\mathrm{r}} = 1$, while its magnitude depends on the actual value of both K_{r} and Γ. Crucially, the value of Γ can be varied independently from the value of K_{r}, thus allowing for design modifications which can improve or stall a motor's performance (but not altering the direction of cycling) without varying its kinetic asymmetry. This kind of effects are explored in the main text and in the next section with the help of numerical simulations.

VI. NUMERICAL SIMULATIONS

In order to better understand the implications of the model for the design of molecular motors, we performed a series of numerical simulations solving numerically dynamical equations (10) while varying key rate constants and plotting the predicted effect on the stationary state current (J in equation (4) in the main text, J^{ss} in equations (31a) and (69)), the thermodynamic efficiency (η, equation (5) in the main text), and the quantity J/I_{F} (stationary state current divided by the rate at which fuel is consumed at the stationary state), which equates to the average number of cycles achieved per molecule of fuel (see equation (43)). As stated in § III A, this last measure is a coefficient of performance which is distinct from efficiency because it is independent of both the energy content of the fuel, instead looking at the effect of each fuel molecule, and of whether the energy is dissipated mechanically or chemically, only reflecting how well fuel use correlates with unidirectional movement. In all the simulations, thermodynamic consistency was always guaranteed by enforcing Wegscheider's conditions (36).

It should be noted that the current is unbounded and can be positive or negative, indicating forward or backward movement respectively, thermodynamic efficiency is bounded between 0 and 1, and J/I_{F} is bounded between 0.5 and -0.5 (the sign indicating direction). The value has a maximum of 0.5 because at minimum 2 molecules of fuel are required for a complete cycle as the rotary motor is a two-stroke design, with two barriers to move past per cycle.

A. Parameters

The parameters in Table I were adopted as reference in the numerical simulations of the model introduced in Section I. The chosen values are intended to be realistic and give a correct qualitative outcome. A precise quantitative analysis would require more experimental data and is out of the scope of the present work. Apart where explicitly said or shown in the graphs, reference parameters are kept constant in the numerical simulations.

B. Supplementary analysis of the numerical simulations

1. *Chemical gating of the fueling reaction*

In this simulation, the sum of the rates of the fueling reactions and the chemical gating ratio of the fueling reaction were varied (Fig. 3a,b in the main text, Fig. 1). This is the only source of chemical gating as no chemical gating is introduced via the waste forming reactions in this simulation, as was the case in the experimental rotary motor (white dot). With no chemical gating (white line) there can be no current in the motor and therefore thermodynamic efficiency and the number of cycles per unit of fuel are also always zero. For intermediate rates of the fueling reaction, the current increases as the chemical gating increases. This is because an increased kinetic bias means the motor spends more time

Table I: Reference parameters employed in the numerical simulations. Rate constants $k^{\mathrm{d}}_{+\mathrm{F}}$, $k^{\mathrm{p}}_{+\mathrm{F}}$, $k_{-\mathrm{W}}$ and k_{Δ} are estimated based on data collected in reference 1, where equations (1) hold, and related rotaxanes[27]. Rate constants $k^{\mathrm{d}}_{-\mathrm{F}}$ and $k_{+\mathrm{W}}$ are calculated by using equation (33) and assuming, based on known enthalpy-of-formation data, a difference of the order of 10^2 $kJ\ mol^{-1}$ in the standard chemical potentials between fuel and waste species ($\mu^{\circ}_{\mathrm{F}} - \mu^{\circ}_{\mathrm{W}}$). The rate constant $k^{\mathrm{p}}_{-\mathrm{F}}$ is obtained by using equation (36a) to guarantee thermodynamic consistency. The total concentration of motor's species L_{M} is the same as in reference 1. The parameters involving chemostatted concentrations ([Fmoc−Cl], [DBF] · [CO_2] and [HCl]) are estimated based on the original experiment[1] and other known data[28]. The order of magnitude of parameters [DBF] · [CO_2] and [HCl] does not significantly affect the results of simulations, since the microscopic reverses of fueling and waste-forming reactions (rate constants $k^{\mathrm{p/d}}_{-\mathrm{F}}$ and $k_{+\mathrm{W}}$) are highly unfavorable.

$k^{\mathrm{d}}_{+\mathrm{F}}$	$8 \cdot 10^{-3}$ mol^{-1} dm^{3}s^{-1}
$k^{\mathrm{d}}_{-\mathrm{F}}$	$1 \cdot 10^{-27}$ mol^{-1} dm^{3}s^{-1}
$k^{\mathrm{p}}_{+\mathrm{F}}$	$2 \cdot 10^{-3}$ mol^{-1} dm^{3}s^{-1}
$k^{\mathrm{p}}_{-\mathrm{F}}$	$2.5 \cdot 10^{-28}$ mol^{-1} dm^{3}s^{-1}
$k_{-\mathrm{W}}$	$8 \cdot 10^{-6}$ s^{-1}
$k_{+\mathrm{W}}$	$1 \cdot 10^{-26}$ mol^{-2}dm^{6}s^{-1}
k_{Δ}	$1 \cdot 10^{1}$ s^{-1}

L_{M}	$1 \cdot 10^{-2}$ mol dm^{-3}
[Fmoc−Cl]	$3 \cdot 10^{-2}$ mol dm^{-3}
[DBF] · [CO_2]	$1 \cdot 10^{-5}$ mol^2 dm^{-6}
[HCl]	$1 \cdot 10^{-18}$ mol dm^{-3}

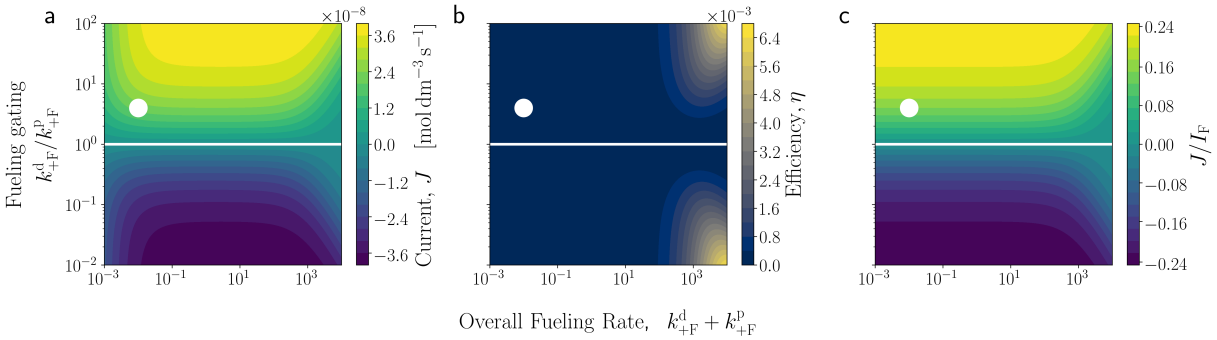

Supplementary Figure 1: Graphs depicting the variation in current, efficiency, and J/I_{F} as overall fueling rate (x-axis) and fueling gating (y-axis) are changed. The white dot indicates the approximate parameters of the experimental rotary motor.

moving in the forward direction. A plateau is reached at higher values of chemical gating, indicating that other values (for instance, shuttling rate or waste formation rate) may become limiting to the current under these conditions. In this case, the waste-forming reaction is likely to be limiting, as it can be seen that the corresponding plateau in the 'cycles per fuel molecule' graph is at a value of approximately ±0.25. This is the theoretical limit (with perfect fueling gating) for a two stroke motor with no chemical gating of the waste-forming reaction (minimum two fuel molecules per cycle because there are two barriers, but half the fuel molecules will lead to no step because of a backwards waste-forming reaction).

Very slow fueling rates (far left of the graphs) slow the motor to a near-stall, as the rate of reaction limits how fast the rotation can be. The graph of cycles per unit fuel shows that the motor is not actually stalled, just extremely slow as the motor still achieves the same number of cycles for each unit of fuel under these conditions. Less intuitively, very fast fueling rates (far right of the graphs) can actually stall the motor. This is because the fueling reaction is so fast that the mechanical distribution is effectively trapped as there is not sufficient time for mechanical equilibration before both co-conformers react. This promotes futile cycles, so fuel is still used despite less directional motion being achieved and therefore fewer cycles are performed for each fuel molecule used. Directional motion is still possible, but a greater chemical gating ratio is needed to achieve it. Under these conditions with a relatively very fast fueling reaction, a motor can be effectively stalled even if the chemomechanical cycle has kinetic asymmetry arising from the chemical gating.

The optimal thermodynamic efficiency balances the competing factors of a fast fueling rate, allowing the mechanical state to be pushed further from equilibrium, and fueling rates that are slow enough to limit futile cycles. The symmetric hotspots (thermodynamic efficiency is independent of direction) are therefore on the right of the graph, towards faster fueling rates where this balance is struck best. The current and J/I_{F} graphs are anti-symmetric around the horizontal axis with a chemical gating ratio of one (i.e., with the chemical gating ratio inverted, the same current and J/I_{F} are

achieved but in the opposite direction).

2. *Chemical gating of the waste-forming reaction*

In this simulation, the overall rate and chemical gating ratio of the waste-forming reaction were varied, while the chemical gating ratio of the fueling reaction was retained at a value of 4 (based on experimental measurements[1], Fig. 2, shown by the white dot in the figures). Therefore, even in the absence of waste-formation chemical gating, there is a

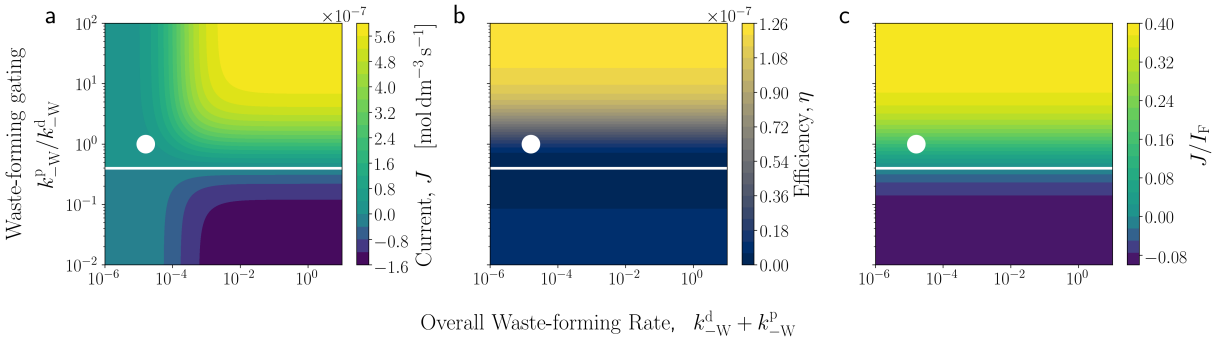

Supplementary Figure 2: Graphs depicting the variation in current, efficiency, and J/I_F as overall waste-forming rate (x-axis) and waste-forming gating (y-axis) are changed. The white dot indicates the approximate parameters of the experimental rotary motor.

driving force for the directional mechanical movement in the rotary motor from a positive information flow. Primarily this simulation shows the same as the fueling gating equivalent, while also showing that the waste-forming gating can cancel out the free energy transfer to the mechanical processes from the fueling gating and stall the motor. This gives the chemomechanical cycle no net kinetic asymmetry which is a condition synonymous with zero mechanical dissipation due to the absence of net free-energy flow between chemical and mechanical transitions. Where this direct negation occurs (white line), the current, efficiency and number of cycles per unit fuel are all inherently zero.

An interesting difference is that fast waste-forming reaction do not appear to cause a loss of current, efficiency, or cycles per fuel molecule. This is because the states preceding a waste-forming reaction (2_H or 2_D) are not able to undergo mechanical exchange and are therefore inherently always at mechanical equilibrium (precluding the mechanism by which fast fueling leads to a lower current, efficiency, and cycles per fuel). However, as the current model neglects the possibility for the rotary motor to lose both barriers, which is more likely to occur with faster waste-forming reactions, deviations from this behavior are expected. If this detail were included, it would be expected that faster waste-forming reactions would also lead to a loss of current, efficiency, and cycles per fuel.

3. *Further exploration of chemical gating*

Better currents and efficiencies are theoretically obtainable with double-gated machines, in which both the fueling and waste-forming processes are chemically gated[29]. A simulation in which the gating ratios of both reactions could be independently varied (Fig. 3) supports this idea, showing that the highest currents and efficiencies are predicted for motors in which both chemical processes are gated (top right and bottom left). Furthermore, no matter the magnitude of gating for one process, the motor would be stalled if the other process is biased in the opposite direction (white line, bottom right to top left of the graphs), leading to zero total kinetic asymmetry and precluding mechanical dissipation. Although the overall rates of the fueling and waste-forming reactions are different within the model, it appears that the contributions of fueling and waste-forming gating are symmetric and of equal importance for current, efficiency, and J/I_F. Additionally, this was the only simulation to approach the theoretical maximum limit of 0.5 cycles per fuel molecule, demonstrating that this requires large chemical gating values for both chemical processes. Under the conditions in which this limit is reached (top right and bottom left), it follows that further improvements to current and efficiency would have to come from other parts of the chemomechanical cycle. The limiting factor in this simulation is most probably the overall rates of the fueling and waste-forming reactions, though could plausibly be shuttling rate under other conditions.

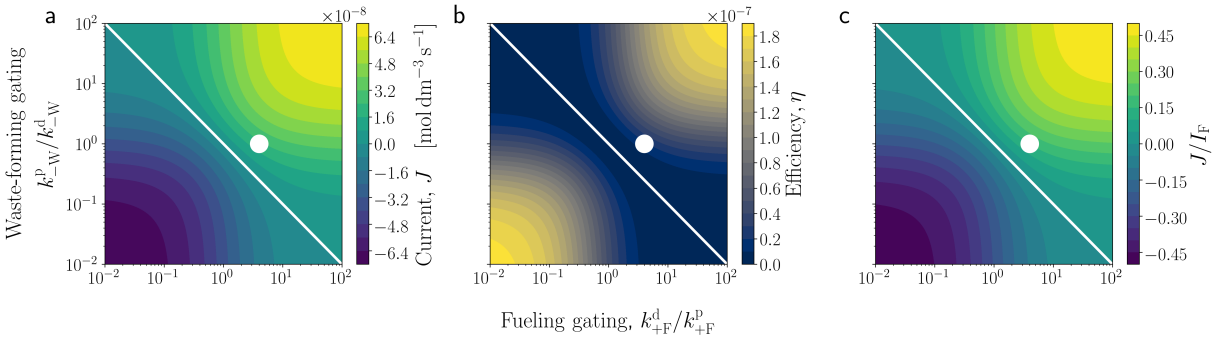

Supplementary Figure 3: Graphs depicting the variation in current, efficiency, and J/I_{F} as chemical gating of the fueling reactions (x-axis) and the waste-forming reactions (y-axis) are changed. Shuttling rates and overall rates of the fueling and waste-forming reactions are kept constant at experimental values throughout. The white dot indicates the approximate parameters of the experimental rotary motor.

4. *Introducing energy flow with power strokes without varying kinetic asymmetry*

In this simulation, the shuttling rate and ratio of clockwise and anticlockwise shuttling rates were varied (Fig. 3c,d in the main text, Fig. 4), introducing energy flow via two power strokes. The simulation treats both halves of the rotary

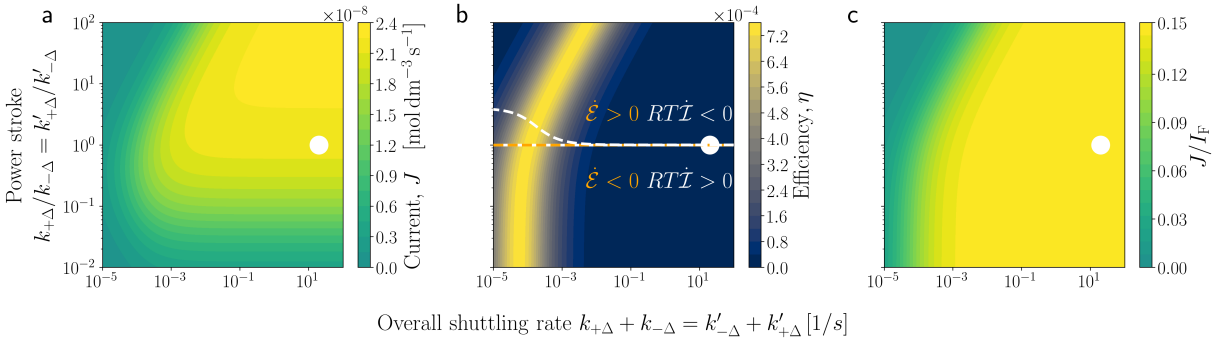

Supplementary Figure 4: Graphs depicting the variation in current, efficiency, and J/I_{F} as overall shuttling rate (x-axis) and power stroke magnitude (y-axis) are changed. The power strokes are added in such a way as to keep the transition state energies and hence the kinetic asymmetry constant by compensating for changes to the mechanical transitions with the rates of the chemical transitions (see the Methods section of the main text). The white dot indicates the approximate parameters of the experimental rotary motor.

motor cycle (Fig. 2) as identical ($k_{+\Delta} = k'_{+\Delta}$, $k_{-\Delta} = k'_{-\Delta}$). As explained in the Methods section of the main text, in this simulation Wegscheider's consistency conditions (equations (36)) were imposed by varying rate constants $k^{\mathrm{p}}_{+\mathrm{W}}$ and $k^{\mathrm{p}}_{+\mathrm{F}}$ according to variations in shuttling rate constants, such that the kinetic asymmetry (K_{r}) of the chemomechanical cycle is not changed by the introduction of power strokes (effectively keeping the absolute transition state energies of the chemical transitions constant), which can nevertheless vary the positive factor Γ in equation (69). This allows us to explore changes caused only by power strokes to identify if, and how, power strokes have any effect on the behavior of the molecular motor.

For relatively slow shuttling rates (far left of the graphs) the motor is effectively stalled, with no significant current, thermodynamic efficiency, or cycles per unit fuel. As well as slow shuttling leading directly to low current, this situation is synonymous with the fast fueling reaction condition described above, in which the mechanical equilibration is slow enough that the mechanical distribution is trapped out by the relatively fast fueling reaction. Fast shuttling rates (far right of the graphs) do not appear detrimental to either the current or the number of cycles per fuel molecule, but thermodynamic efficiency with respect to how free energy is dissipated is strongly adversely affected. This is because fast shuttling hinders the generation of a concentration bias with respect to the equilibrium distribution in the mechanical states by more rapidly enabling equilibration. The position of optimal thermodynamic efficiency is determined by a trade-off between shuttling slow enough that the mechanical states are significantly far from their equilibrium distribution in the steady state, but fast enough not to too strongly promote futile cycles. It is particularly noticeable from the graphs that the optimal region of thermodynamic efficiency contours around the region in which J/I_{F}, the number of

cycles per fuel molecule, moves from a non-productive plateau (left of the graphs) to a productive plateau (right of the graphs). This is because slow shuttling decreases both efficiency and J/I_F, while the latter is independent of the path by which the energy from the fuel is dissipated. As a result, it is unaffected as the degree of energy dissipated through the mechanical processes decreases because of faster shuttling.

A key difference can be seen between graphs in the region describing negative energy flow from backwards power strokes (bottom, where $k_{+\Delta}/k_{-\Delta} = k'_{+\Delta}/k'_{-\Delta} < 1$, so clockwise shuttling requires gain of chemical potential). In this region, the thermodynamic efficiency and the number of cycles per unit fuel are independent of the magnitude of the power stroke and dependent only on the overall shuttling rate. Conversely, the current is strongly dependent on the power stroke magnitude. This arises because the current is directly reduced by the slow forward mechanical transitions associated with backward power strokes which limit the rate of the forwards chemomechanical cycles. However, efficiency and J/I_F are not affected as the decrease in the current (J) is offset by the decrease in the fuel consumption rate (I_F).

In the region with a positive energy flow arising from forwards power strokes, (top, where $k_{+\Delta}/k_{-\Delta} = k'_{+\Delta}/k'_{-\Delta} > 1$, so clockwise shuttling lowers standard chemical potential) all three quantities are dependent on both the overall shuttling rate and the magnitude of the power stroke. If the power stroke is too large or overall shuttling rate is too small (top and left of the graphs), futile cycles are favored, decreasing the current and thermodynamic efficiency and requiring more fuel per cycle on average. This is because the proximal species ($1^{\mathrm{H}}_{\mathrm{D}}$ or $1^{\mathrm{D}}_{\mathrm{H}}$) are sufficiently destabilized so that the unwanted proximal fueling reaction is faster than mechanical shuttling. It is especially unfavorable if a large power stroke and slow overall shuttling rate are combined.

The maximum current is seen in a region with positive energy flow from forward power strokes but faster mechanical transitions (top right of the graphs). This is because, at steady state, the energy flow is increased by adding power strokes faster than information flow is decreased by biasing the mechanical equilibrium. This is a specific property of nonequilibrium regimes, where the standard chemical potentials and mutual information contributions to the total free-energy flow, which must inherently cancel at equilibrium, may differ in a nonequilibrium steady state. In mathematical terms we have, for the sum of energy and information flows:

$$\dot{\mathcal{E}} + RT\dot{\mathcal{I}} = J(\mu^{\circ}_{1^{\mathrm{D}}_{\mathrm{H}}} - \mu^{\circ}_{1^{\mathrm{D}}_{\mathrm{D}}} + \mu^{\circ}_{1^{\mathrm{H}}_{\mathrm{D}}} - \mu^{\circ}_{1^{\mathrm{H}}_{\mathrm{H}}} + RT\log\frac{[1^{\mathrm{D}}_{\mathrm{H}}][1^{\mathrm{H}}_{\mathrm{D}}]}{[1^{\mathrm{D}}_{\mathrm{D}}][1^{\mathrm{H}}_{\mathrm{H}}]}) \geq 0\,. \tag{70}$$

At mechanical equilibrium, both the current J and the quantity in parenthesis are individually zero, since the concentrations are distributed accordingly to the exponential of the the difference in standard chemical potentials divided by RT. As soon as the system is driven out of equilibrium, the difference in standard chemical potentials stays constant (and positive in the region we are considering). In the presence of kinetic gating in the forward direction, the magnitude of the logarithm (negative, in the region we are considering) decreases. This is because, while the equilibrium favors $1^{\mathrm{D}}_{\mathrm{D}}$ over $1^{\mathrm{H}}_{\mathrm{D}}$ and $1^{\mathrm{H}}_{\mathrm{H}}$ over $1^{\mathrm{D}}_{\mathrm{H}}$, the fueling kinetic gating is such to flatten this correlation, thus reducing mutual information. As a result, the mutual information contribution decreases towards more negative values slower than the standard chemical potential contribution increases towards positive values, so that the sum in the parenthesis is positive. In the presence of fast shuttling, the concentration distribution stays very close to the equilibrium one and the quantity in parenthesis is very small, thus making the efficiency very low. In other words, when the shuttling is fast, the mechanical transitions stay very close to equilibrium. This does not contradict the fact that we observe a high current in the stationary state, because ratio $k_{+\Delta}[1^{\mathrm{D}}_{\mathrm{H}}]_{\mathrm{ss}}/k_{-\Delta}[1^{\mathrm{D}}_{\mathrm{D}}]_{\mathrm{ss}} = k'_{+\Delta}[1^{\mathrm{H}}_{\mathrm{D}}]_{\mathrm{ss}}/k'_{-\Delta}[1^{\mathrm{H}}_{\mathrm{H}}]_{\mathrm{ss}}$ being close to 1 does not imply that the difference giving the current $J = k_{+\Delta}[1^{\mathrm{D}}_{\mathrm{H}}]_{\mathrm{ss}} - k_{-\Delta}[1^{\mathrm{D}}_{\mathrm{D}}]_{\mathrm{ss}} = k'_{+\Delta}[1^{\mathrm{H}}_{\mathrm{D}}]_{\mathrm{ss}} - k'_{-\Delta}[1^{\mathrm{H}}_{\mathrm{H}}]_{\mathrm{ss}}$ is small. Indeed, this is a clear example showing why the entropy production, not the current or J/I_F, is a measure of how far from equilibrium this system operates. Despite the increased current, the average number of cycles per fuel molecule remains unchanged between the high-current area (top right of the graphs) and the region with no or negative energy flow (bottom of the graphs), showing that only current is affected. In the same area, the efficiency plot shows that a very low percentage of the fueling free-energy is made available to the mechanical transitions, indicating that this regime, while optimizing current (J) and J/I_F, may not be optimal to perform work (e.g., transporting cargoes).

5. Introducing energy flow with a power stroke together with varying kinetic asymmetry

In contrast to the previous case, if Wegscheider's consistency conditions are imposed by varying rate constants $k^{\mathrm{p}}_{+\mathrm{W}}$ and $k^{\mathrm{p}}_{-\mathrm{F}}$ (and not $k^{\mathrm{p}}_{+\mathrm{W}}$ and $k^{\mathrm{p}}_{+\mathrm{F}}$) according to variations in shuttling rate constants, the introduction of a power stroke will change the kinetic asymmetry of the chemomechanical cycle (Fig. 5). Unsurprisingly, the graphs produced for this scenario appear to display a combination of the features seen when power stroke magnitude (Fig. S.4) and kinetic asymmetry (Figs. S.1 and S.2) are altered independently. In the region with a positive power stroke and the associated larger kinetic asymmetry, the current and J/I_F increase. As with the fueling gating variation (Fig. S1) J/I_F, the number of cycles per fuel molecule, approaches the theoretical cap of ±0.25 for a motor with an unbiased waste-forming reaction.

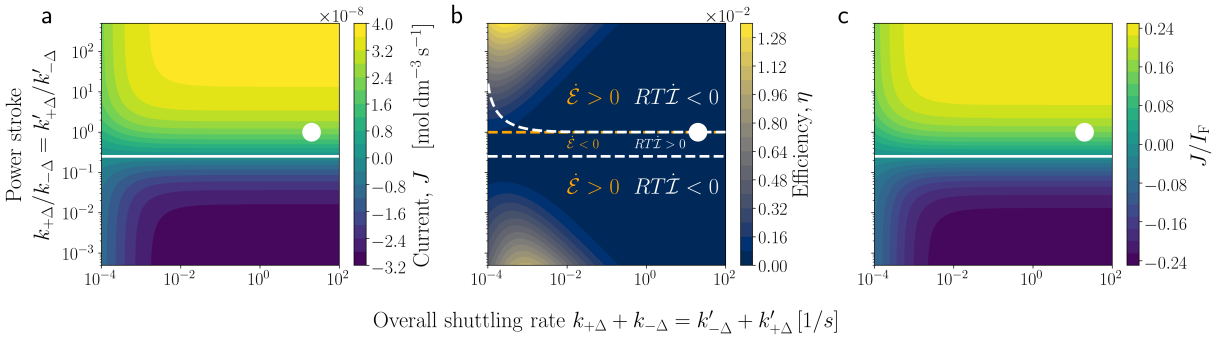

Supplementary Figure 5: Graphs depicting the variation in current, efficiency, and J/I_F as overall shuttling rate (x-axis) and power stroke magnitude (y-axis) are changed. The total power stroke magnitude is not compensated by changes in fuel addition and waste removal transition rates (k^{p}_{+F} and k^{p}_{-W}), therefore allowing the kinetic asymmetry to change. Instead, the transition rates of reverse processes (waste addition and fuel removal, k^{p}_{+W} and k^{p}_{-F}) are altered to retain Wegscheider's conditions and thermodynamic validity (see the Methods section of the main text). The white dot indicates the approximate parameters of the experimental rotary motor.

This is because the heights of the waste-forming transition states do not change (and hence remain identical to each other within the model) so any change in the power stroke is compensated by a corresponding change in the rates of the waste-forming reactions. The maximum efficiency in the region with positive power strokes is the highest seen in any simulation, appearing in the region with slower absolute shuttling for same reasons as previously discussed (see § VI B 1, VI B 2, and VI B 4), indicating that this combined approach, introducing power strokes with concomitant increase in kinetic asymmetry, may be an efficient design for molecular motors.

As with the simulations varying kinetic asymmetry by altering chemical gating of the fueling or waste-forming reactions, the direction of the rotary motor can be inverted with sufficiently negative power strokes. However, these graphs are not symmetrical and a lower maximum current and efficiency are seen in the negative current region as the chemical gating inherent to the system (*i.e.*, with no power strokes) favors a positive (clockwise) current.

6. *Causing power strokes to cancel out*

In this simulation (Fig. 6), shuttling rate and power stroke magnitude are, again, altered. This time, however, the

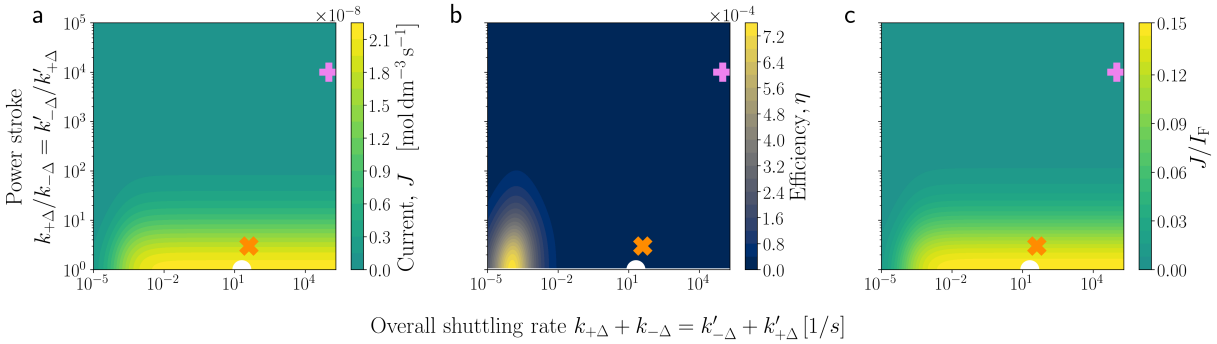

Supplementary Figure 6: Graphs depicting the variation in current, efficiency, and J/I_F as overall shuttling rate (x-axis) and power stroke magnitude (y-axis) are changed. The power strokes are introduced so that they cancel out (i.e., energy release by the first mechanical transition is always mirrored by an identical energy gain in the second) and lead to no net energy flow within the chemomechanical cycle. The pink plus and orange cross indicate the properties expected from changing one fumaramide group to a succinamide. The pink plus indicates the values obtained from single-molecule experiments[30], while the orange cross shows the values found in a related rotaxane-based system[31]. The white dot indicates the approximate parameters of the experimental rotary motor.

direction of one power stroke is always opposite to the other while they retain the same magnitude, cancelling out each other's contribution. Therefore, no energy flow is introduced across the full chemomechanical cycle and kinetic asymmetry remains inherently unaltered. This is most easily realized by switching one binding site for a more weakly or

more strongly coordinating station. In the figures, the orange cross marks the predicted position of a motor equivalent to the experimental motor but with one station that binds the macrocycle 2.7 kJ mol^{-1} more strongly than the other, equating to a 3 : 1 bias in occupancy. This motor is predicted to operate at about 80% of the current of the original design as it appears futile cycles would be promoted and ≈ 20% fewer cycles would be achieved, despite the same overall rate of fuel use. If the difference in binding strength is increased to 23 kJ mol^{-1}, the difference measured for the binding of the benzylic amide macrocycle used in the rotary motor to a fumaramide site compared to a succinamide site[30], the motor is effectively stalled, achieving no significant current, efficiency, or number of cycles per fuel molecule.

As before (see § VI B 1, VI B 2, VI B 4, and VI B 5), slow shuttling (left of the graphs) can be seen to stall the motor as futile cycles are favored, and once again, the area of maximum efficiency comes where this effect best balances with the degree to which the mechanical states are kept away from equilibrium in the steady state. Fast shuttling does not affect the current or the number of cycles per fuel molecule.

All graphs indicate that any change away from degenerate stations (moving up the y-axis) will always be detrimental for the motor in terms of current, efficiency, and the number of cycles per fuel molecule. This arises from a decreased capacity to support information flow in the motor as one station becomes more favored, which in turn decreases the ability of the motor to sustain a current. The full details and origins of this effect are not fully explored in this current work and warrant further experimental and theoretical investigation.

7. Conclusion

While the above by no-means represents an exhaustive analysis of all possible design feature alterations, even for the specific small-molecule motor analyzed in this paper, several important considerations have been identified. Furthermore, as future experimental systems become available to study, we envisage that similar analyses will help establish more general design considerations for molecular motors. These may become invaluable when putting molecular motors to work and may help clarify the driving forces behind the functioning of biological molecular motors.

[1] Wilson, M. R. *et al.* An autonomous chemically fuelled small-molecule motor. *Nature* **534**, 235–240 (2016).
[2] Laidler, K. J. *Chemical Kinetics* (HarperCollins Publishers, New York, 1987).
[3] Wachtel, A., Rao, R. & Esposito, M. Thermodynamically consistent coarse graining of biocatalysts beyond michaelis–menten. *New J. Phys.* **20**, 042002 (2018).
[4] Astumian, R. D. How molecular motors work — insights from the molecular machinist's toolbox: the nobel prize in chemistry 2016. *Chem. Sci.* **8**, 840–845 (2017).
[5] Astumian, R. D. Kinetic asymmetry allows macromolecular catalysts to drive an information ratchet. *Nat. Commun.* **10**, 3837 (2019).
[6] Das, K., Gabrielli, L. & Prins, L. J. Chemically-fueled self-assembly in biology and chemistry. *Angew. Chem. Int. Ed.* **60**, 20120 (2021).
[7] Avanzini, F., Falasco, G. & Esposito, M. Thermodynamics of non-elementary chemical reaction networks. *New J. Phys.* **22**, 093040 (2020).
[8] Rao, R. & Esposito, M. Nonequilibrium thermodynamics of chemical reaction networks: Wisdom from stochastic thermodynamics. *Phys. Rev. X* **6**, 041064 (2016).
[9] Feinberg, M. Complex balancing in general kinetic systems. *Arch. Ration. Mech. Anal.* **49**, 187–194 (1972).
[10] King, E. L. & Altman, C. A schematic method of deriving the rate laws for enzyme-catalyzed reactions. *The Journal of Physical Chemistry* **60**, 1375–1378 (1956).
[11] Hill, T. L. *Free energy transduction in biology* (Academic Press, New York, 1977).
[12] Mirzaev, I. & Gunawardena, J. Laplacian dynamics on general graphs. *Bulletin of Mathematical Biology* **75**, 2118–2149 (2013).
[13] Schnakenberg, J. Network theory of microscopic and macroscopic behavior of master equation systems. *Rev. Mod. Phys.* **48**, 571–585 (1976).
[14] Mou, C. Y., Luo, J. & Nicolis, G. Stochastic thermodynamics of nonequilibrium steady states in chemical reaction systems. *The Journal of Chemical Physics* **84**, 7011–7017 (1986).
[15] Lebowitz, J. L. & Bergmann, P. New approach to nonequilibrium process. *Physical Review* **99**, 578–587 (1955).
[16] Katz, S., Lebowitz, J. L. & Spohn, H. Phase transitions in stationary nonequilibrium states of model lattice systems. *Phys. Rev. B* **28**, 1655–1658 (1983).
[17] Esposito, M. Stochastic thermodynamics under coarse graining. *Phys. Rev. E* **85**, 041125 (2012).
[18] Maes, C. Local detailed balance. *SciPost Phys. Lect. Notes* **32**, 1–17 (2021).
[19] Feng, Y. *et al.* Molecular pumps and motors. *J. Am. Chem. Soc.* **143**, 5569–5591 (2021).
[20] Falasco, G. & Esposito, M. Local detailed balance across scales: From diffusions to jump processes and beyond. *Phys. Rev. E* **103**, 042114 (2021).
[21] Gaspard, P. Comment on "validity of path thermodynamics in reactive systems". *Phys. Rev. E* **103**, 016101 (2021).

[22] Petersen, J., Förster, K., Turina, P. & Gräber, P. Comparison of the h+/atp ratios of the h+-atp synthases from yeast and from chloroplast. *Proc. Natl Acad. Sci. USA* **109**, 11150–11155 (2012).
[23] Horowitz, J. M. & Esposito, M. Thermodynamics with continuous information flow. *Phys. Rev. X* **4**, 031015 (2014).
[24] Geertsema, E. M., van der Molen, S. J., Martens, M. & Feringa, B. L. Optimizing rotary processes in synthetic molecular motors. *Proc. Natl. Acad. Sci. U.S.A.* **106**, 16919–16924 (2009).
[25] Ragazzon, G. & Prins, L. J. Energy consumption in chemical fuel-driven self-assembly. *Nat. Nanotechnol.* **13**, 882–889 (2018).
[26] Astumian, R. & Bier, M. Mechanochemical coupling of the motion of molecular motors to atp hydrolysis. *Biophys. J.* **70**, 637–653 (1996).
[27] Leigh, D. A., Wong, J. K. Y., Dehez, F. & Zerbetto, F. Unidirectional rotation in a mechanically interlocked molecular rotor. *Nature* **424**, 174–179 (2003).
[28] Shirono, K., Morimatsu, T. & Takemura, F. Gas solubilities (CO_2, O_2, Ar, N_2, H_2, and He) in liquid chlorinated methanes. *J. Chem. Eng. Data* **53**, 1867–1871 (2008).
[29] Borsley, S., Leigh, D. A. & Roberts, B. M. W. A doubly kinetically-gated information ratchet autonomously driven by carbodiimide hydration. *J. Am. Chem. Soc.* **143**, 4414–4420 (2021).
[30] Lussis, P. *et al.* A single synthetic small molecule that generates force against a load. *Nat. Nanotechnol.* **6**, 553–557 (2011).
[31] Alvarez-Pérez, M., Goldup, S. M., Leigh, D. A. & Slawin, A. M. Z. A chemically-driven molecular information ratchet. *J. Am. Chem. Soc.* **130**, 1836–1838 (2008).